MODELING AND SIMULATION OF PANTOGRAPH-CATENARY SYSTEMS

by

DAVID O'CONNOR

SUBMITTED TO THE DEPARTMENT OF
MECHANICAL ENGINEERING IN
PARTIAL FULFILLMENT OF THE
REQUIREMENTS FOR THE DEGREE OF

MASTER OF SCIENCE IN MECHANICAL ENGINEERING

at the

MASSACHUSETTS INSTITUTE OF TECHNOLOGY

February 1984

Author_____

Department of Mechanical Engineering
February 27, 1984

Certified by_

David N. Wormley
Thesis Supervisor

Accepted by_

Warren M. Rohsenow
Chairman, Mechanical Engineering Graduate Committee

MODELING AND SIMULATION OF PANTOGRAPH-CATENARY SYSTEMS

by

DAVID O'CONNOR

ABSTRACT

This research examines pantograph-catenary systems to evaluate
dynamic performance. A pantograph-catenary time-domain simulation and a
pantograph frequency response computer simulation are developed to study
different catenary materials, to investigate the influence of pantograph
parameters on dynamic performance, and to evaluate different pantograph
configurations. An all-aluminum catenary is compared with a catenary con-
sisting of a copper contact wire, aluminum messenger wire, and stainless
steel droppers. All-aluminum catenaries are shown to yield smaller con-
tact force variations and may be more suitable for two pantograph op-
erations. Pantograph parameter studies have evaluated head mass, frame
mass, and head spring rate and damping on dynamic performance. A com-
parison of pantographs using spring-cam suspensions with those using
air cylinder suspensions shows the latter performs significantly better.
The parameter and suspension studies are used to form an optimum set of
pantograph parameters. The optimum pantographs contact force variation
is 44% lower at 170 km/hr than a typical high-speed design. A frame-
actuated, actively controlled pantograph is designed using modern con-
trol techniques. For the 170 km/hr case, the active design contact force
variation is 58% lower than the typical high-speed pantograph and 25% lower
than the optimum pantograph. The case where two pantographs are run
under the same catenary is also discussed.

Thesis Supervisor: David N. Wormley
        Title: Professor of Mechanical Engineering

ACKNOWLEDGEMENTS

TABLE OF CONTENTS

LIST OF FIGURES

LIST OF TABLES

CHAPTER 1

INTRODUCTION

1.1 Background

Electrification of rail systems offers increased efficiency of power conversion in comparison to petroleum-based systems. With increases in fossil fuel prices likely to continue, the economic advantage that electric rail systems offer will increase. Electric locomotives also offer increased reliability over non-electric locomotives. In both Europe and Japan, major sections of track are already electrified with more extensive electrification planned.

Providing power to an electrified train is usually done in one of two ways. The first is with a live "third rail" which is positioned somewhere on the railbed. The other uses a live overhead wire called a catenary. The safety hazard posed by an exposed third rail causes the majority of intercity systems to use catenaries. Japan's Shinkansen and France's TGV both have catenary systems.

The major disadvantage to electrification is the high capital cost, over half of which is associated with overhead wire installation. Thus any developments that result in a lower-cost catenary may have a significant impact on the future of electrification.

The current in the catenary is transferred to the train through a mechanical arm known as a pantograph. The pantograph must exert enough force on the catenary to ensure good electrical contact. Excessive force

however, introduces wear and dynamic problems. The pantograph must also be able to operate over a wide range of wire heights, typically 0.5 to 2.0 m,[1] to accomodate the drop in catenary height when a tunnel is approached. Most pantographs have two stages: a frame to accomodate gross motion and a head to follow small fluctuations in wire height.

The dynamic interaction between the pantograph and catenary has a significant effect on performance. Ideally the pantograph should touch the wire hard enough to ensure good electrical contact, but lightly enough so the catenary is never significantly displaced. Increasing uplift force does not always ensure better electrical contact. Catenaries are relatively stiff at the support towers and comparatively soft in between; increasing uplift force causes larger variations in catenary displacement which leads to greater dynamic excitation. These excitations may cause the pantograph to lose contact in the stiffest regions of the catenary; indicating that the ideal catenary has a uniform stiffness. If too little uplift force is used, small disturbances cause losses in contact. When loss of contact happens, not only is power to the train interrupted, but also an arc occurs. Arcing can severely damage a catenary and greatly decrease its operating life.

Many catenary designs exist. The simplest, a single tensioned wire supported by towers, is called a trolley wire (Figure 1.1a). It is the

---

[1]Some systems specifically designed for high-speed operation have smaller height variations. France's SNCF high-speed line has a height variation under 40 cm (16 in) and Japan's Shinkansen has even less [1].

Tower

FIGURE 1.1a   TROLLEY WIRE

Messenger Wire
Contact Wire
Dropper
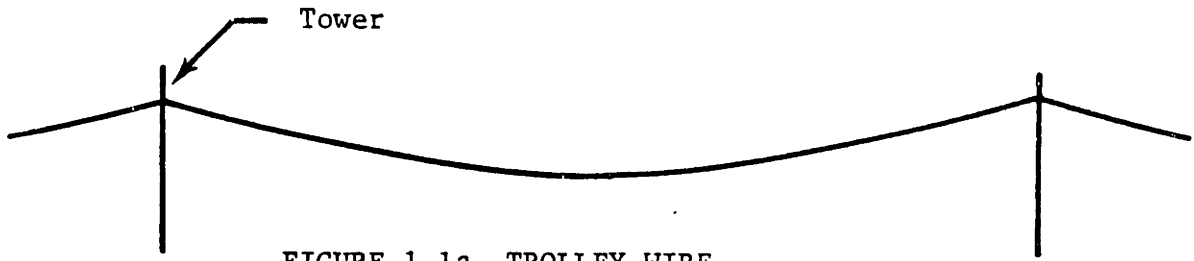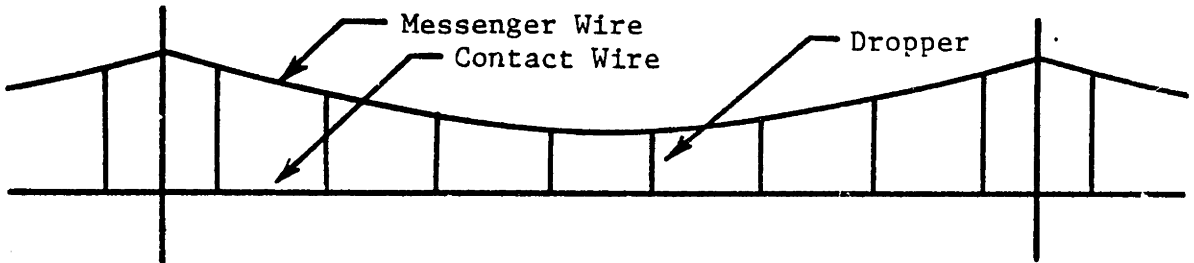
FIGURE 1.1b   SIMPLE CATENARY

Stitch Wire
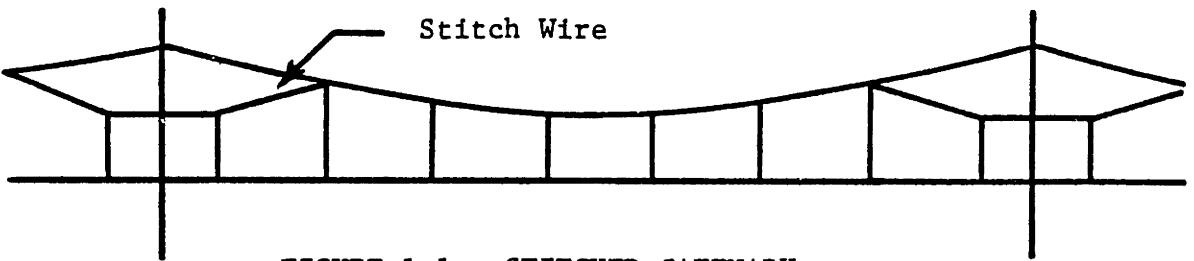
FIGURE 1.1c   STITCHED CATENARY

Auxiliary Wire
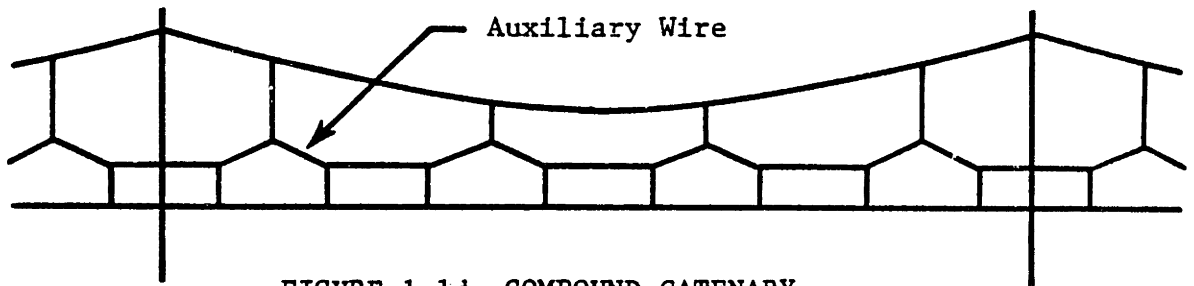
FIGURE 1.1d   COMPOUND CATENARY

FIGURE 1.1   COMMON CATENARY CONFIGURATIONS

least expensive type of catenary to build and is commonly used for low speed, intracity travel. Extreme variation in spring rate and large sag make its use inappropriate for speeds over 50 km/hr (30 mi/hr).

More complex designs have two goals: One is to make the stiffness uniform and the other is to reduce sag. Figure 1.1b shows a "simple catenary". It consists of two wires: the messenger wire, supported by the towers and the contact wire, suspended from the messenger wire by droppers. The droppers are of varying length to reduce sag. Since the contact wire is not directly attached to the towers, the stiffness is more uniform.

The stitched catenary shown in Figure 1.1c is similar to the simple catenary but has an additional wire hung from the messenger wire bypassing each support tower. The stitch reduces the stiffness of the catenary at the towers giving the catenary a more uniform stiffness. Stitched catenaries are used by the French on the SNCF line.

Figure 1.1d shows a compound catenary. It features a third auxillary wire between the messenger and the contact wire. The addition of an auxillary wire helps isolate the contact wire from the droppers as well as the towers yielding a catenary with an even more uniform stiffness. Compound catenaries are used on Japan's Tokiado line. Japan's newest catenary system, the Sanyo line, uses a combination of the compound and stitched configurations.

1.2 Literature Review

Over the past 20 years, much research has been performed in the area of pantograph-catenary dynamics. In this chapter, some of the more important works will be discussed.

1.2.1 Pantograph Studies

Much of the research has concentrated on improving pantograph performance. A better-performing pantograph makes possible the construction of less expensive catenaries and allows higher-speed operation under existing systems. The most frequently made suggestion for improving performance is to reduce head mass [2,3,4,5,6]. To maintain contact with the wire, the head must be able to respond to all wire motions. A lighter head, having less inertia, is able to react to high-frequency vibrations more quickly. Gostling and Hobbs [4] support this recommendation and also recommend the head suspension be kept soft. Belyaev, et al. [7] tested two Soviet pantographs. The lighter of the two performed better at higher speeds, although the authors were concerned with its sturdiness. They also found that the addition of viscous head damping resulted in more uniform contact force for both pantographs.

Boissonade and Pierre [2], who tested the Faiveley high speed pantograph on the French SNCF line, recommended reducing head mass. He also recommends increasing frame damping on all pantographs (they use $30 \frac{N \cdot S}{m}$). Further he suggests that "one-way" damping, resistance only to downward motion of the pantograph head, could decrease loss of contact between

pantograph and catenary. Boissonnade, Pierre, and Dupoint [1] have done over 200 tests on pantograph-catenary systems at speeds up to 308 km/hr. All tests were run under a 40 year old catenary with 90 m spans. Only minor modifications were made to the catenary for thest tests. The Faiveley (AM) pantograph was shown to perform well up to 230 km/hr. It is felt that this pantograph could be modified for speeds as high as 300 km/hr under existing catenary systems.

Peters [8] tested both single and dual stage Faiveley pantographs. Loss of contact duration was used as the performance criteria. He reports that short separations, less than 5 ms, result in small, low-temperature electric arcs that cause no damage to the pantograph head or contact wire. Medium duration separations, 5 ms to 20 ms, are the most damaging to the catenary and pantograph head. For durations greater than 20 ms, the forward velocity of the train extinguishes the arc; this causes loss of power to the train, but no additional damage. These tests were made with an uplift force of 90N and a pantograph head mass of 15 kg. Significant performance improvements were achieved by increasing the uplift force to 125N and reducing head mass from 15 kg to 13 kg. Peters reported that 45% of the total separation time was spent during separations of 2 ms to 5 ms. The more prominent separations tended to occur at the support towers. He showed that unacceptable contact behavior occurred when the standard deviation in contact force equaled one-third the uplift force.

Coxen, et al [9] have reported on the development of a simple, high performance pantograph by British Rail and Brecknell-Willis. The panto-

graph features a torsional spring suspension for a set of light collectors, airfoils to overcome aerodynamic asymmetries, and a pneumatic cylinder as part of the frame suspension. Flow to and from the cylinder is through a small orifice, so there is a constant uplift force only for low-frequency motions. To high-frequency excitation, the cylinder acts as a spring in series with a damper to ground, improving frame response.

Vesely [10] did frequency response testing on an August-Stemman pantograph. The results were compared with a general pantograph model that incorporates geometric nonlinearities as well as head stops and Coulomb friction. The model correlated well with experimental data up to a 13 hz excitation frequency. After this unmodelled structural effects of the links became important. The two-mass model was shown to be a very accurate description of the actual system for displacements under 20 cm.

Several researchers have considered the use of active elements to improve pantograph performance. Hydraulic actuators were incorporated by Sikorsky Aircraft [11] into the frame of an August-Stemman pantograph. Two configurations were tested. The first was frame actuated and responded to the difference between head and frame displacement. The second used the same measurement but had an additional actuator between the head and frame. A stable control system was not achieved for either design.

Behjaev, et al. [7], discusses a TS-IM type pantograph with an active pneumatic cylinder designed to stabilize contact pressure on the catenary. The system also provided a means for raising the pantograph from its

lowered position. Wann [12], compared passive and several classically designed active pantographs. Simulations showed that active elements have the potential to significantly improve pantograph performance. Vinayalinyam [13] simulated two active pantograph designs. One frame actuated design and his own "panhead inertia compensated" design. Neither design showed any significant reduction in contact force variation.

1.2.2 Catenary Studies

The other elements in an overhead current collection system is the catenary. Several studies stress wave speed as an important parameter. The wave speed dictates the speed of propagation of a displacement or a force through the catenary. It is defined as [2,14]:

$$V_{wave} = \frac{\Sigma T}{\Sigma \rho}$$

where:

ΣT is the sum of the tensions in the contact wire, messenger wire, and auxillary wires.

$\Sigma \rho$ is the sum of the linear densities of the contact wire, messenger wire, and auxillary wires.

Critical speed, the maximum speed before serious degradation of performance or loss of contact occurs, is generally defined as a fraction of wave speed.

Thomet [14] claims that a catenary resonance is excited when the train velocity is 45% of the wave speed. He feels that this is the critical speed and recommends keeping the train velocity at least 10%

below this value. Thomet also recommends that wire tension be made as large as possible. Higher tension increases the wave speed and makes the catenary's stiffness more uniform.

Some authors feel that catenary sag should not be eliminated entirely. As the pantograph moves from a tower to midspan the catenary becomes more compliant and displaces more. If the catenary sags, the pantograph must overcome the sag by lifting the wire. Since this inertial resistance has the greatest effect where the catenary stiffness is smallest, displacements are reduced. Estimations of how much sag is useful varies. Some proposed ratios of sag to span length are 0.6/1000 [3], 1.0/1000 [15], and 1.3/1000 [16].

Recently there has been an increased interest in aluminum catenaries. The primary motivation has been increasing copper prices. However, there are some other advantages. For an equivalent current carrying capability, an aluminum cable is approximately one-half the weight and can hold the same tension as a copper one [17]. Since tensions are the same but weight is less, aluminum has higher wave speeds. Problems include greater sensitivity to solar heating, less resistance to wind loading and questionable wear characterstics.

Several authors have addressed the wear issue. Thomas [18] in 1966 examined a French composite contact wire used in Bordeaux with an aluminum cable and a steel core. He claimed that after 500,000 pantograph passes, the life of a copper catenary, the wire showed little wear and had the possibility of 100,000 more passes. Recently, Carlson and Griggs [19]

did wear testing of aluminum and copper conductors. They reported that wear rates were about the same for aluminum and copper after an initial break-in period during which aluminum wore faster.

1.2.3 Pantograph-Catenary Models

To better understand the dynamic interactions between pantographs and catenaries, many attempts to develop system models have been made. The pantograph portion of the model generally uses the two-mass representation where the first mass represents the head mass and the second mass represents the frame structure. Most of the effort is usually spent developing a good catenary model.

In 1964 Morris [20] developed an analog computer simulation for a model including a simple two-mass pantograph and a catenary consisting of lumped masses connected by a tensioned wire and suspended from a spring-damper system. The simplified catenary representation was necessary to reduce the problem to a size that an analog computer could handle. The simplifications were severe enough to make this model of limited value. Gilbert and Davis [21] developed an analytic solution for catenary motion. The catenary was modeled as a massless tensioned spring embedded in an elastic medium whose stiffness was varied sinusoidally.

Abbot [22] modeled a trolley wire and replaced the differential equations of motion by finite difference equations. The equations were solved using numerical methods. Levy, et al. [23] developed a model of a simple catenary which considers wire tension, wire mass, bending stiffness, tower stiffness, dropper stiffness and wire sag. The catenary was modeled

using modal analysis and incorporated the first 45 models of vibration. The pantograph was represented with the standard two-mass model. More recently, Armbruster [17] used a similar modal analysis approach to model the catenary. His pantograph model also incorporated nonlinear damping elements.

Scott and Rothman [24] developed several computer programs to evaluate various catenary systems. Their critical speed predictions agreed well with experiments conducted by Willets and Edwards [25]. Percent separation time predictions, however, did not agree closely.

Hobbs [26] developed a finite-element model and conducted experiments to verify it. He showed that wire bending stiffness can be neglected but wire mass must be considered. The test catenary was shaken by a hydraulic ram and accelerometers mounted on the wire were monitored. The model compared well with the experiment up to 10 Hz.

1.3 Scope of Study

The objectives of this study are the following:

- Evaluate the effect of constructing catenaries from lower cost materials

- Examine the effect of catenary sag on performance

- Study the effect of pantograph parameters on performance and form a set of optimum parameters

- Examine new passive and active pantograph configurations

- Study the performance of two pantographs traveling under the same catenary

-22-

To complete the above studies, two analytical models are developed. The first is a pantograph-catenary system model. For the catenary portion of the model a simple-style catenary is modeled using modal analysis. The effects of tension in the wires, wire mass, wire sag, bending stiffness, wire damping, tower stiffness and dropper stiffness are considered. The pantograph portion of the model is a linear two-mass representation: one mass for the head and the other for the .frame. A pantograph frequency response model is also developed. It too uses the two-mass representation of the pantograph.

In recent years, copper has become increasingly expensive. After copper, aluminum is the next best feasible electrical conductor and is considerably cheaper. Already some catenaries are using aluminum messenger wires. An all-aluminum catenary will be compared with a standard catenary to evaluate its dynamic performance.

The cost of a pantograph when compared to a catenary system is small. An improved pantograph would allow the use of a cheaper catenary or possibly an existing catenary and still achieve good performance. Pantograph parameters are examined in this study to determine their effect on performance. Alternate suspension configurations are also investigated. The results are used to form a set of best possible parameters. A frame actuated actively-controlled pantograph is also designed and simulated. The best passive and active designs are then compared with a typical high-speed pantograph currently in use. The case where two pantographs are mounted on the same train is also considered.

CHAPTER 2

MODEL DEVELOPMENT

In this chapter, the modeling and solution technique for a pantograph-catenary system time domain simulation is described. The pantograph and catenary models are first considered separately; then the coupling between the two is investigated. The methods used to model the system and the solution technique are only outlined here. A detailed derivation of the model is presented in Appendices A and B.

A frequency response program for the pantograph is also developed here. The two-mass model is used to describe the pantograph. One mass represents the head structure and the other mass represents the frame structure. The simulation outputs the magnitude and phase of the contact force, head displacement, on frame displacement to a sinusoidal catenary input.

2.1 Pantograph-Catenary Model Description

The catenary simulated is a simple-style catenary. It was chosen because it has all the characteristic dynamic effects present in advanced catenary designs without the additional complexities involved in modeling stitched and compound catenary designs. A diagram of the model is given in Figure 2.1, the catenary is of finite length and has the following features:

- A simple style catenary containing a contact wire and messenger wire.

- The spacing between droppers and towers can be assigned arbitrarily.
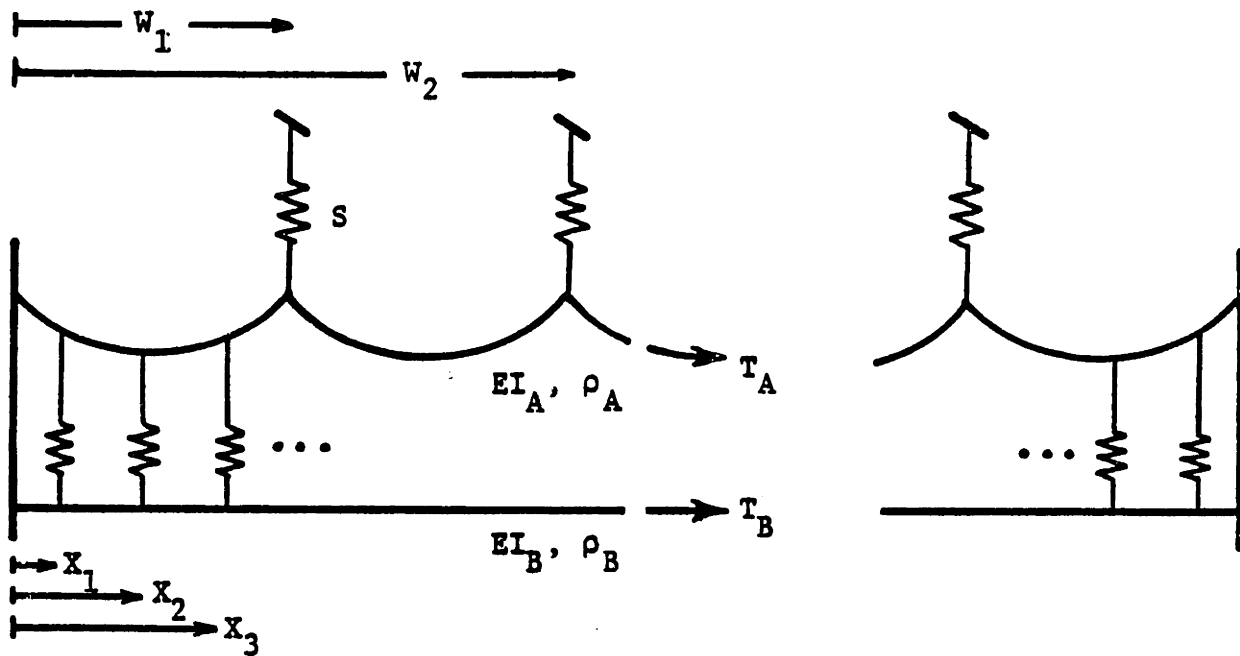
Tower Stiffness: S

Dropper Stiffness: K

Distance to the jth Tower: W_j

Distance to the ith Dropper: X_i

Stiffness of the Two Wires: EI_A, EI_B

Density of the Two Wires: ρ_A, ρ_B

Tension in the Two Wires: T_A, T_B

FIGURE 2.1: CATENARY MODEL

- Contact and messenger wires are each modeled with a bending stiffness, constant tension, and a uniform density.

- Damping is distributed proportionally to the mass of the wires to ensure orthogonality of the natural modes.

- The two wires are connected by droppers modeled as massless linear springs.

- The messenger wire is supported by towers which are also modeled as massless springs.

Figure 2.2 shows a typical "symmetric" pantograph design. It consists of two main elements, a head structure and a two-sided frame structure. The head is mounted to the frame through a spring suspension. The frame's suspension uses springs in combination with a system of links to apply a constant uplift force to the frame over the operating range.

Figure 2.3 illustrates an "asymmetric" pantograph. It also consists of a head and frame structure. The head is mounted to the frame through a torsional rather than a translation spring suspension and the frame uses a pneumatic air cylinder for its suspension.

For both pantographs, the links of the head structure move together and the links of the frame structure move together. However, the two elements can move independently of each other. When operating under a level catenary, pantograph displacements are small. So it is felt that nonlinear pantograph equations of motion can be linearized to a two-mass, two-degree-of-freedom model where one mass represents the head and the other represents the frame. Vesely [10], using both experimental and analytical pantograph tests, showed that the linear two-mass model is a valid repre-

HEAD

HEAD
SUSPENSION

UPPER
FRAME
LINK

LOWER
FRAME
LINKS
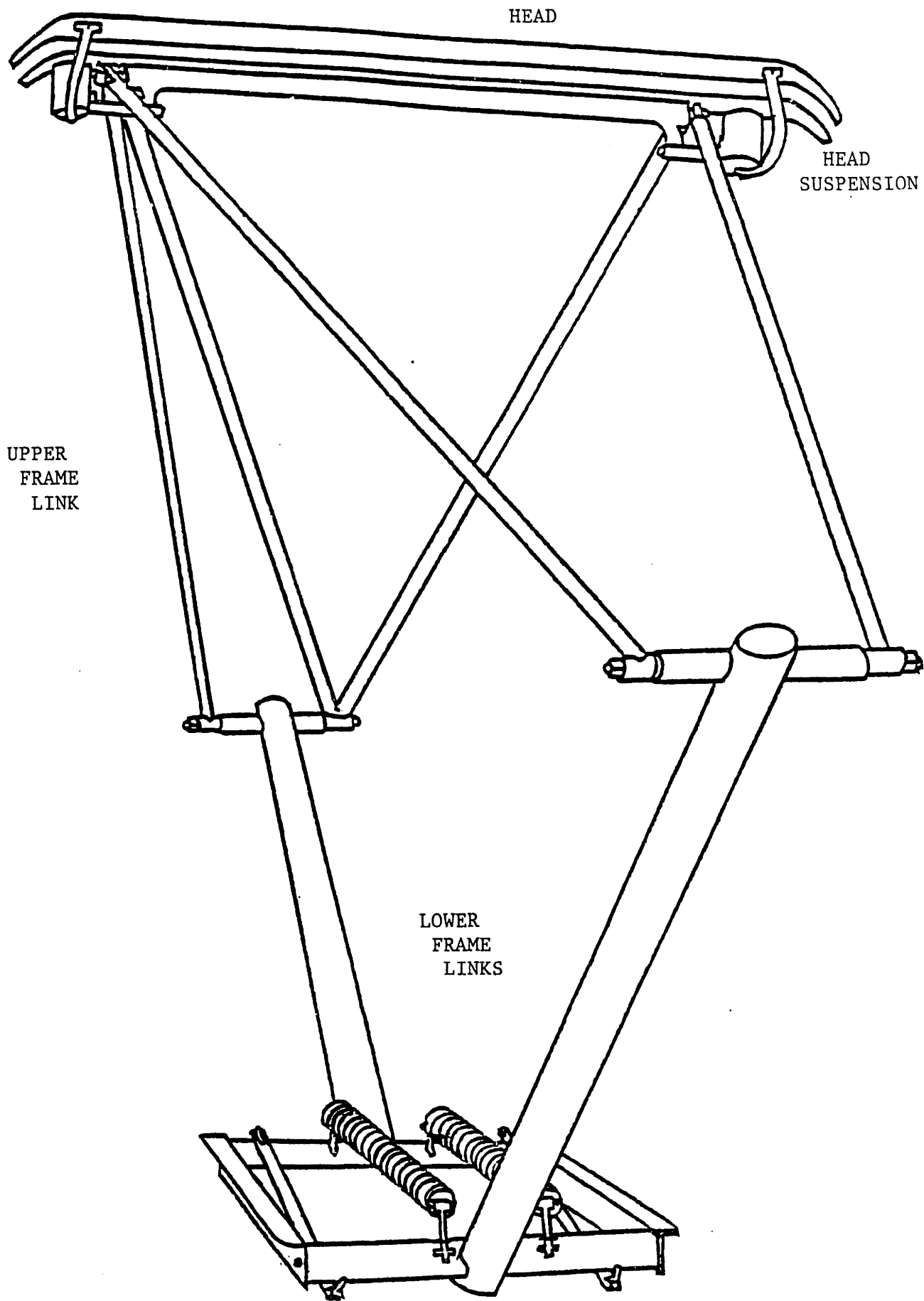
FIGURE 2.2:   TYPICAL SYMMETRIC PANTOGRAPH

HEAD

FRAME
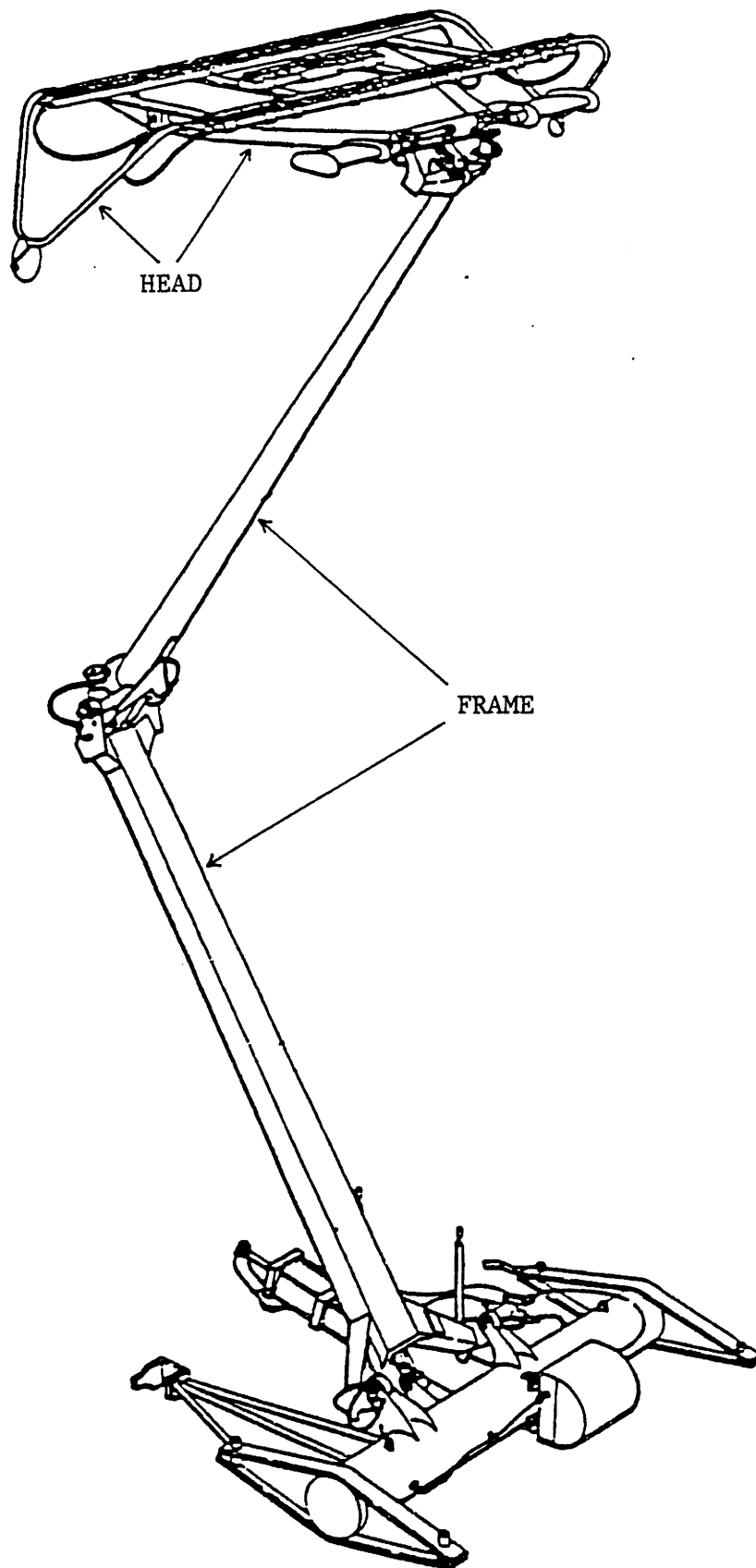
FIGURE 2.3: TYPICAL HIGH SPEED PANTOGRAPH

sentation as long as displacements are under 20 cm and the head non-linearities are not too severe. These nonlinearities include Coulomb friction and limited operating range of the head. The pantograph motion in the simulations presented in Chapter 3 never exceed 10 cm. In most high performance pantograph designs, Coulomb friction is minimized [9]. The range of head motion is often limited in some pantograph designs; so mechanical stops must be included in the model. They are easily incorporated into the two-mass model and will be used here. The simulation's two-mass pantograph model has the following features.

- The motion of the pantograph is modeled with two masses. The first represents the pantograph head and the second the pantograph frame.

- The stiffness of the contact strips and pantograph shoe are modeled by a linear spring, K_s.

- The stiffness between the head and the frame is modeled by a linear spring, K_H.

- Mechanical stops are included to limit the motion between head and frame.

- The uplift force is modeled by a constant force, F_o.

- Two types of damping elements between the head and the frame are modeled: linear and one-way damping.

- There are two suspension choices: the first is a linear spring, linear damper, and a one-way damper in parallel (Figure 2.4). The second is a linear spring and damper in series (Figure 2.5).

- The model contains a full-state feedback, frame-actuated, active controller.
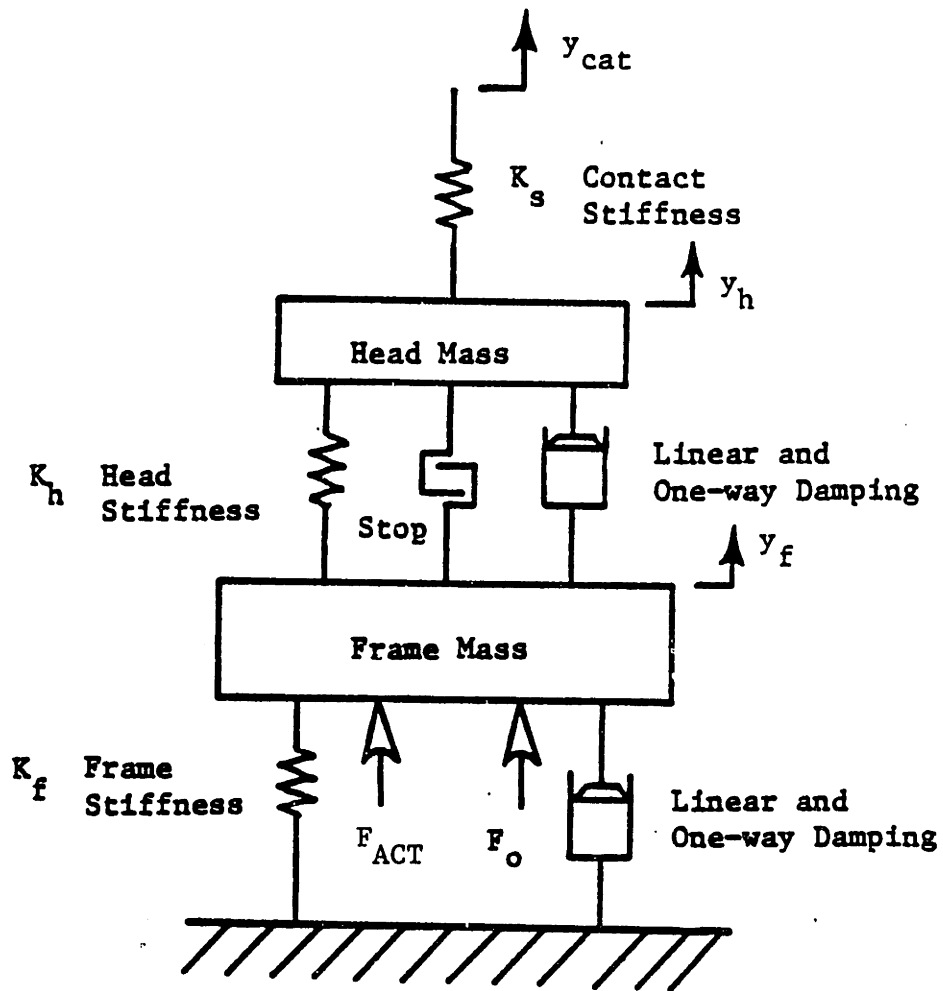
FIGURE 2.4: PANTOGRAPH MODEL, FIRST SUSPENSION OPTION
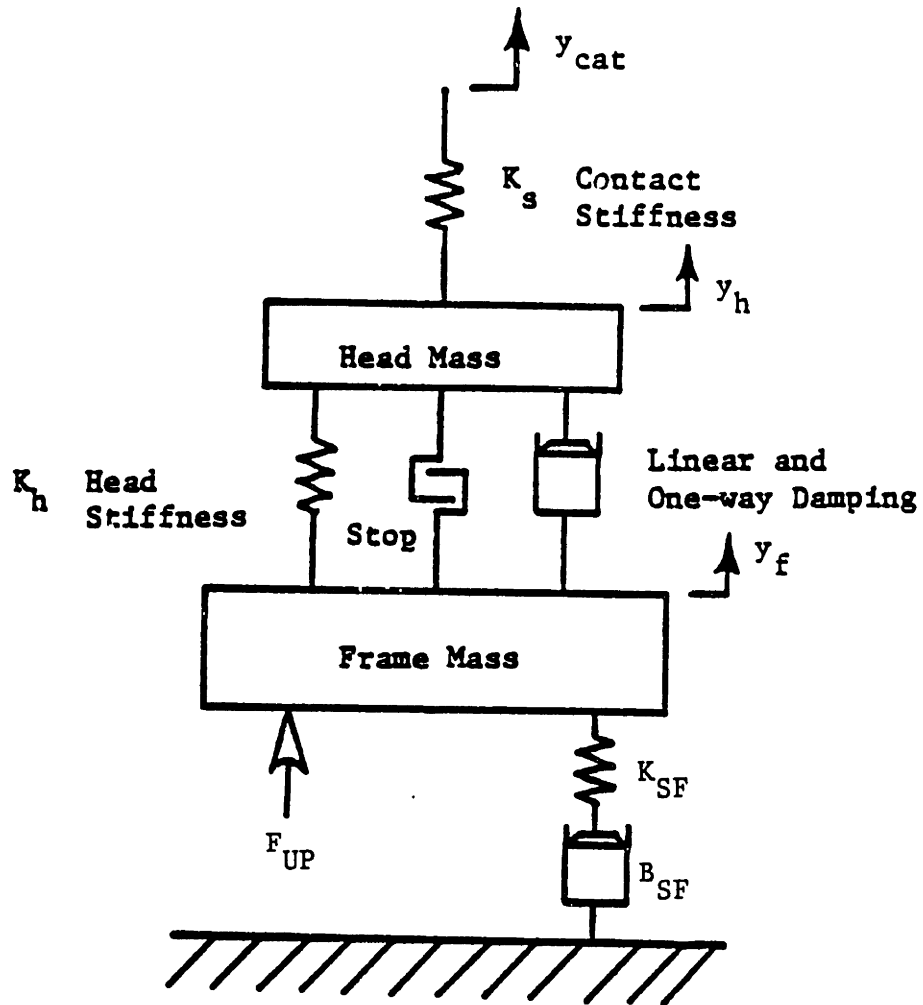
FIGURE 2.5: PANTOGRAPH MODEL, SUSPENSION OPTION TWO

The two models are coupled through the spring that represents the stiffness of the carbons on flexure of the head, k_s (Figure 2.6). The pantograph's uplift force presses it against the catenary compressing k_s. The force through the compressed spring is the contact force. Since the head is not attached to the catenary, k_s can be compressed but never tensioned. If at any point in the simulation the spring becomes tensioned, the contact force is set to zero. A tensioned spring represents a loss of contact. The dynamics of the two systems are considered separately until the pantograph head and catenary move close enough together to compress k_s, thus re-establishing contact.

2.2 Pantograph-Catenary Equation Development

The equations governing the response of the catenary are obtained in three basic steps. First, the displacement of the contact wire and messenger wire are expressed as Fourier sine series expansions. Second, the kinetic energy of the wires and the potential energy of the wires, dropper, and towers are expressed in terms of these series expansions. Lagrange's equation is then used to obtain the homogeneous, undamped equations of motion. From these equations, the natural mode shapes are found. Third, with knowledge of the natural frequencies and displacement amplitudes, modal analysis techniques can be used to find the response of each catenary mode to a forcing function. The response of the individual modes can be summed to obtain the total response. A brief description of this method follows here and is developed in greater detail in Appendix A.

K_s

Direction
of Travel
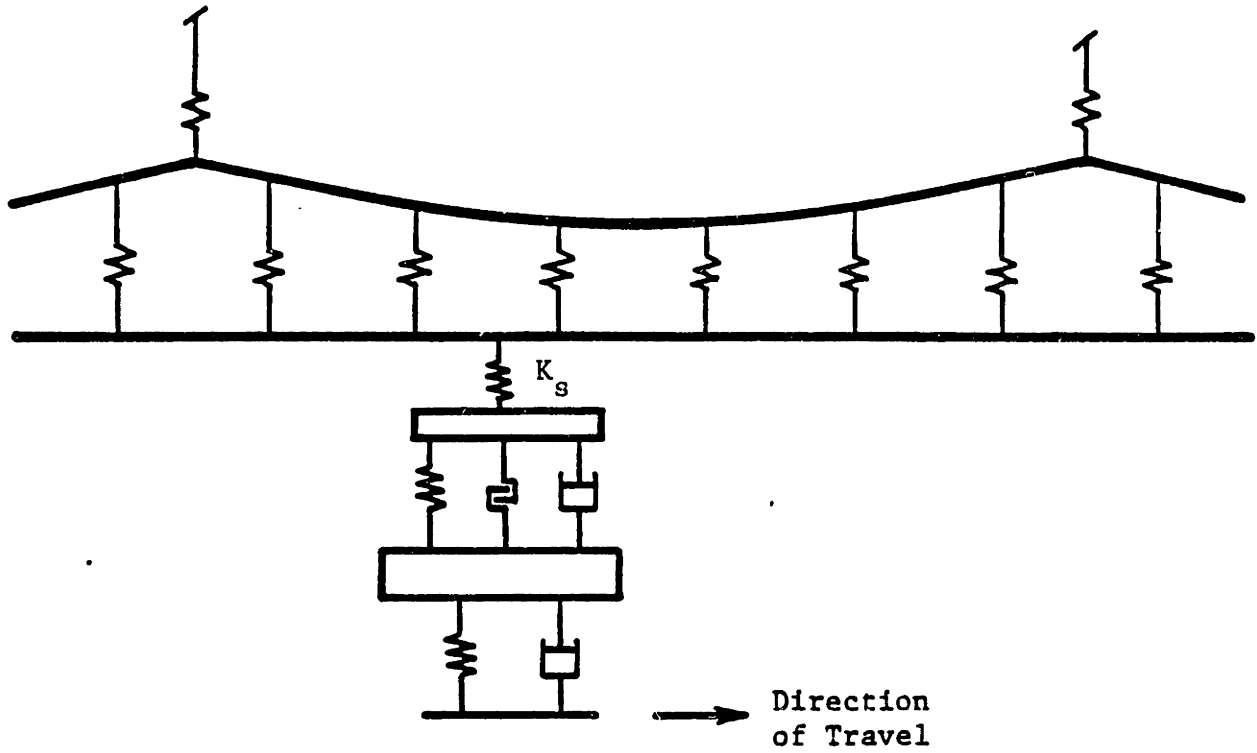
FIGURE 2.6: COUPLING OF THE PANTOGRAPH AND CATENARY MODELS

The displacement shapes of the contact wire and messenger wire from equilibrium are each expressed as Fourier sine-series expansions. A result from Fourier analysis states that any shape with fixed ends can be mathematically described by a superposition of an infinite set of sine functions if their amplitudes are correctly chosen. A good approximation of the shape is possible if enough terms are used. Approximating the shape with a finite series reduces the problem from one with an infinite number of degrees of freedom to one with a finite number of degrees of freedom. The series expansions are given below:

$$y_A(x,t) = \Sigma A_m(t) \sin(\frac{m\pi x}{L}) \quad \text{(messenger wire)}$$

$$(2.1)$$

$$y_B(x,t) = \Sigma B_m(t) \sin(\frac{m\pi x}{L}) \quad \text{(contact wire)}$$

where:

    y = the wire displacement

    A_m = the amplitude of the mth sine term for the messenger wire

    B_m = the amplitude of the mth sine term for the contact wire

    x = the displacement along the catenary

    L = the total length of the catenary

    m = an integer, designates the harmonic number.

The kinetic energy of the wires and the potential energy of the catenary due to tension, bending, dropper stiffness, and tower stiffness are then expressed in terms of these series expansions. Using Lagrange's method, these energy terms are transformed into the unforced homogeneous

equations of motion for the catenary. Since the shape of the wire is expressed as a function of amplitude terms and the time variation of the wire is a function of the amplitude terms' time variation only; it is felt that they are a good choice of generalized coordinates and will be used here. Because this part of the analysis is only concerned with finding natural frequencies and the mode shape amplitudes, forcing functions and damping terms have been neglected. Therefore, the equations of motion will contain only displacement and acceleration terms (A, $\ddot{A}$, B, and $\ddot{B}$). The equation are arranged with the second derivative terms on the left and the amplitude terms on the right.

The catenary equations of motion are linear, so they will always vibrate in some combination of the natural modes of the catenary. Then, when the system is excited, the catenary's response must be harmonic so the acceleration terms can be written as:

$$\ddot{A}_m = -\omega^2 A_m$$

$$\ddot{B}_m = -\omega^2 B_m$$

(2.2)

where:

ω = the natural frequency of vibration

To find the natural frequencies and mode shape amplitudes, the acceleration terms are replaced with Equation (2.2). The substitution leaves the equations as a function of amplitude terms and the frequency of vibration.

For convenience, the catenary equations are arranged in matrix-vector form. The amplitudes of the messenger wire, A_m, and the amplitudes of the contact wire, B_m, are written as a single vector, Γ.

$$\omega^2\, I\Gamma = H\Gamma \qquad (2.3)$$

where:

$\dot{\omega}$ = the frequency of vibration

I = the identity matrix

Γ = vector of amplitude terms

H = the dynamic matrix

With the equations of motion in this form, the natural frequencies and mode shape amplitudes are easily found. The eigenvalue of the H matrix are the squares of the natural frequencies and the eigenvectors contain the mode shape amplitudes. Each natural mode shape is determined by using Equation (2.1) and inserting the amplitude terms from each eigenvector.

The natural modes of the catenary are orthogonal and can be considered separately. A result from modal analysis technique gives the equation for each mode as:

$$M_i\ddot{z}_i + 2\xi_i\omega_i M_i\dot{z}_i + \omega_i^2 M_i Z_i = Q_i \qquad (2.4)$$

where:

$z_i(t)$ = the ith model response

m_i = the ith modal mass

ξ_i = the damping ratio

ω_i = the ith natural frequency

Q_i = the ith modal forcing function

The influence of the pantograph and the gravitational forces which cause sag on the catenary equations of motion are represented in the modal forcing function:

$$Q_i = \int_o^\ell f(x,t)\phi_i(x)dx \qquad (2.5)$$

where:

$f(x,t)$ = the applied force distribution

ϕ_i = the ith natural mode shape

The above equation must be evaluated for each mode. It can accomodate more than one pantograph.

The catenary's dynamic response can be found by superimposing the individual modal responses using the following result from modal analysis:

$$y(x,t) = \Sigma z_i(t)\phi_i(t) \qquad (2.6)$$

where:

z_i = the ith modal response function

ϕ_i = the ith natural mode shape.

The modal catenary equations of motion and the pantograph equations are solved simultaneously on a digital computer using a 4th-order Runge-Kutta routine.

2.3 Pantograph Frequency Response Model

A frequency domain model has been developed to study the response of the pantograph to different catenary inputs. The pantograph model used is the same two-mass model described on page 29 and shown in Figure 2.2 and 2.3. However, since frequency response methods are for linear systems only, the head stops and one-way dampers have been removed. All other features of the model are the same.

To find the frequency response, the equations of motion for the pantograph are written in state space form. The displacements and velocities of the pantograph head and frame masses are used as state variables. The catenary height is the input.

$$\dot{x} = Ax + By_{cat} \qquad\qquad (2.7)$$

where:

 x = the state variable vector

 A = the system matrix

 B = the input vector

 y_{cat} = the catenary height

Taking the Laplace transform of equation 2.7 and putting the state variables on the same side of the equation yields:

$$[SI - A]x = By_{cat} \qquad\qquad (2.8)$$

For a purely sinusoidal response. the Laplace operator can be replaced by $j\omega$, where ω is the frequency of the input and j indicates an

imaginary number. Making the substitution for S and solving for the state variable vector results in:

$$\underline{x} = [j\omega I - A]^{-1} By_{cat} \qquad (2.9)$$

With the use of a digital computer, ω is varied over the range of interest. For each value of ω, the matrix inversion in equation 2.9 is made using the Gaussian elimination technique. The result is multiplied by the B matrix to find the response of each state variable to the input for the frequency in question. The program will produce magnitude and phase plots of any of the state variables. By using the head response y_H/y_{cat} and Equation (2.10) the contact force response can also be plotted.

$$\frac{F_{contact}}{y_{cat}} = k_s \left(\frac{y_H}{y_{cat}} - 1 \right) , \qquad (2.10)$$

CHAPTER 3
RESULTS

The time simulation and frequency response programs discussed in Chapter 2, have been used for several different investigations: evaluating the effect of sag on performance, determining if an all aluminum catenary has acceptable dynamics, investigating the effects of pantograph parameters on performance, determining what pantograph parameters yield the best passive pantograph, evaluating actively controlled pantographs, comparing the best passive and active configurations with an existing high speed pantograph, studying the interaction between two pantographs under the same catenary, and determining critical speed.

The baseline pantograph was chosen so its parameters are typical of a well-designed, high-speed pantograph. All simulations were done under the baseline catenary. This catenary is similar to those used on the British Rail and ISCOR systems [27]. The parameters for the baseline pantograph and catenary are summarized in Tables 3.1 and 3.2. Simulation results for the baseline system are presented in the following section.

3.1 Baseline Performance

The time response for the baseline pantograph and catenary is presented in this section. A three span catenary is used. The velocity of the train is 170 km/hr. Figures 3.1 through 3.6 show the time history of the contact wire shape plotted at 0.1 second intervals. Each plot contains only five shapes for clarity, and the six figures span a total of 3 seconds. The position of the pantograph at each response time is indicated by the

TABLE 3.1

BASELINE PANTOGRAPH PARAMETERS

Head Mass:	9.1 kg	20 lbm
Frame Mass:	17.2 kg	38 lbm
Stiffness of the Pantograph Shoe:	82.3 kN/m	470 lb/in
Stiffness Between the Head and Frame:	7.0 kN/m	40 lb/in
Stiffness Between the Frame and Base:	0.0 kN/m	0.0 lb/in
Damping Between the Head and Frame:	130 Ns/m	.743 lb sec/in
Damping Between the Frame and Base:	30 Ns/m	.171 lb sec/in
Uplift Force:	90 N	20.2 lb

o   Data represents a Faively Pantograph, See Reference

TABLE 3.2

BASELINE CATENARY PARAMETERS

Material:

    Contact Wire   —   Copper, 4/0 Hard Drawn

    Messenger Wire   —   Aluminum/Steel re-inforced

    Droppers   —   Stainless Steel

Length:	196.6 m	645 ft
Tower Spacing:	3 Spans	
	65.5 m	215 ft
Dropper Spacing:	6 per Span	
	10.92 m	35.8 ft
Tower Stiffness:	12.51×10^6 N/m	$71.43 \times 10^3 \frac{lb}{in}$
Dropper Stiffness:	1.75×10^6 N/m	$1.0 \times 10^4 \frac{lb}{in}$
Tension:		
Upper Wire	9,340 N	2,100 lb
Lower Wire	12,000 N	2,700 lb
Density:		
Upper Wire	0.2722 kg/m	0.183 lb/ft
Lower Wire	0.955 kg/m	0.642 lb/ft
Rigidity:		
Upper Wire	81.53 Nm^2	28,410 $lb\text{-}in^2$
Lower Wire	121.62 Nm^2	42,380 $lb\text{-}in^2$
Catenary Damping Ratio	0.02	
Voltage	25 kV	
Current	600 amp	
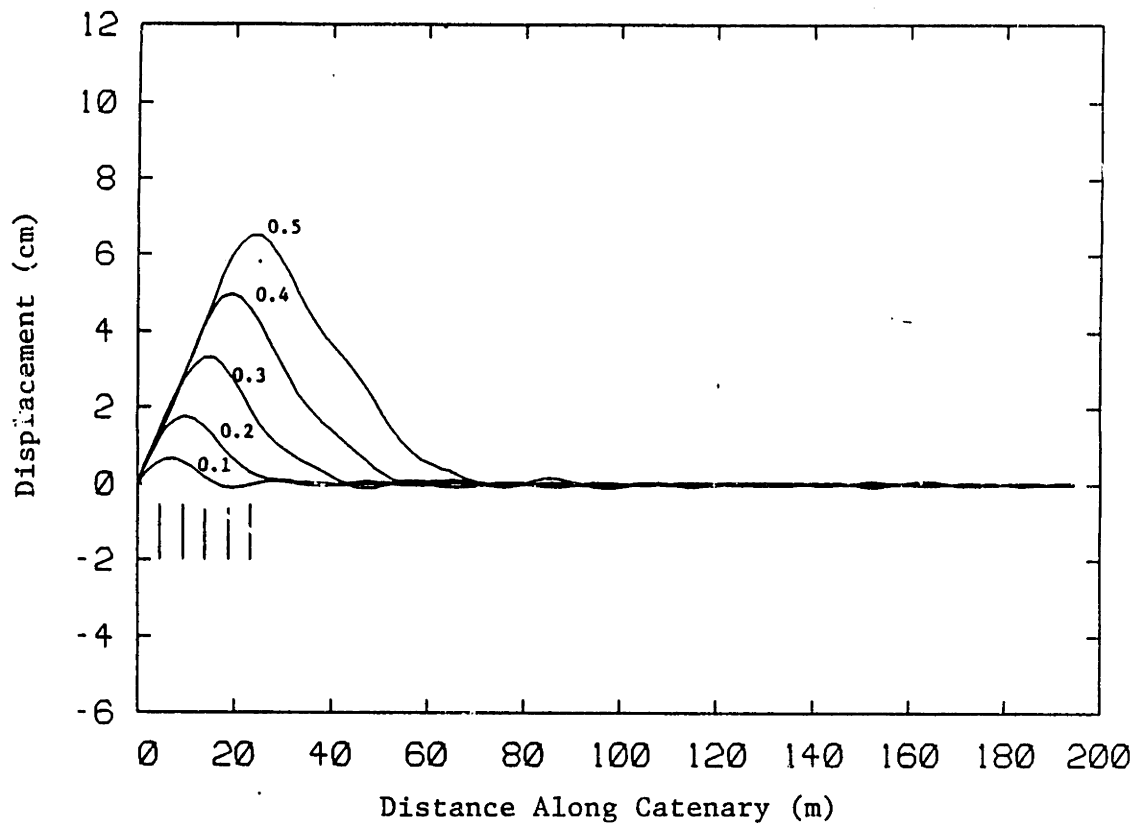
FIGURE 3.1: CATENARY SHAPE BETWEEN 0.1 AND
0.5 SECONDS
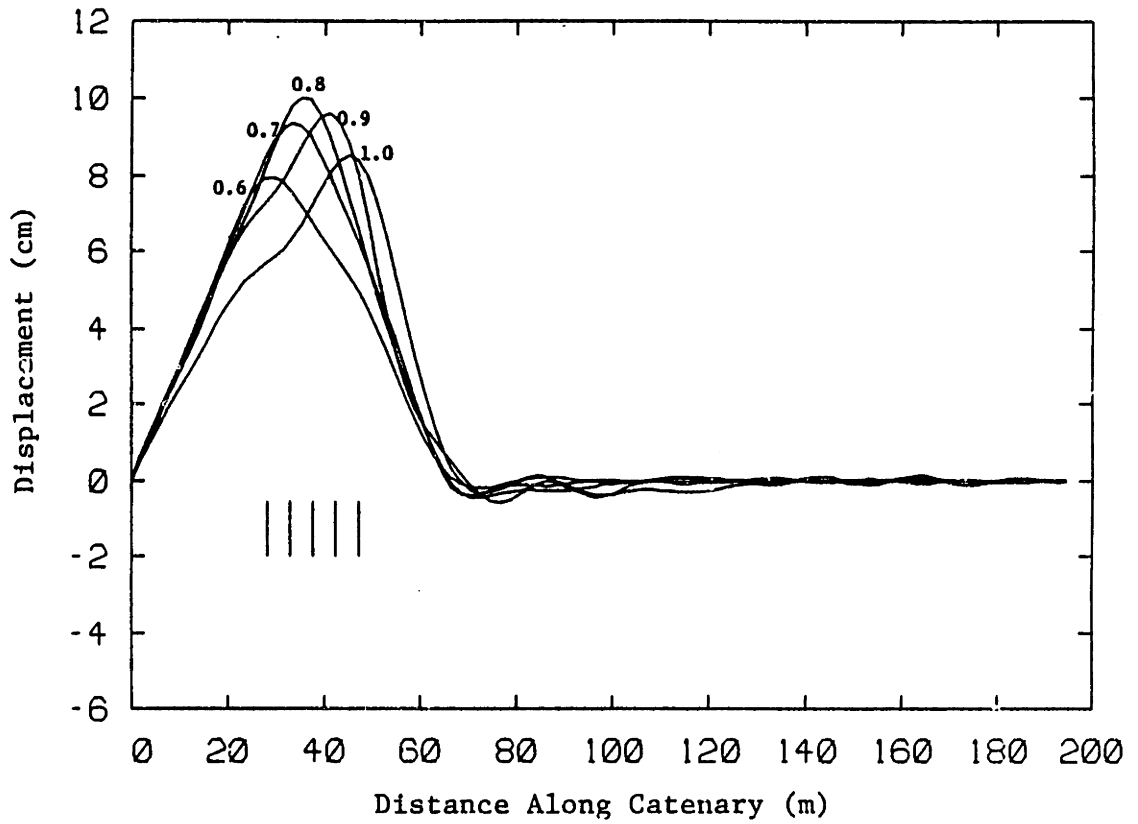
FIGURE 3.2: CATENARY SHAPE BETWEEN 0.6 AND
1.0 SECONDS
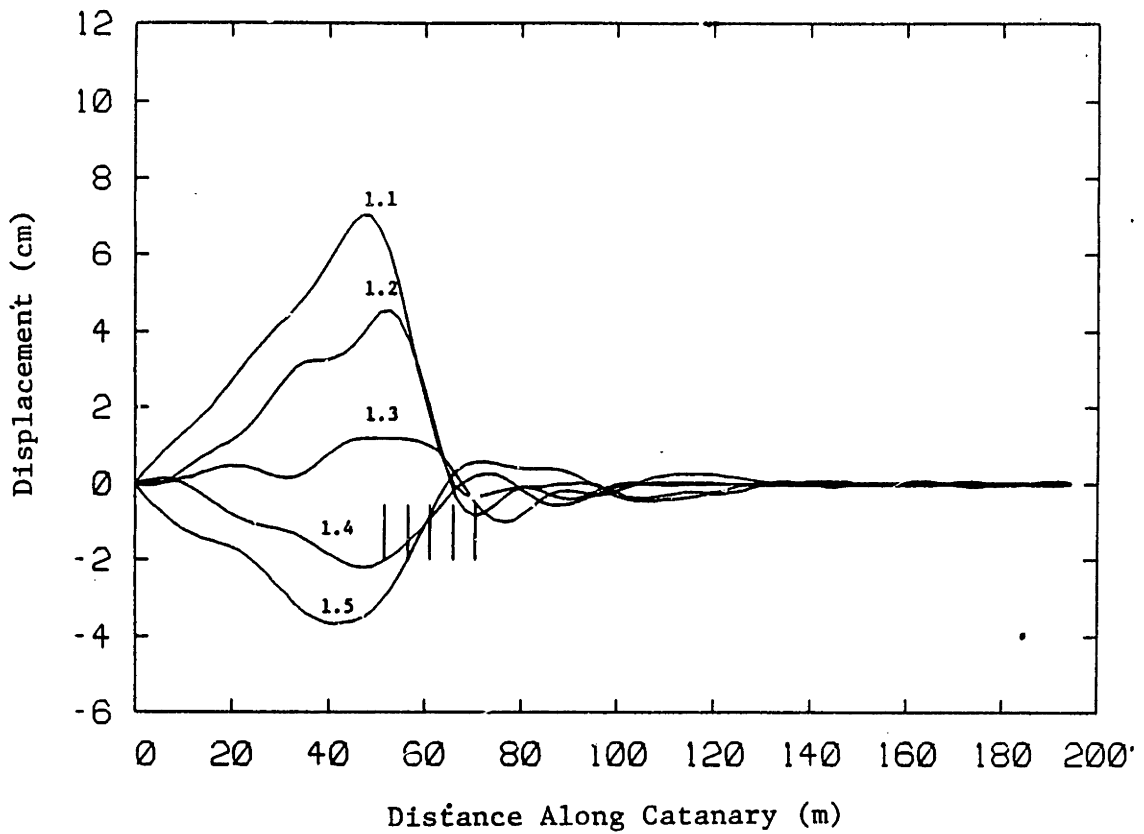
FIGURE 3.3: CATENARY SHAPE BETWEEN 1.1 AND
1.5 SECONDS
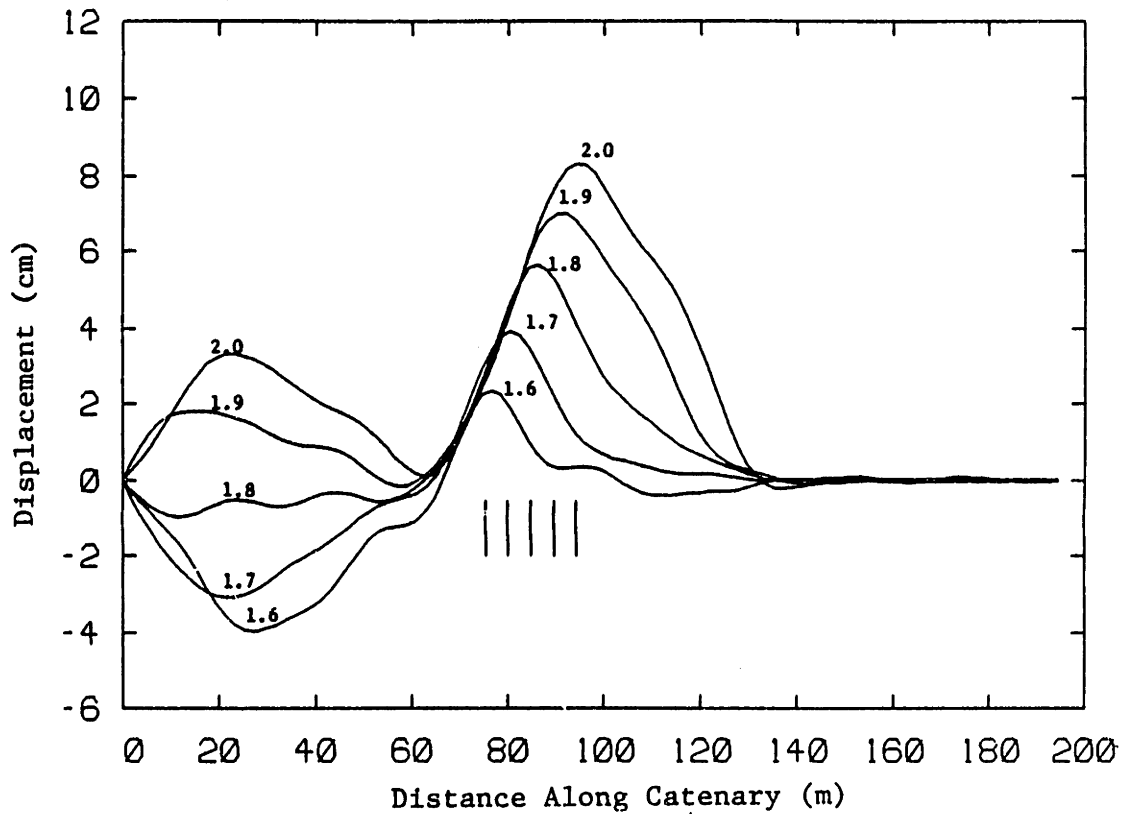
FIGURE 3.4: CATENARY SHAPE BETWEEN 1.1 AND
1.5 SECONDS
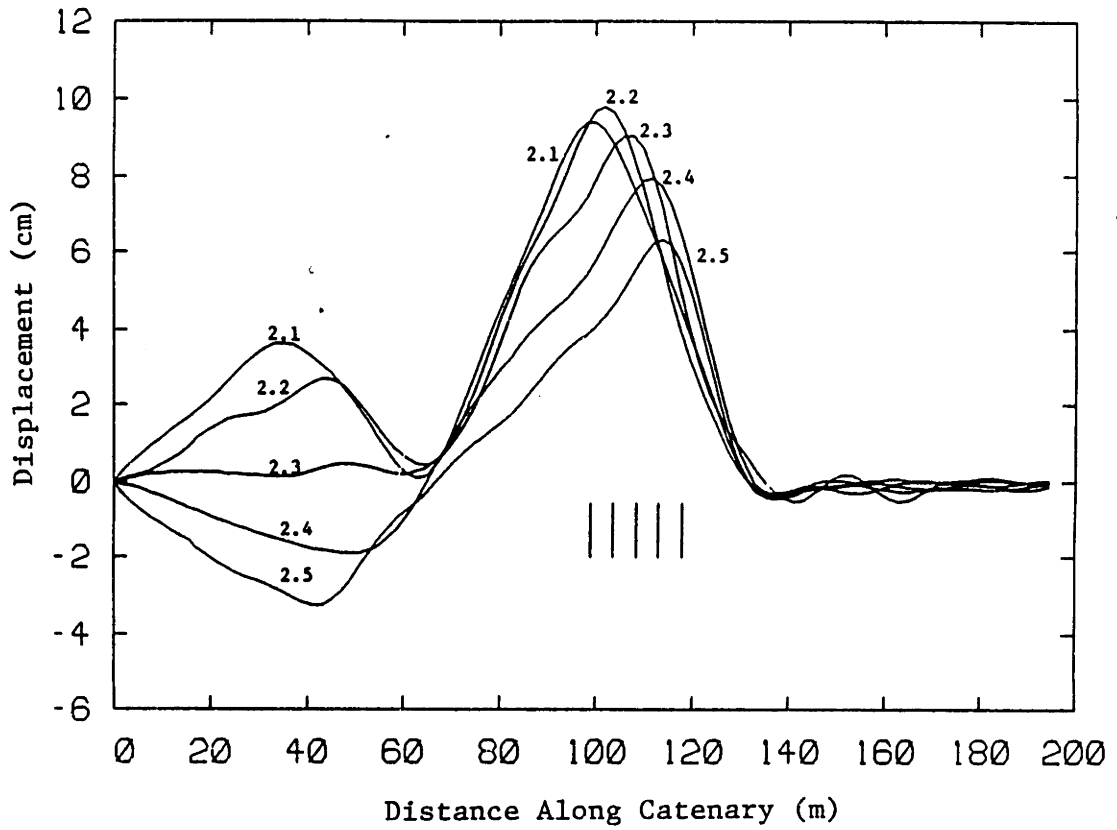
FIGURE 3.5:   CATENARY SHAPE BETWEEN 2.1 AND
2.5 SECONDS
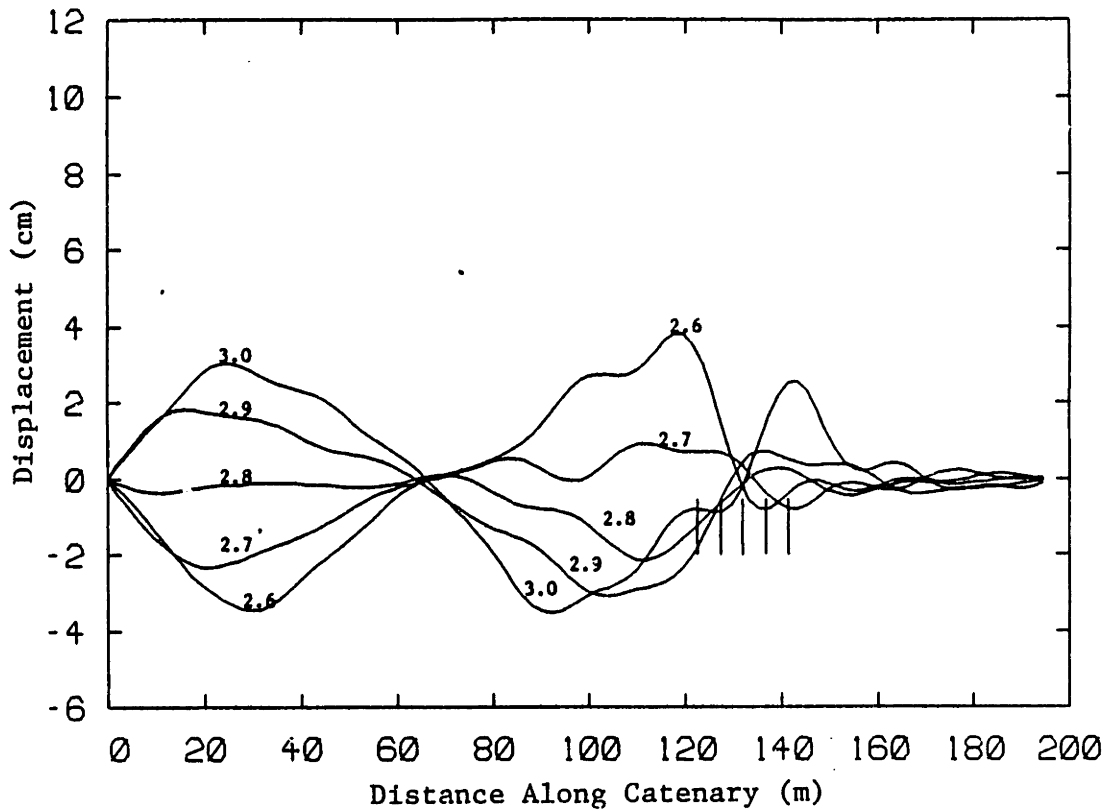
FIGURE 3.6:   CATENARY SHAPE BETWEEN 2.6 AND
3.0 SECONDS

vertical lines.

In the early stages of the simulation (0.0 - 0.8 sec), the contact wire displaces upward as the pantograph moves along the wire. The displacement grows because the catenary's spring rate becomes much smaller as the contact point moves from the towers to midspan. Figure 3.7 shows the catenary's static spring rate over one span. Between 0.8 and 0.9 seconds, the catenary displacement reaches its maximum, and then begins to descend. Because the catenary is much stiffer at the support towers than at midspan, the contact wire's displacement must lessen as the support tower is approached. ·

The pantograph approaches the first tower from 0.9 to 1.3 sec. The wire slope is very steep. Since the wire is constrained to move downward, the pantograph must also move downward; this briefly raises the contact force.

The pantograph passes the first tower at 1.36 sec and the catenary begins to rise again. The contact wire changes shape at the towers from a steep descent to a moderate incline. Downward inertia developed by the pantograph as a tower is approached makes this change difficult to track, especially at higher speeds.

When the pantograph passes through a span, it displaces the catenary which causes the wire to vibrate after the pantograph has passed. Between 1.6 and 2.6 sec the first span makes an excursion from full negative displacement to positive and back to negative (± 4 cm), vibrating in the first natural mode, 1 Hz. The dissipative term in the catenary equations
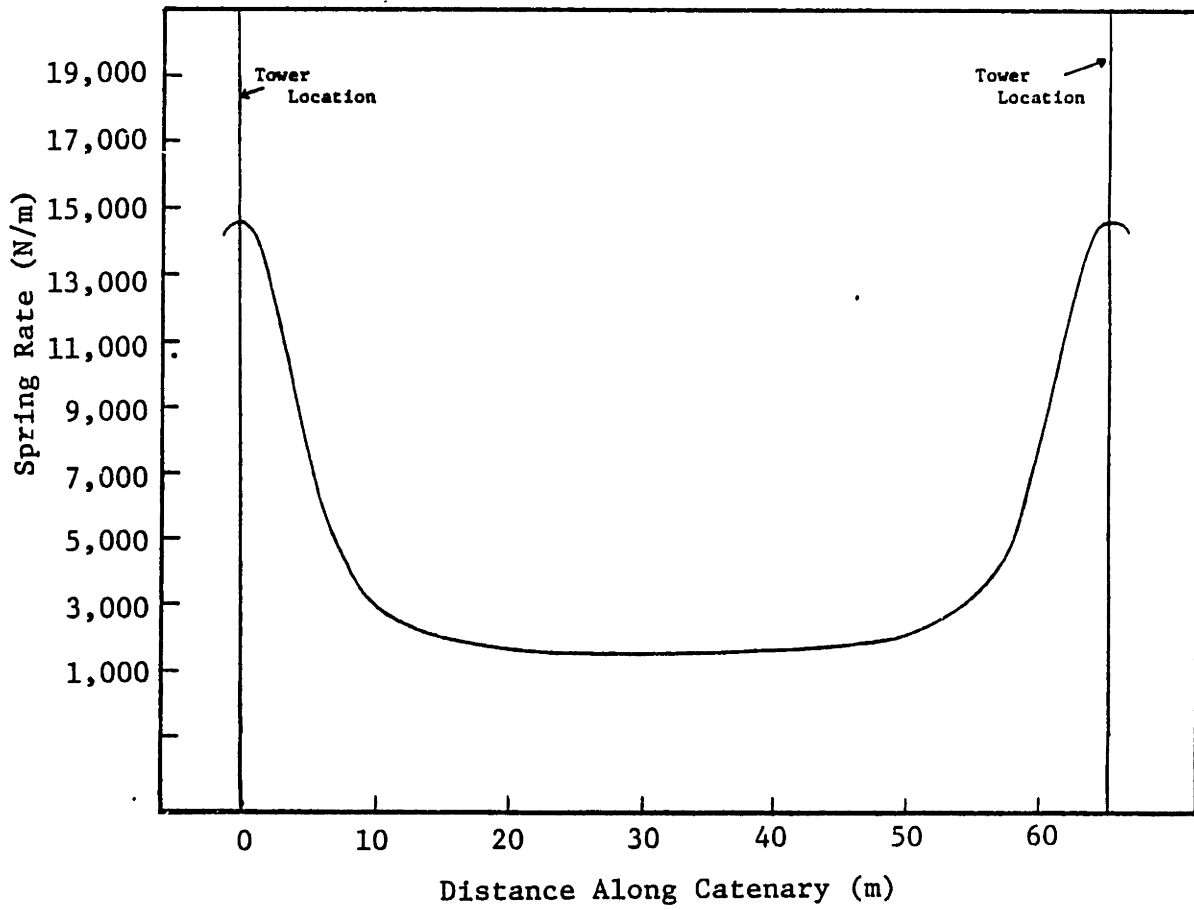
FIGURE 3.7: CATENARY SPRING RATE vs. DISTANCE
FOR ONE SPAN

of motions, $2\xi\,\omega_n\dot{z}$, indicates the lower modes will dissipate less energy over the same time period. This vibration may present problems for trains using multiple pantographs.

The catenary's response in the second span is the same as it is in the first span. After the pantograph passes the first tower, the displacement of the wire increases linearly as the pantograph moves into a "softer" region of the catenary. When the pantograph has passed the second span, the catenary vibrates freely and is dominated by the first mode. The consistent behavior between consecutive spans justifies considering a finite length of catenary.

The displacements of the catenary, pantograph head, and pantograph frame at the instantaneous contact point for the above system are shown in Figure 3.8. The plots are of the displacement from the datum at the contact point versus time. Displacements of the catenary and pantograph increase nearly linearly until a peak is reached, and then decrease rapidly as a support tower is approached. The maximum catenary displacement occurs at 0.79 sec., well past the middle of the span. The peak occurs further from the center of the span as train speed increases and catenary wave speed decreases. This shift, coupled with the constraint imposed by the stiff support towers, causes the wire to descend steeply as a tower is approached. The further the peak displacement occurs past center, the steeper the descent.

The change in catenary shape at the towers, from a steep descent to an incline has a great effect on pantograph performance. At higher
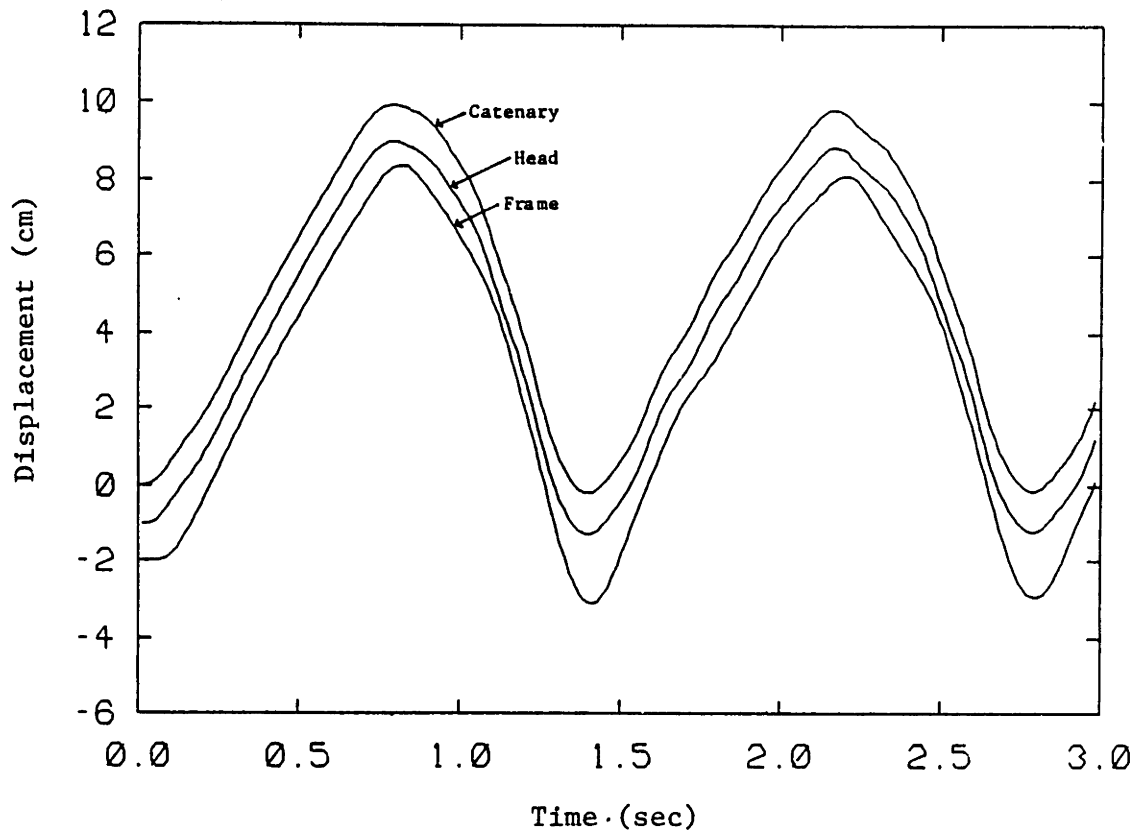
FIGURE 3.8:   DISPLACEMENT OF CATENARY, HEAD, AND FRAME
VS. TIME, BASELINE SYSTEM, 170 km/hr
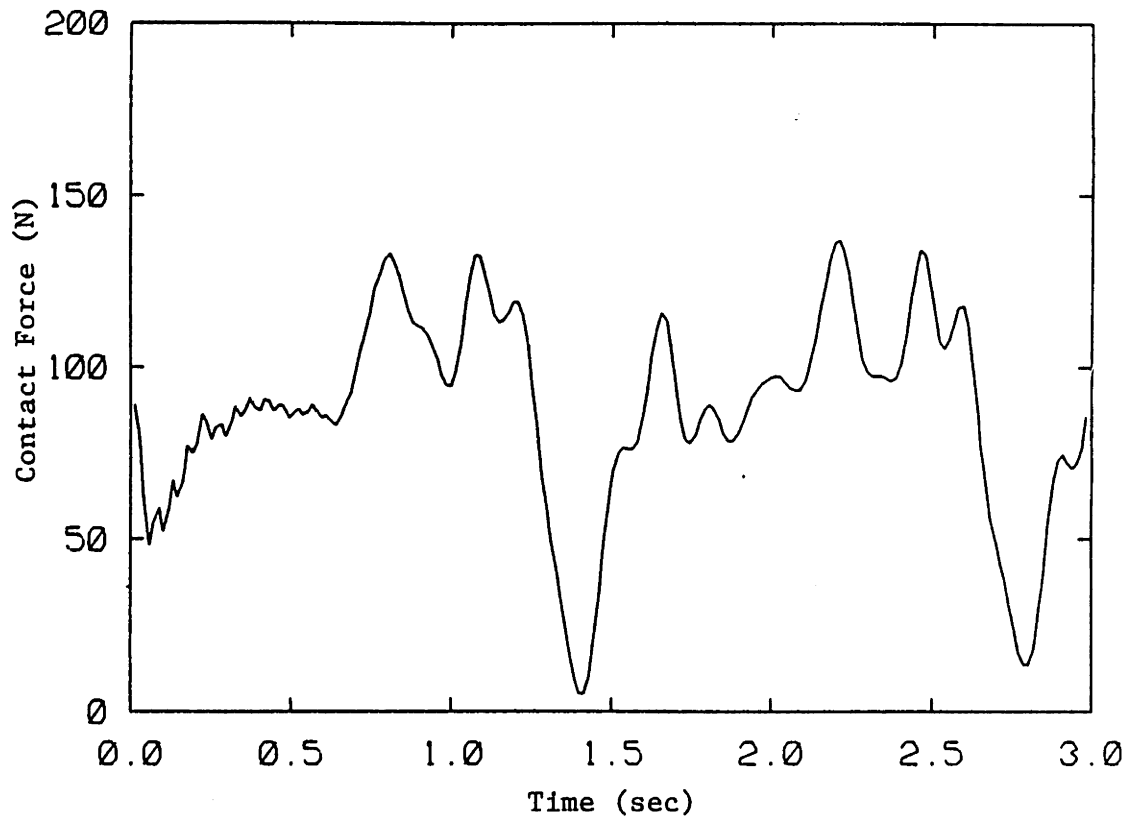
FIGURE 3.9:   CONTACT FORCE, BASELINE SYSTEM, 170 km/hr

speeds, loss of contact often occurs. At 170 kph the pantograph head is able to maintain contact, but the pantograph frame, which is heavier and cannot respond as quickly, undershoots when the pantograph passes a tower. The head suspension is able to accomodate the larger displacement between the head and frame, but the slow response of the frame mass results in a lower contact force.

The contact force versus time plot is shown in Figure 3.9. There are two peaks in contact force in each span. The first is found at 0.79 sec, which corresponds to the change from a rising to a falling catenary on the displacement plot. The second peak at 1.07 sec. occurs during the steepest part of the catenary's descent, where the pantograph inertia resists the downward motion imposed by the catenary. A minimum in contact force appears just after the pantograph passes a tower. The momentum developed by the pantograph during the tower approach keeps the frame moving downward even though the head has begun displacing the catenary upward. This pattern is repeated in the next span.

The baseline system was run at several other speeds. The contact force and displacement plots for 135 km/hr are found in Figures 3.10 and 3.11, and for 150 km/hr in Figures 3.12 and 3.13. For each train speed, Table 3.3 shows the time when maximum catenary displacement is reached, the corresponding distance from the last tower passed, the value of maximum displacement, and the contact force variation.
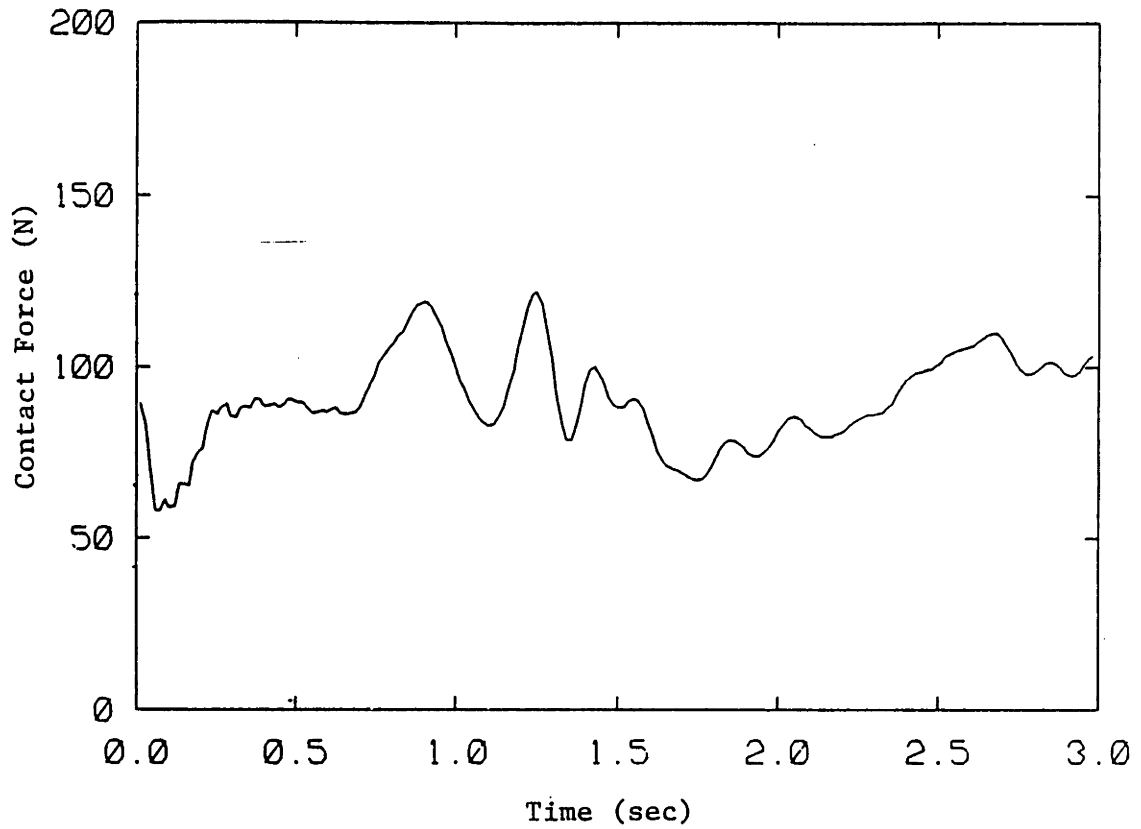
FIGURE 3.10:   CONTACT FORCE VS. TIME,
               BASELINE SYSTEM, 135 km/hr
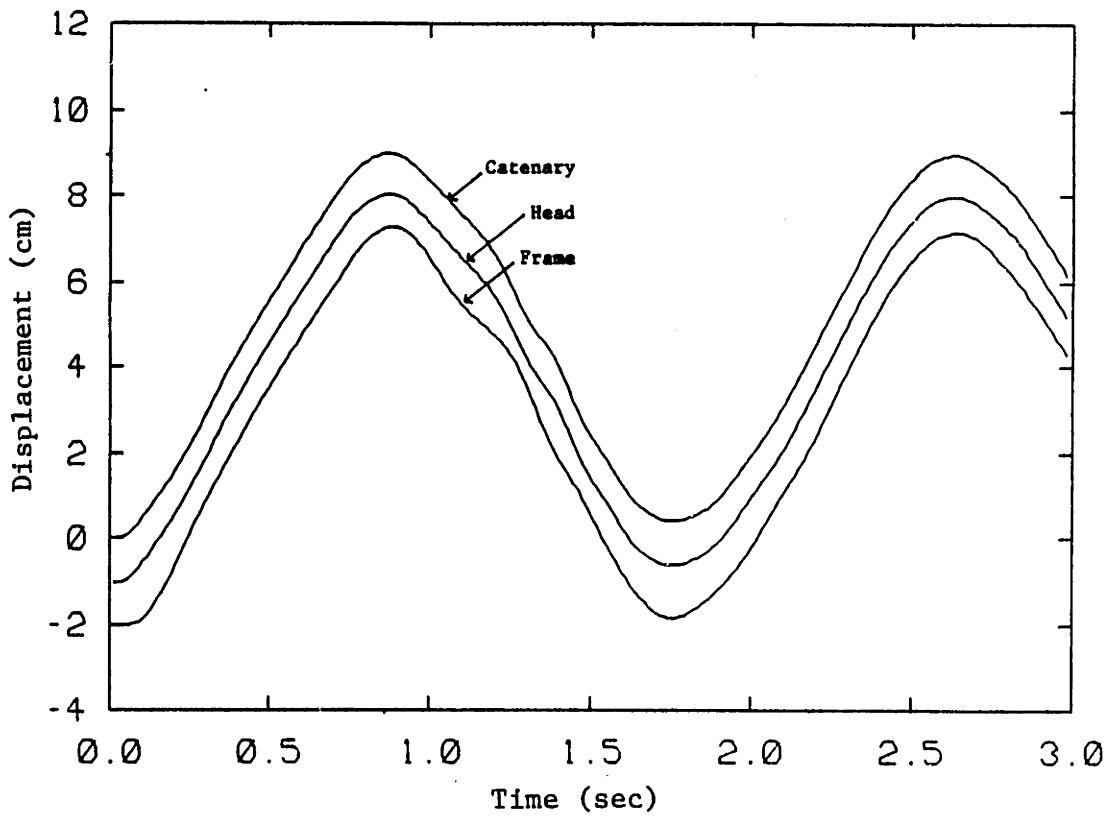
FIGURE 3.11:   DISPLACEMENT OF CATENÁRY, HEAD,
               AND FRAME vs. TIME, BASELINE
               SYSTEM, 135 km/hr
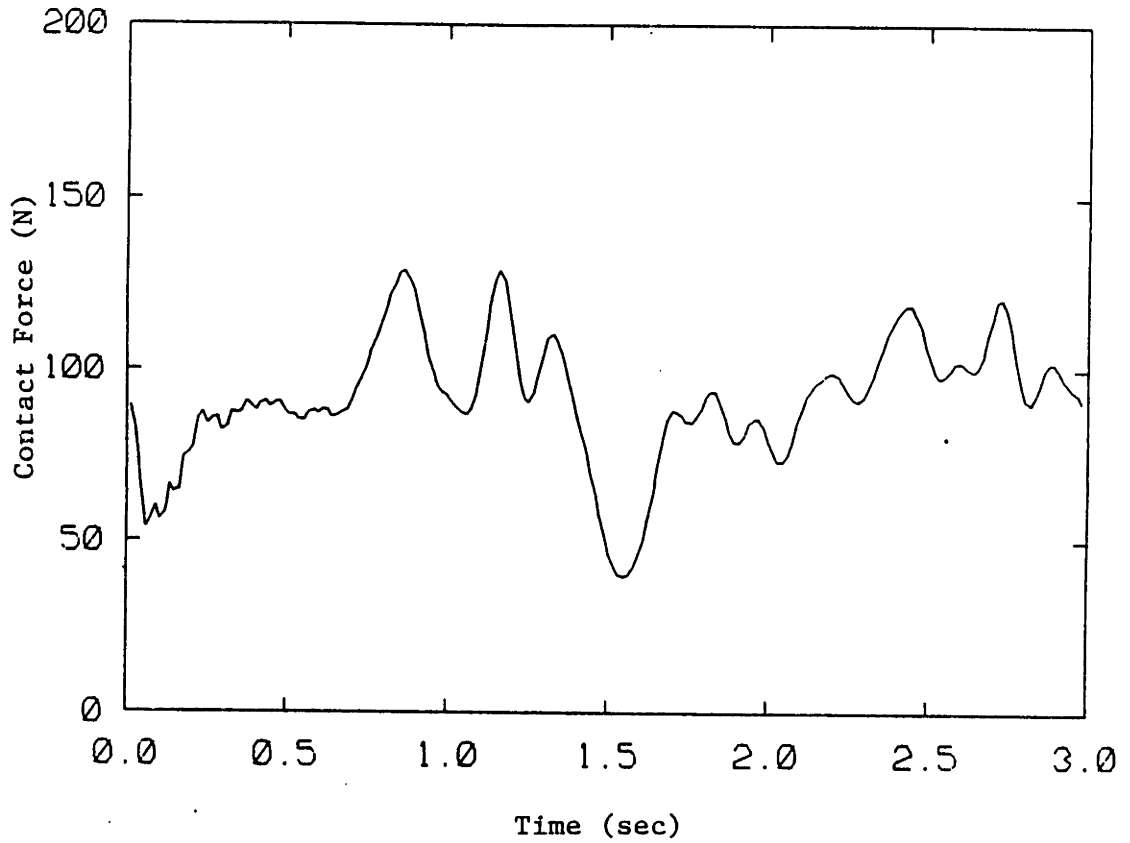
FIGURE 3.12:   CONTACT FORCE VS. TIME, BASELINE
SYSTEM, 150 km/hr
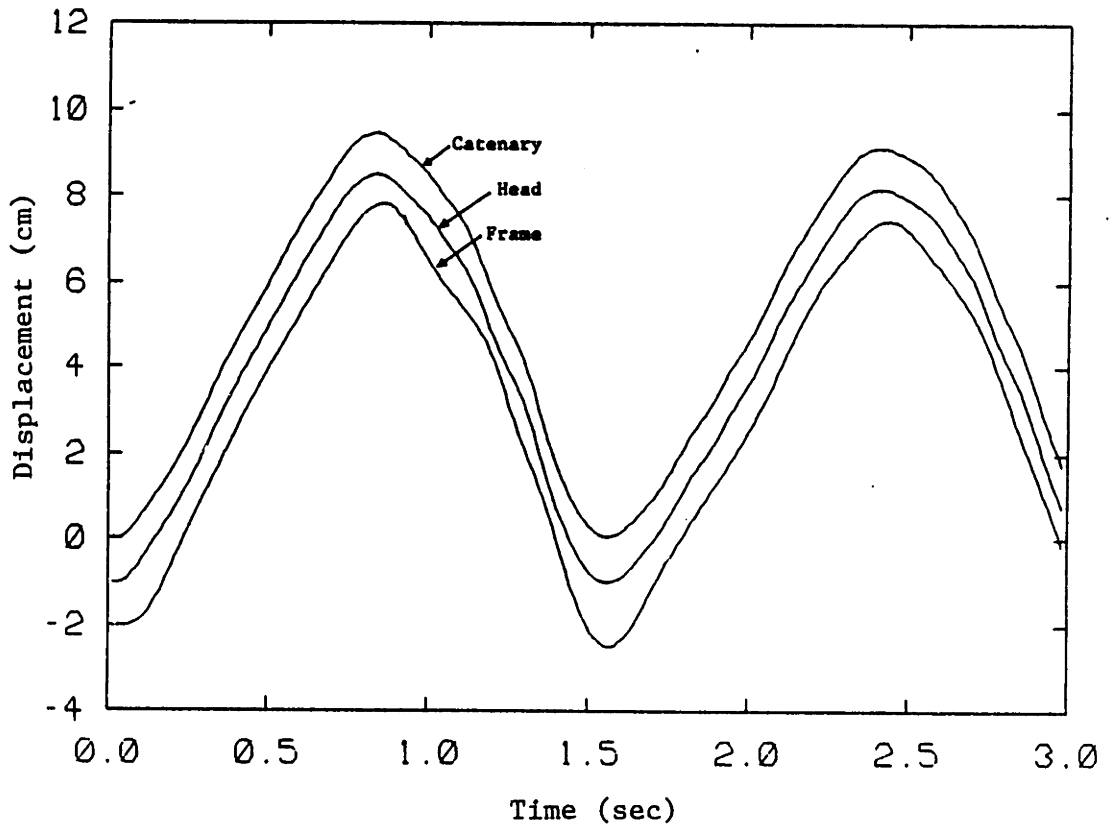
FIGURE 3.13:   DISPLACEMENT OF CATENARY, HEAD,
AND FRAME vs. TIME, BASELINE
SYSTEM, 150 km/hr

TABLE 3.3

CATENARY DISPLACEMENT CHARACTERISTIC vs. VELOCITY

Speed	Time of Maximum Displacement	Location of Maximum Displacement	Maximum Displacement	Contact Force Variation
135 km/hr	0.864 sec	32.4 m	9.0 cm	54.7 N
150 km/hr	0.839 sec	35.0 m	9.4 cm	87.5 N
170 km/hr	0.788 sec	37.2 m	10 cm	130 N

As train velocity increases, the maximum catenary displacement occurs closer to the tower and is larger in magnitude. The shift in maximum displacement is caused by the train traveling closer to the wave speed. Until the disturbance caused by the pantograph reaches the tower, the catenary cannot react to the towers' increased stiffness and decrease its displacement. Since the catenary reacts to the tower later, it has more time to displace upward, which is why maximum displacement increases with speed.

Contact force variation also increases with speed. Higher peak forces occur as speed increases because the pantograph is forced down a larger distance over a shorter period of time. Since the pantograph moves down with increased velocity, it develops greater downward momentum that causes larger drops in contact force. At 175 km/hr this downward momentum causes the pantograph to lose contact with the catenary. The amount of time the pantograph is separated from the catenary increases as the train velocity increases beyond this speed.

3.2 Aluminum Catenary Performance

Because of the high cost of copper, there recently has been an increased

interest in all-aluminum catenaries. In this section, the typical response of an aluminum catenary is studied and compared to the baseline system. The contact wire parameters of the aluminum system were chosen so that it could carry the same voltage and current as the baseline catenary. Dropper spacing, tower spacing and wire tensions were chosen to ensure structural integrity, not to exceed material limitations, and to minimize cost [27]. The aluminum catenary parameters are given in Table 3.4. As with the baseline typical response, the simulation was made at 170 km/hr with the same pantograph.

The time history of the aluminum catenary shape is shown in Figures 3.14 through 3.19. The lower wire displaces linearly at first (0.0 - 0.6 sec), and peaks between 0.6 and 0.7 sec. As the pantograph approaches the first tower (0.7 to 1.4 sec) the catenary's displacement declines. This pattern is repeated in the second span.

The instantaneous displacements at the point of contact of the catenary, pantograph head, and pantograph frame are shown in Figure 3.20. The maximum displacement occurs at t = 0.73 sec, closer to midspan. The contact force versus time plot is shown in Figure 3.21. Peak forces occur as a tower is approached and minimum forces occur at tower locations, just like the baseline response. While minimums and maximums in contact force occur in roughly the same locations, they are of lesser magnitude. The contact force variation is 63 N, 51% less than the copper case.

The descent of the aluminum catenary is not as steep when a tower is approached. Since its' wave speed is higher than the baselines, the effect

TABLE 3.4

ALUMINUM CATENARY PARAMETERS

Materials:

Contact Wire	-	Aluminum, 6201-T81
Messenger Wire	-	Aluminum, Steel Re-inforced
Droppers	-	Aluminum

Length: 194.77 m   639 ft.

Tower Spacing: 3 Spans
64.92 m   213 ft.

Dropper Spacing: 4 per Span
16.23   53.3 ft.

Tower Stiffness: 12.51×10^6 N/m $71.43 \times 10^3 \frac{lb}{in}$

Dropper Stiffness: 1.75×10^6 N/m $1.0 \times 10^4 \frac{lb}{in}$

Tension:

Upper Wire	8,000 N	1,800 lb
Lower Wire	16,400 N	3,700 lb

Density:

Upper Wire	0.216 kg/m	0.145 lb/ft
Lower Wire	0.537 kg/m	0.361 lb/ft

Rigidity:

Upper Wire	51.31 Nm^2	17.88×10^3 lb-in^2
Lower Wire	214.93 Nm^2	74.9×10^3 lb-in^2

Wave Speed: 180.2 m/s

Catenary Damping Ratio

Voltage	25 kV
Current	600 amps
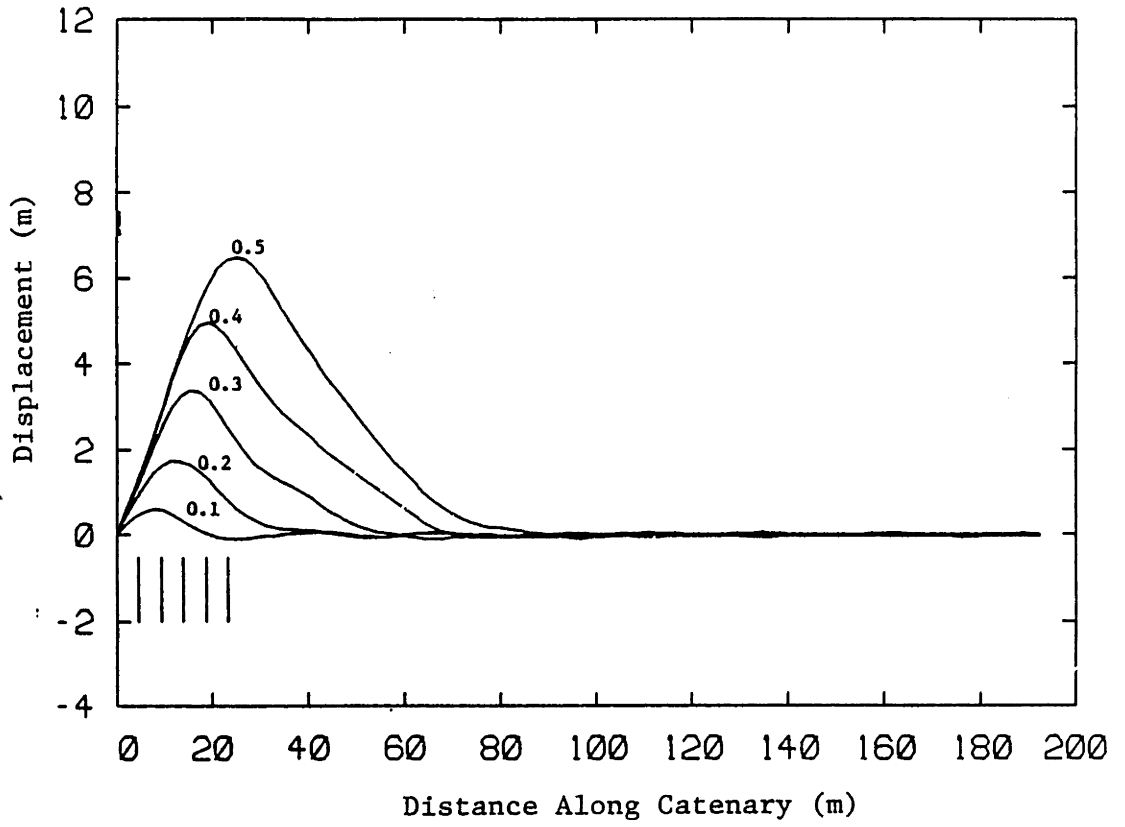
FIGURE 3.14: ALUMINUM CATENARY SHAPE BETWEEN 0.1
AND 0.5 SECONDS
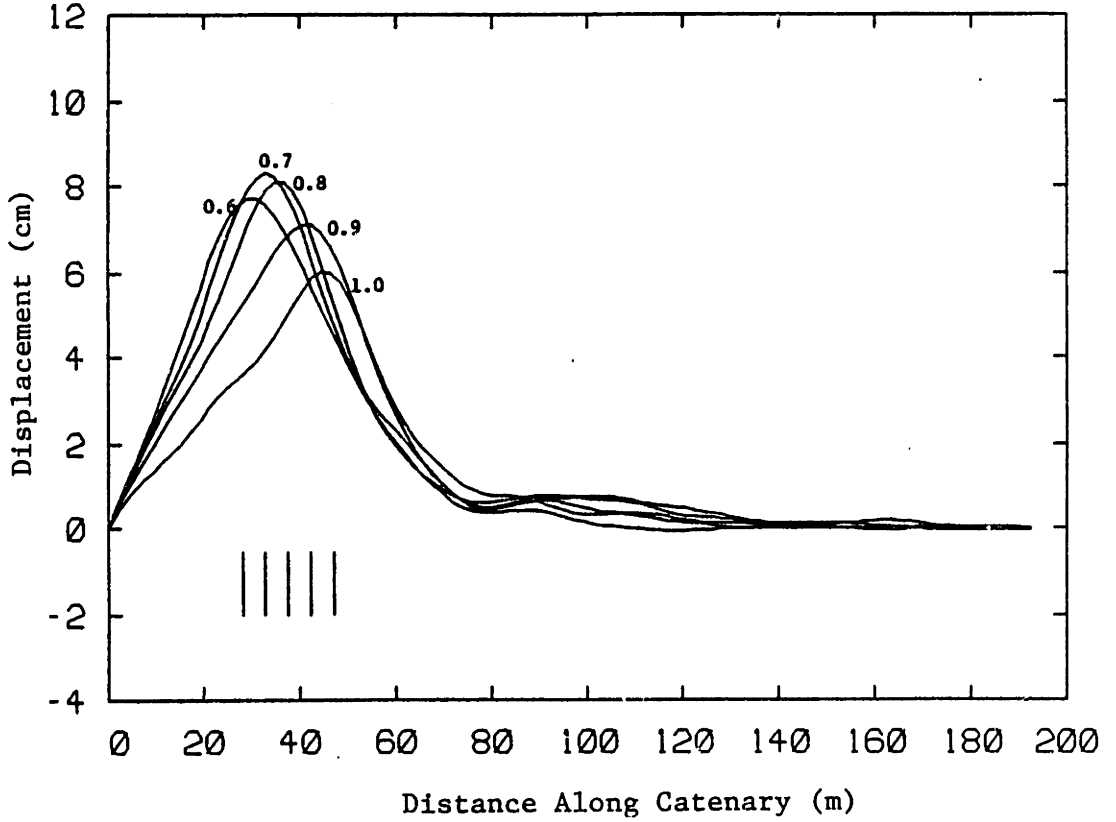
FIGURE 3.15: ALUMINUM CATENARY SHAPE BETWEEN 0.6
AND 1.0 SECONDS
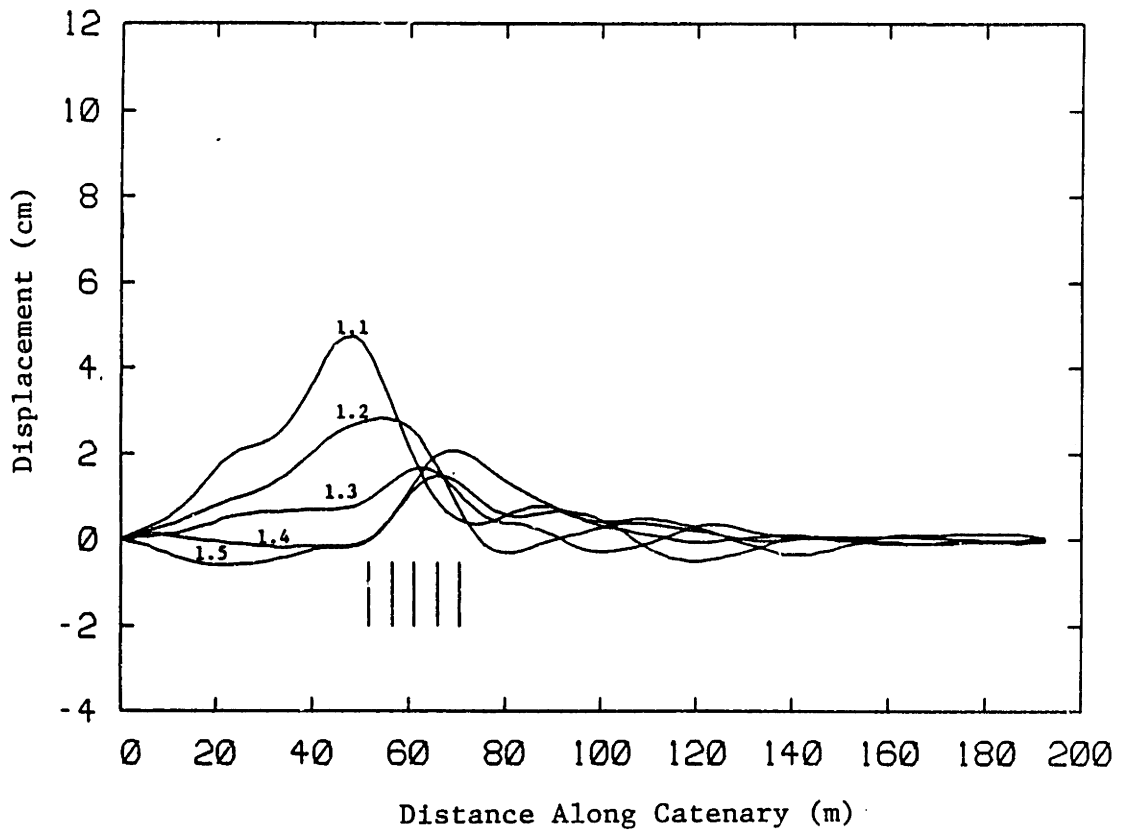
FIGURE 3.16: ALUMINUM CATENARY SHAPE BETWEEN
1.1 AND 1.5 SECONDS
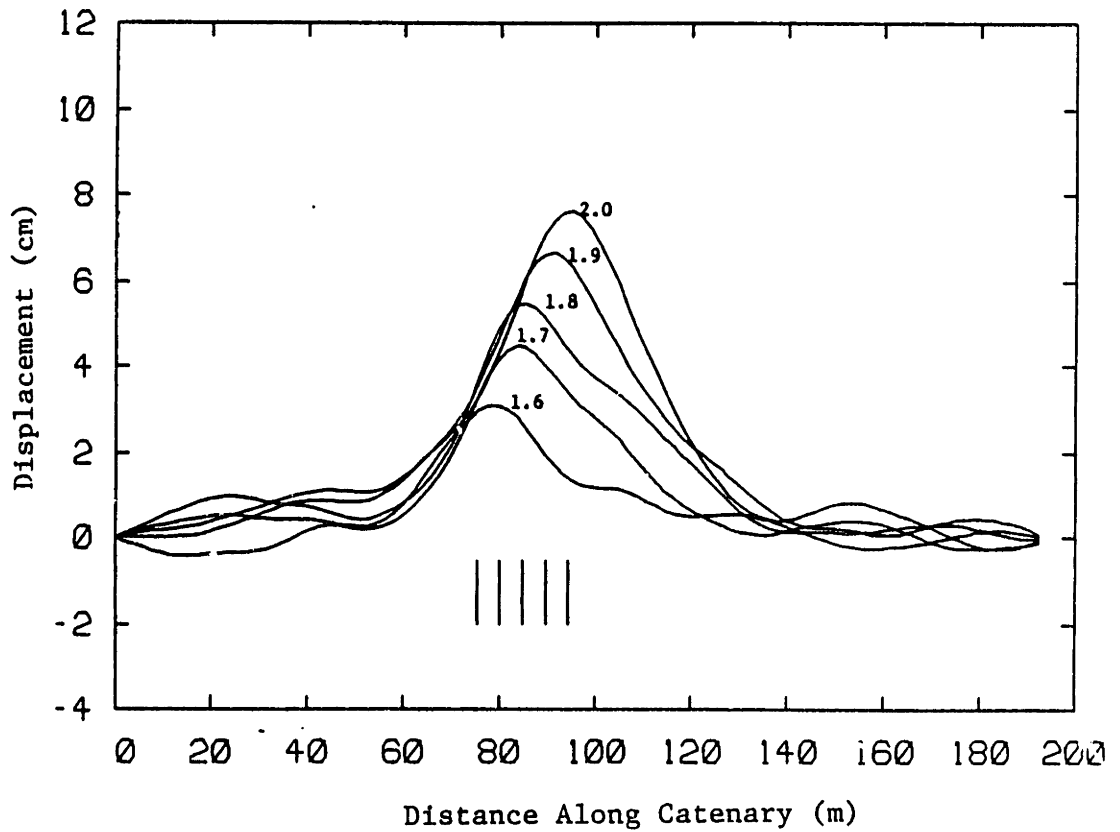
FIGURE 3.17: ALUMINUM CATENARY SHAPE BETWEEN
1.6 AND 2.0 SECONDS
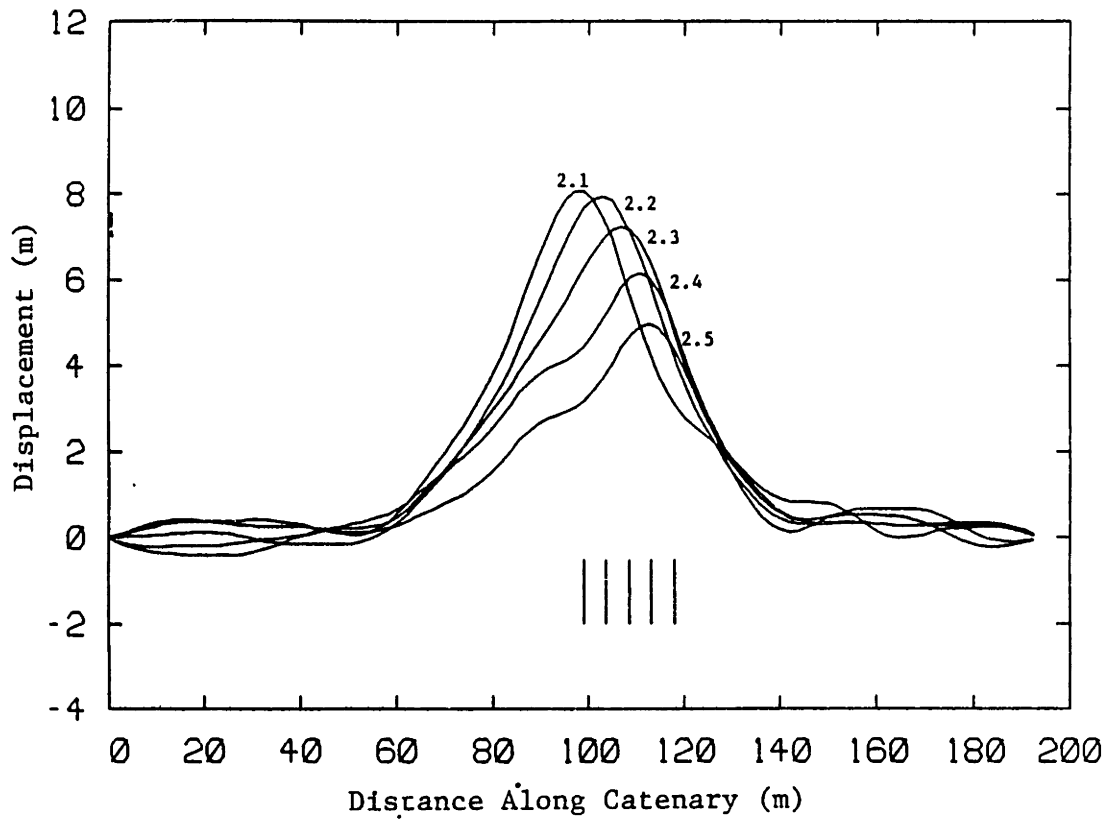
FIGURE 3.18: ALUMINUM CATENARY SHAPE BETWEEN
2.1 AND 2.5 SECONDS
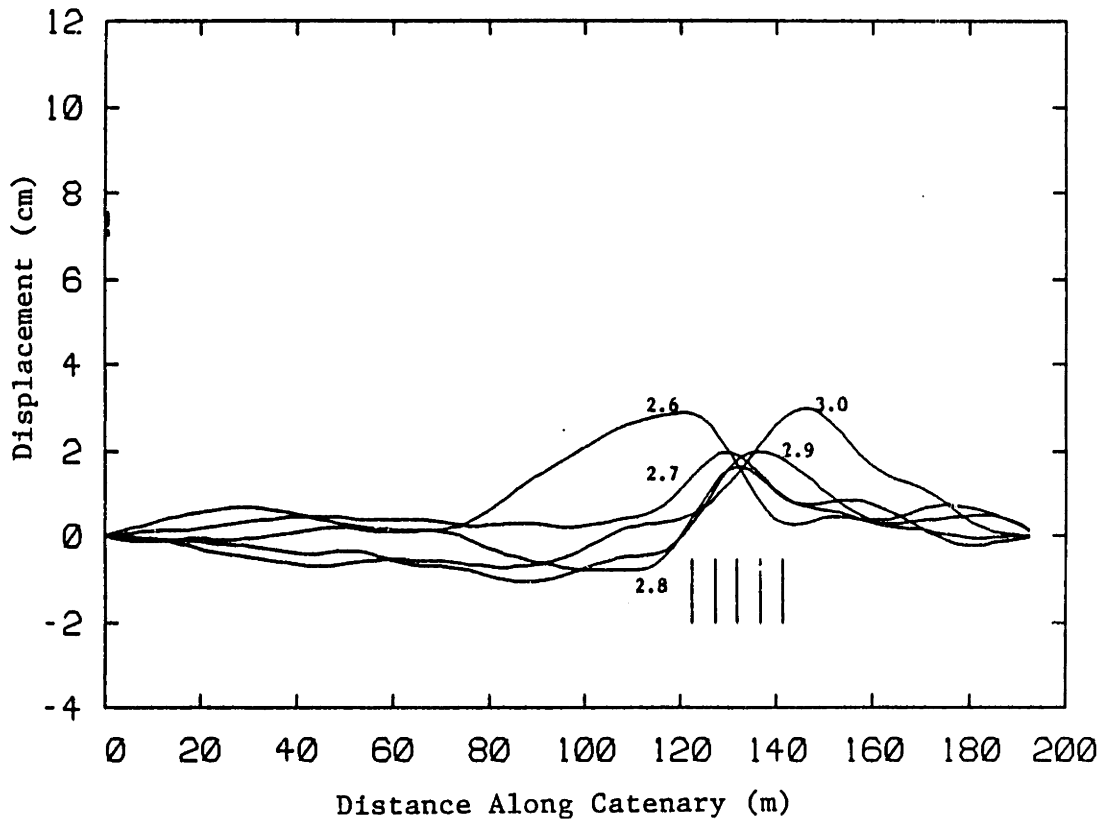
FIGURE 3.19: ALUMINUM CATENARY SHAPE BETWEEN
2.6 AND 3.0 SECONDS
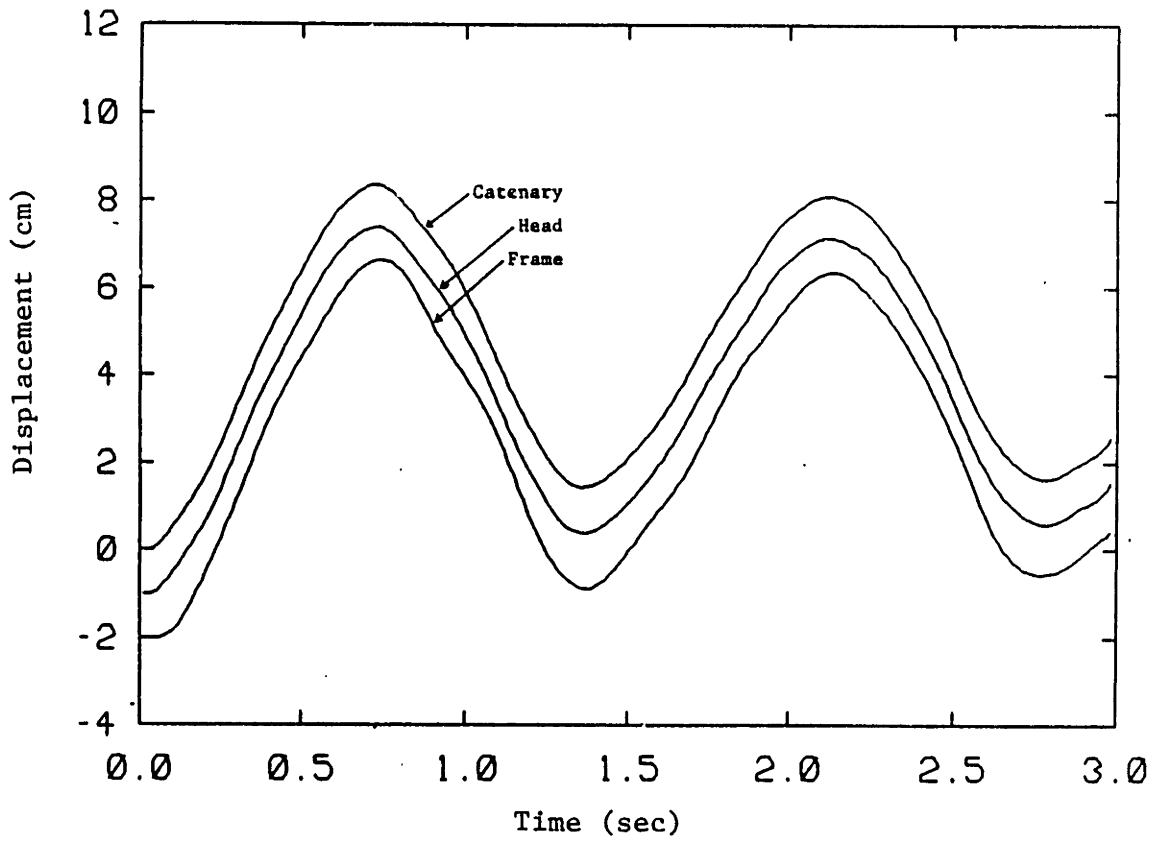
FIGURE 3.20: DISPLACEMENT OF CATENARY, HEAD, AND FRAME vs. TIME, ALUMINUM CATENARY, 170 km/hr
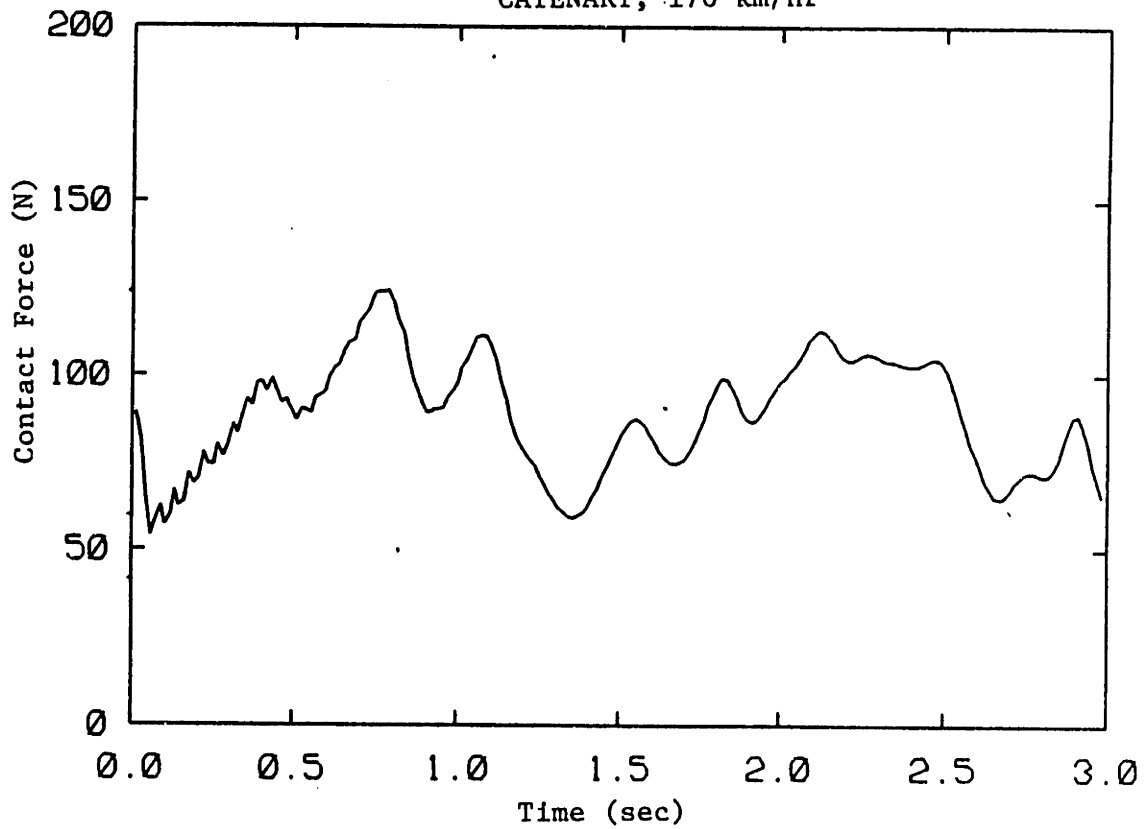
FIGURE 3.21: CONTACT FORCE, ALUMINUM CATENARY, 170 km/hr

of the approaching towers is felt sooner. With the wire descent more
gradual, the contact forces developed before a tower passing are smaller.
Since less force is applied to the pantograph during descent, it has less
downward momentum when it passes a tower, thus attenuating the sudden drop
in contact force that occurs at a tower. The pantograph is able to main-
tain contact with the catenary at speeds up to 260 km/hr; 85 km/hr faster
than the baseline separation speed.

The catenary's vibrations, caused by the pantograph are of smaller
amplitude and damp out faster for the aluminum case than for the baseline
case. The reduction in vibration can be seen by comparing the catenary's
shape in the first span when the pantograph is in the second span (Figures
3.6 and 3.19). The dissipative term from the catenary equation of motion
is $2\xi\omega_1\dot{z}_1$. The aluminum catenary, being lighter, has higher natural fre-
quencies. So, with the damping ratio the same for both cases, the aluminum
catenary dissipates more energy in a given amount of time. Since vibrations
are smaller, aluminum catenaries should improve performance for multiple
pantograph system.

3.3 Influence of Sag

The time simulation was run for values of maximum sag ranging from
0 to 16 cm. The train speed was 170 km/hr, and the baseline catenary and
pantograph parameters were used. Contact force variation versus maximum
sag is summarized in Table 3.5.

A small amount of sag improves performance. Displacement versus
time and contact force versus time plots for the 6 cm sag case are found
in Figures 3.22 and 3.23. The peaks and troughs in contact force occur in

TABLE 3.5

CONTACT FORCE VARIATION VS. MAXIMUM SAG

| Sag in Centimeters	Contact Force Variation in Newtons
0	130
2	106
4	85.9
6	66.1
8	64.8
10	72.7
12	95.3
14	123
16	153
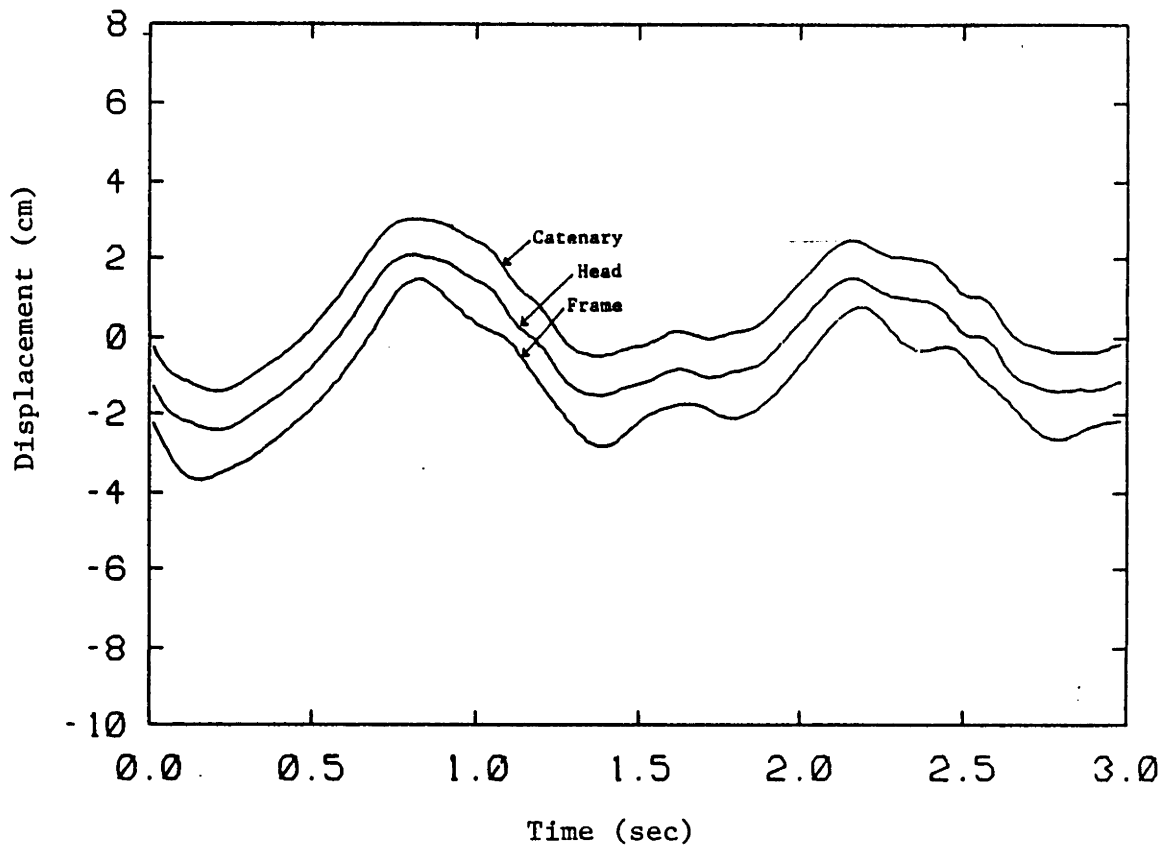
FIGURE 3.22: DISPLACEMENT OF CATENARY, HEAD, AND FRAME vs. TIME. BASELINE SYSTEM, 170 km/hr, 6 cm SAG
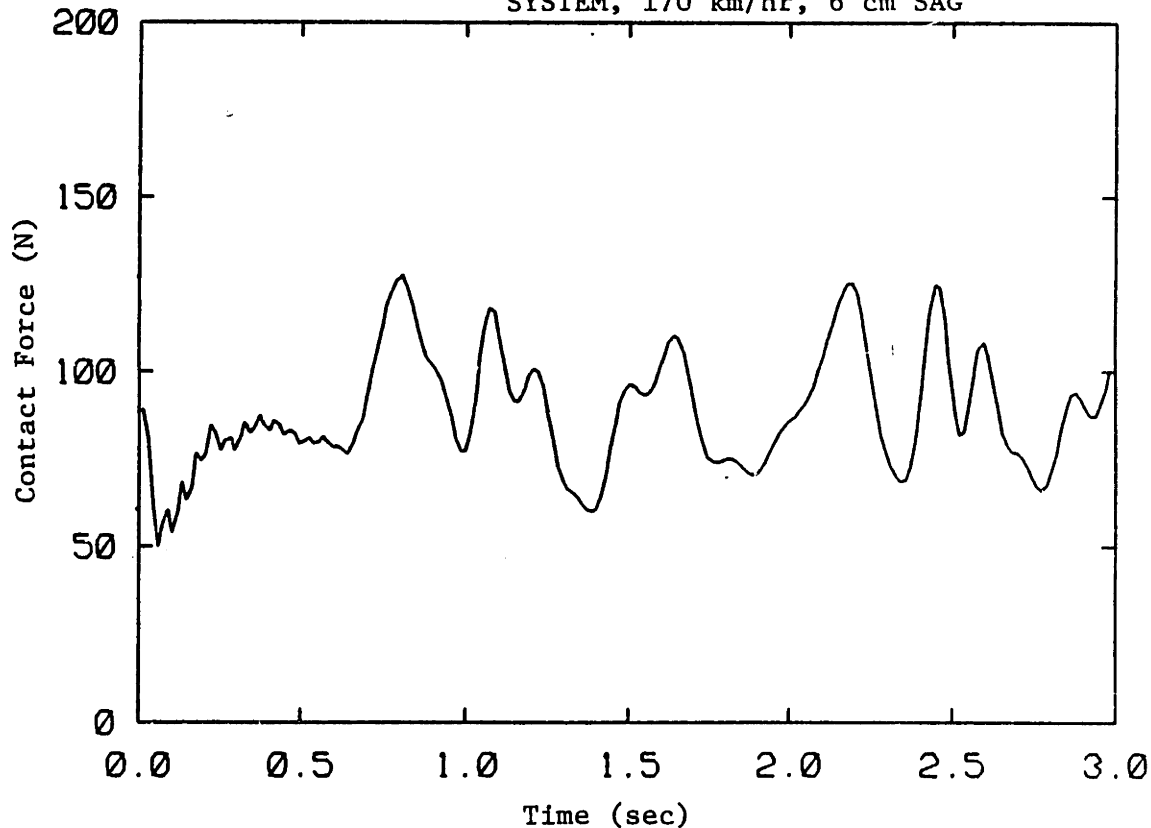
FIGURE 3.23: CONTACT FORCE HISTORY, BASELINE SYSTEM, 170 km/hr, 6 cm SAG

the same locations as the zero sag case, only they are of smaller magnitude. As mentioned above, the center of the span is the most compliant area. As an approaching pantograph attempts to overcome the sag by moving the wire up, it encounters inertial resistance which increases the apparent stiffness of the catenary. Since catenary's stiffness appears more uniform, fluctuations in contact force are smaller. Performance improves with sag up to 8 cm, after which performance degrades with increasing sag.

When the maximum sag becomes larger than the maximum positive displacement for the zero sag case, the contact force characteristics change. Figures 3.24 and 3.25 show the displacement and contact force plots for the 14 cm sag case. Minimums in contact force occur just before a tower is reached. The catenary sags so much that the wire rises as the tower is approached, and it reaches its highest point at the towers. The pantograph, after rising to this point, must suddently change direction. Since its momentum is still in he upward direction large peak forces occur.

The results show that some sag should be allowed in catenary design. Based on the data presented here, a desirable amount of sag is 80% of the maximum catenary displacement for the zero sag case.
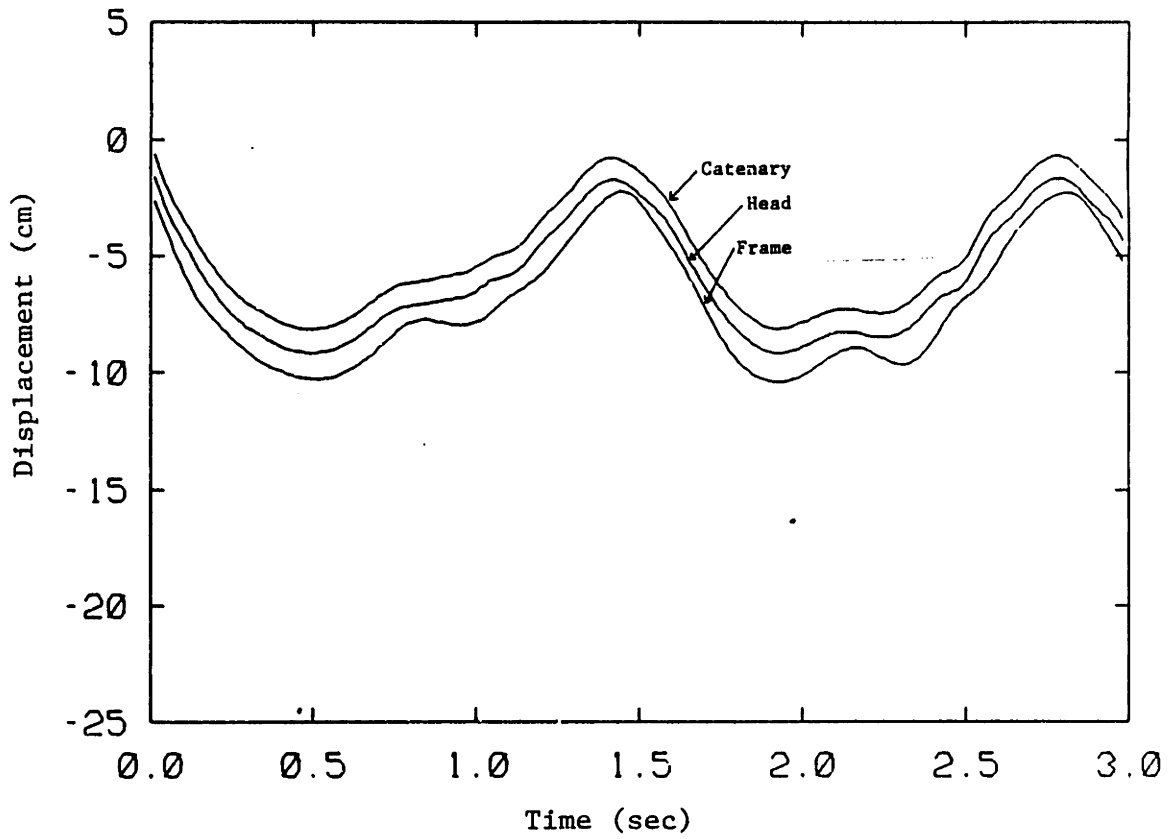
FIGURE 3.24: DISPLACEMENT OF CATENARY, HEAD, AND
FRAME vs. TIME. BASELINE SYSTEM,
170 km/hr, 14 cm SAG
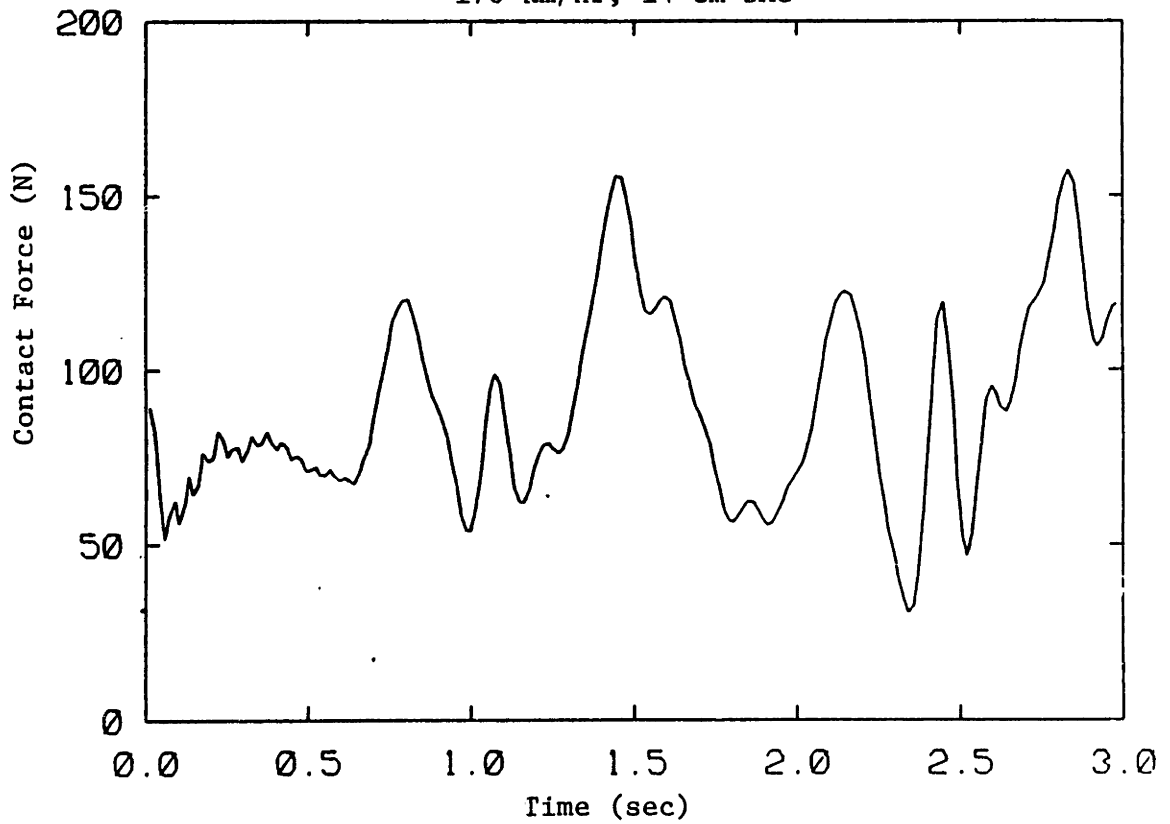
FIGURE 3.25: CONTACT FORCE HISTORY
BASELINE SYSTEM, 170 km/hr, 14 cm SAG

3.4 Parameter Study

The pantograph-catenary model has been used to investigate the effects of pantograph parameters on performance. All pantograph parameters in the simulations that follow are baseline parameters except for those being investigated. The catenary is the baseline catenary and the train speed is 170 km/hr unless otherwise noted.

A frequency response model is also used to aid in the analysis. By examining the displacement plots in the typical response section, the important frequencies and corresponding amplitudes were estimated. The most significant frequencies occur around 1 Hz and 4 Hz. The 1 Hz effect has an amplitude of approximately 10 cm and is associated with the tower-passing frequency. The 4 Hz effect is associated with the sudden change in catenary shape that occurs at the towers. It is referred to as the cusp frequency and has an amplitude of about 2 cm.

3.4.1 Mass Parameter Study

Many studies have suggested reducing the pantograph head mass to improve performance. A ligher head, having less inertia, should be able to react to changes in catenary shape faster. The frequency response program was run with the standard baseline pantograph and with the same pantograph having a 20% reduced head mass. Table 3.6 shows how the variation in contact force divided by displacement input varies with frequency.

TABLE 3.6

CONTACT FORCE VARIATION PER UNIT DISPLACEMENT VS. FREQUENCY
REDUCED MASS

	1 Hz	2 Hz	3 Hz	4 Hz
Base	1,549 N/m	20,270 N/m	6,004 N/m	4,615 N/m
20% Reduced Head	1,424 N/m	18,820 N/m	5,969 N/m	4,494 N/m
20% Reduced Frame	1,271 N/m	19,810 N/m	7,236 N/m	5,145 N/m

It can be seen that the reduced head mass pantograph responds better
at all frequencies in the range of interest. The reduced head mass panto-
graph was also run under the baseline catenary at 170 km/hr. The contact
force and displacement versus time plots are found in Figures 3.26 and 3.27.

A comparison of contact force fluctuation for the baseline pantograph
and the reduced head mass pantograph is given below:

CONTACT FORCE FLUCTUATION

	Baseline	20% Reduced Head
170 km/hr	130 N	118 N

The reduced head mass pantograph lowers contact force fluctuations
by 12N. The performance improvements were not concentrated in any particu-
lar region of the catenary, but rather small improvements occur all along
the catenary. Since the frequency respond data show improvement over the
entire range of interest, this was expected.

The effects of reducing frame mass were also investigated. Both the
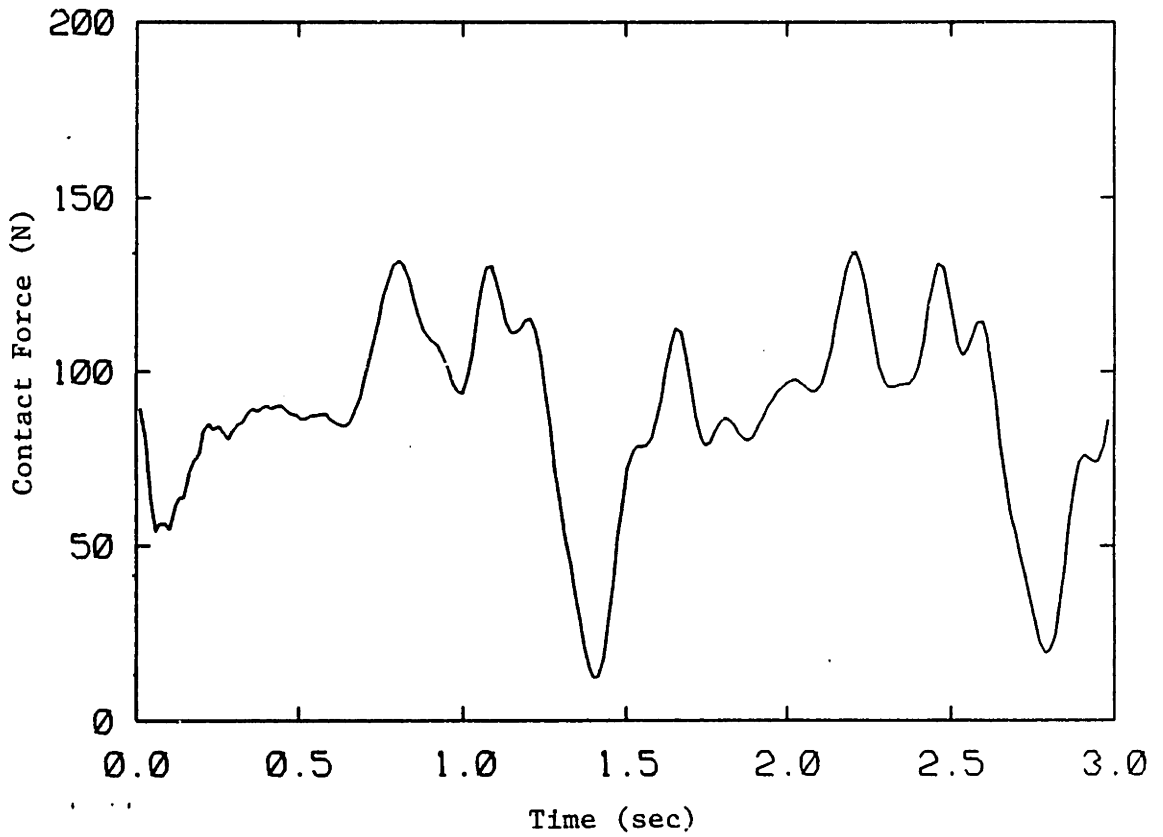
FIGURE 3.26: CONTACT FORCE vs. TIME, 20% REDUCED
HEAD MASS, 170 km/hr
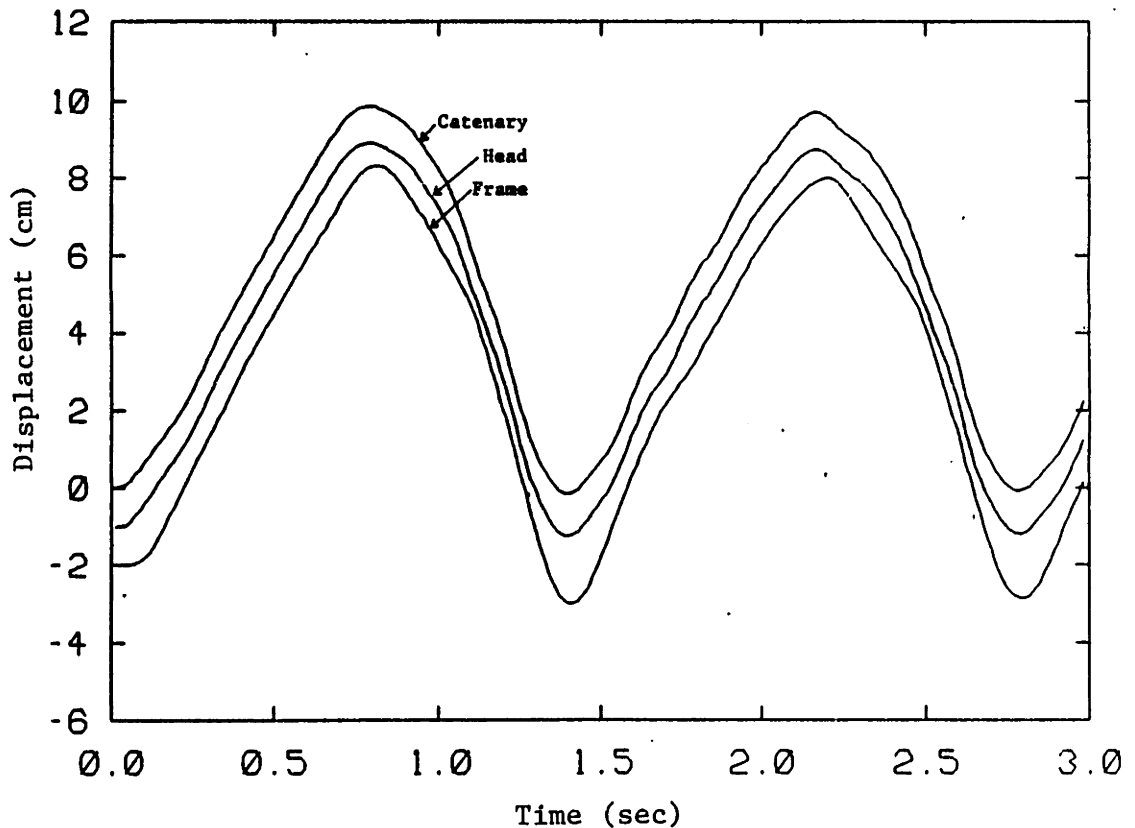
FIGURE 3.27: DISPLACEMENT OF CATENARY, HEAD, AND
FRAME vs. TIME, 20% REDUCED HEAD MASS,
170 km/hr

frequency and time simulations were run with a baseline pantograph having a 20% frame mass reduction. The frequency response, summarized in Table 3.6, shows a large improvement in the 1 Hz range but reduces performance at the cusp frequency.

When comparing frequency response one is comparing the ratio of contact force amplitude to input displacement amplitude. The 1 Hz effect associated with the tower passing frequency has approximately 5 times the amplitude of the 4 Hz cusp effect at the towers, so the improvement is significant.

The time simulation also showed performance improvements. The contact force variation is given below:

CONTACT FORCE VARIATION

	Baseline	20% Reduced Frame
170 km/hr	130 N	109 N

Much of the improvement occurs in reducing the sudden drops in contact force just after a tower is passed. Between spans the catenary is very soft and the pantograph causes a displacement of 10 cm. The towers, being very stiff, do not displace significantly. As the pantograph approaches a tower, the catenary's displacement decreases quickly causing a large downward force on the pantograph. Comparing the displacement and contact force versus time plots in Figures 3.28 and 3.29 one can see that the peak contact forces occur during this descent. When the pantograph reaches a tower, the catenary can no longer displace downward. However, the frame,
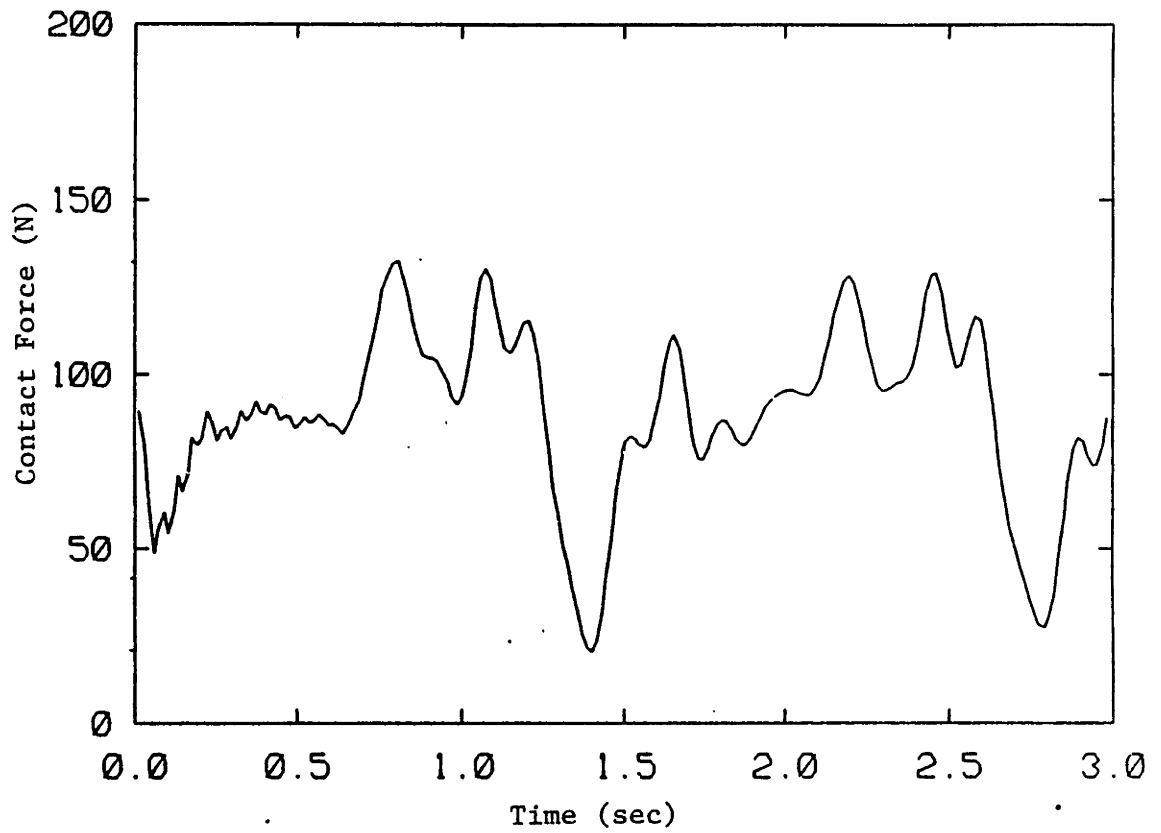
FIGURE 3.28: CONTACT FORCE vs. TIME, 20% REDUCED
FRAME MASS, 170 km/hr
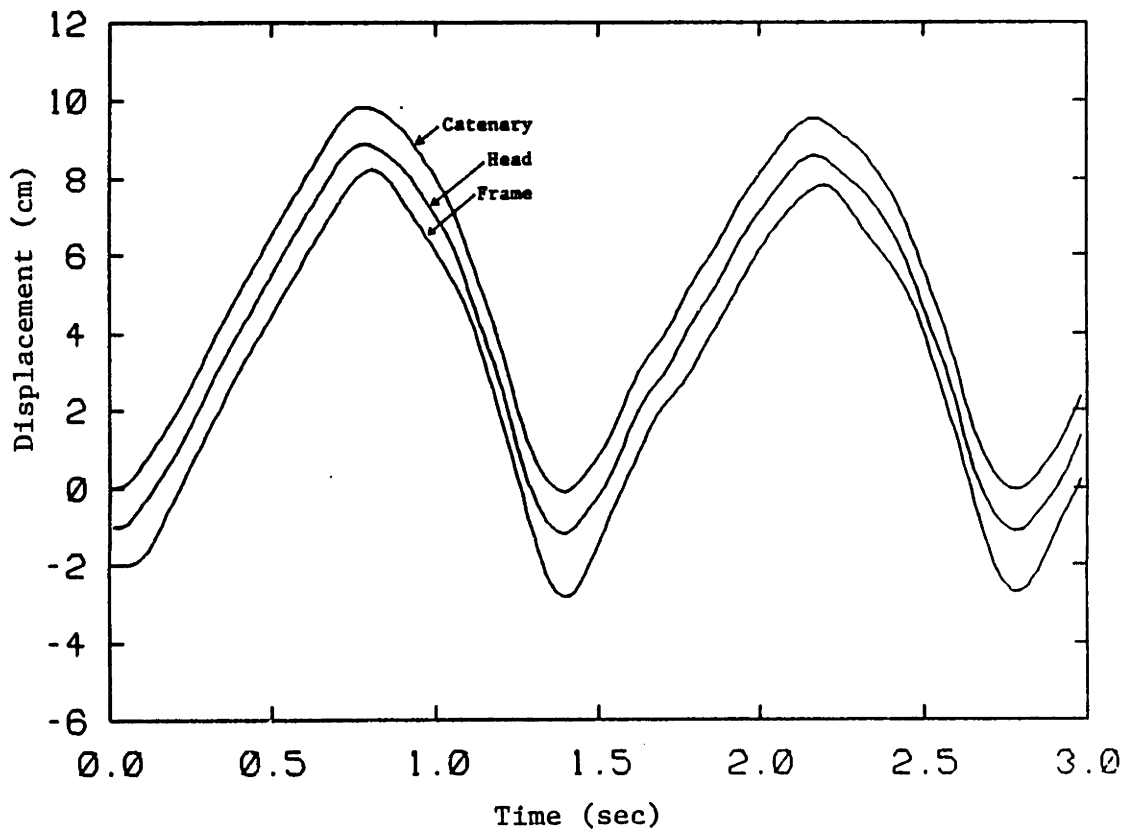
FIGURE 3.29: DISPLACEMENT OF CATENARY, HEAD, AND
FRAME vs. TIME, 20% REDUCED FRAME
MASS, 170 km/hr

which has developed a large downward momentum during its descent, continues to fall. By looking at the displacement plot, one can see that the frame undershoots the tower more than the head does. The contact force plot shows a sudden drop in this region.

Peters [8] did testing of pantograph-catenary systems at the D.O.T. facility in Pueblo, Colorado. He reported that loss of contact generally occurred at the towers. The simulation indicates that this is largely due to frame inertia.

3.4.2 Head Spring Study

The stiffness of the pantograph head spring was varied. The results of the frequency response runs are summarized in Table 3.7.

TABLE 3.7

CONTACT FORCE PER UNIT INPUT VS. FREQUENCY
HEAD SPRING RATE

	1 Hz	2 Hz	3 Hz	4 Hz
Head Spring Rate				
1750 N/m	1,550 N/m	4,120 N/m	5,400 N/m	7,870 N/m
3,500 N/m	1,500 N/m	7,500 N/m	4,700 N/m	5,400 N/m
*7,000 N/m	1,400 N/m	16,750 N/m	5,570 N/m	4,330 N/m
15,000 N/m	1,400 N/m	29,700 N/m	8,460 N/m	6,050 N/m

*Baseline

It can be seen from the frequency response data that increasing spring rate degrades performance. However, decreasing the spring rate a bit appears to improve performance. The time simulation was run with the head

spring rate at 3500 N/m. A comparison of the reduced spring rate and

standard pantograph contact force fluctuations is given below.

TABLE 3.8

CONTACT FORCE VARIATION vs. HEAD SPRING RATE

	Baseline	Reduced Spring Rate
135 km/hr	54.7 N	44.5 N
150 km/hr	87.5 N	73.4 N
170 km/hr	130 N	113 N

A contact force comparison of the baseline and reduced head stiffness

pantograph is found in Figure 3.30.

As the pantograph approaches a tower it must move down because the

catenary becomes stiffer. If the head spring is also stiff it does not

compress much and the frame is forced to move down immediately. A soft

spring, however, compresses as the head is forced down causing more relative

motion between the head and frame and less pure frame motion. The force

through a softer spring causes much of the frame downward motion to occur

closer to the tower. By comparing displacement Figures 3.8 and 3.31, one

can see that the relative distance between the head and frame as a tower is

approached is less for the 3500 N/m head spring case. When the tower is

passed the spring has not fully unloaded; so it applies a force on the

heavy frame and a light head which is pressing against a now softening

catenary. Since there is more motion in the light head, and less frame

motion, not as much downward momentum is developed which reduces the drop

in contact force at the towers.
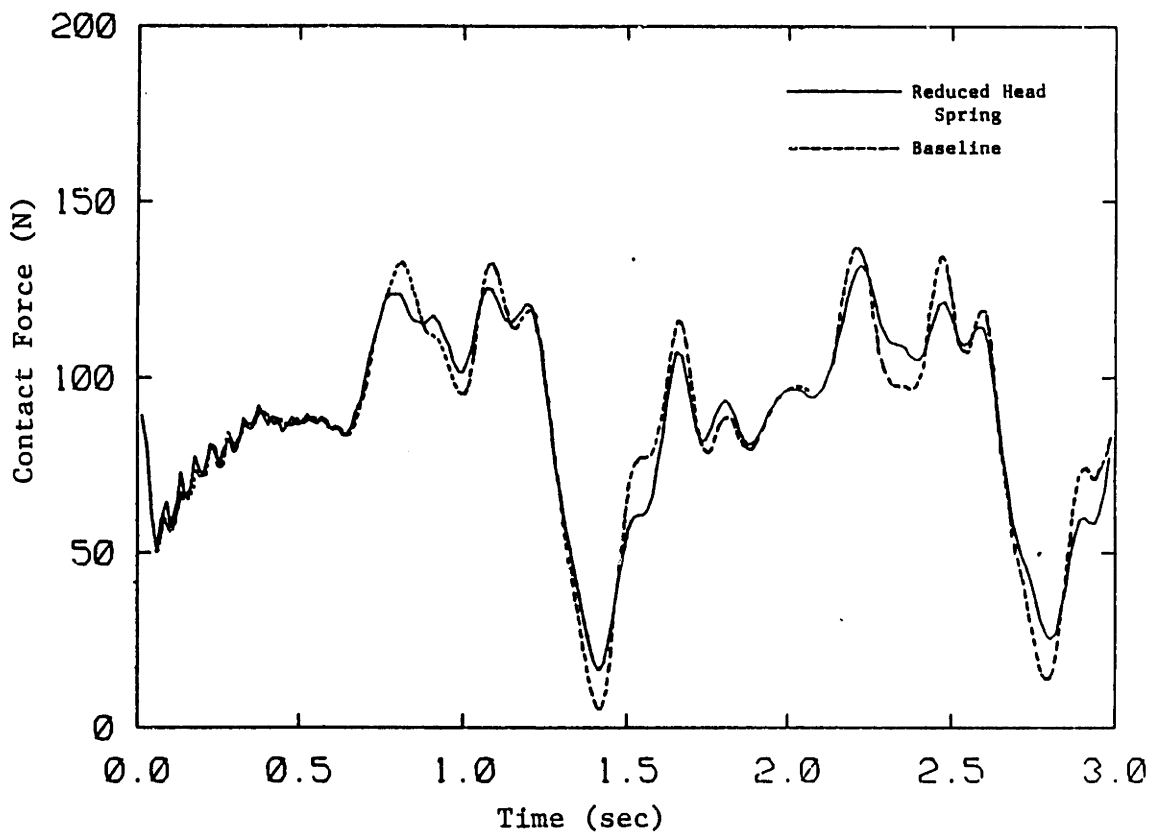
FIGURE 3.30:   CONTACT FORCE vs. TIME,
               COMPARISON OF REDUCED HEAD SPRING
               AND BASELINE PANTOGRAPHS, 170 km/hr
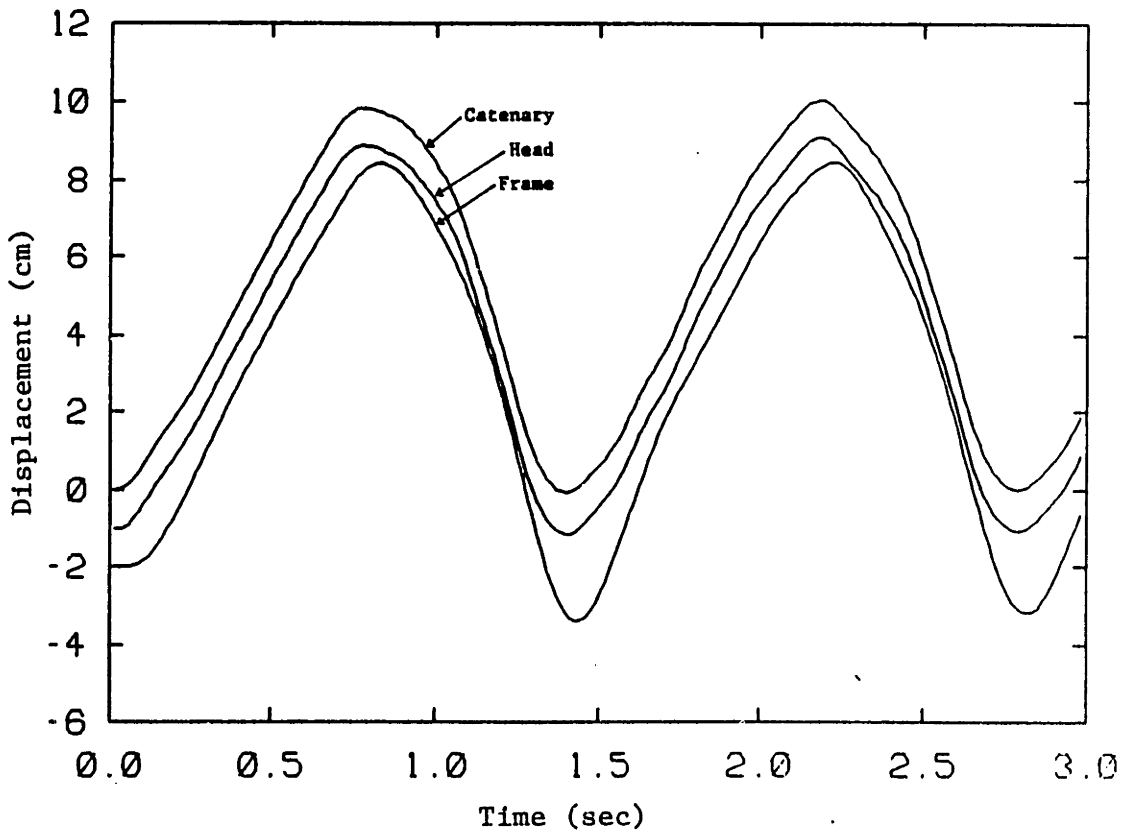
FIGURE 3.31:   DISPLACEMENT OF CATENARY, HEAD, AND
               FRAME vs. TIME, REDUCED HEAD SPRING
               RATE PANTOGRAPH, 170 km/hr

There is a limit to how soft the frame spring can be made. As the

spring becomes softer, the relative motion between the head and frame

becomes greater. The pantograph must be designed to accomodate the

greater range of motion.

3.4.3 Damping Parameter Study

The effect of head damping on performance is evaluated here. The

frequency response data are summarized in Table 3.9. It shows that as damping is

is increased from 50 $\frac{N \cdot s}{m}$ to 1000 $\frac{N \cdot s}{m}$ the response improves in the low-

frequency range and worsens in the high-frequency range. Increased damping

slows the rate at which the head can respond but reduces oscillations, which

makes it easier for the head to follow low frequency inputs. The time

simulation was also run with damping values ranging from 50 $\frac{N \cdot s}{m}$ to

1000 $\frac{N \cdot s}{m}$; the results are summarized in Table 3.10. Performance improves

significantly as damping is increased from 50 $\frac{N \cdot s}{m}$ to 250 $\frac{N \cdot s}{m}$. Very small

improvements in performance occur until damping reaches 500 $\frac{N \cdot s}{m}$. Further

increases cause performance to degrade.

The same test was performed with the frame damper. In this case,

as damping was increased, low-frequency respond was degraded and high-

frequency response was improved. The results are summarized in Table

3.11. Higher damping restricts frame motion which makes it harder for

the pantograph to follow low-frequency, high-amplitude inputs. However,

it is not as easily excited by low-amplitude, high-frequency inputs. The

results of the time simulation are found in Table 3.12. Increasing

damping to 60 $\frac{N \cdot s}{m}$ causes performance to improve, but after 60 $\frac{N \cdot s}{m}$ per-

TABLE 3.9

CONTACT FORCE PER DISPLACEMENT INPUT VS. FREQUENCY
HEAD DAMPING

Head Damping	1 Hz	2 Hz	3 Hz	4 Hz
$50 \frac{N \cdot s}{m}$	$1560 \frac{N}{m}$	$23,600 \frac{N}{m}$	$5,600 \frac{N}{m}$	$3,770 \frac{N}{m}$
$100 \frac{N \cdot s}{m}$	$1560 \frac{N}{m}$	$21,300 \frac{N}{m}$	$5,800 \frac{N}{m}$	$4,280 \frac{N}{m}$
$130 \frac{N \cdot s}{m}$	$1550 \frac{N}{m}$	$20,270 \frac{N}{m}$	$600 \frac{N}{m}$	$4,615 \frac{N}{m}$
$250 \frac{N \cdot s}{m}$	$1550 \frac{N}{m}$	$17,300 \frac{N}{m}$	$6,840 \frac{N}{m}$	$5,640 \frac{N}{m}$
$500 \frac{N \cdot s}{m}$	$1510 \frac{N}{m}$	$16,910 \frac{N}{m}$	$8,440 \frac{N}{m}$	$6,470 \frac{N}{m}$
$1000 \frac{N \cdot s}{m}$	$1470 \frac{N}{m}$	$19,630 \frac{N}{m}$	$9,805 \frac{N}{m}$	$6,790 \frac{N}{m}$

TABLE 3.10

CONTACT FORCE VARIATION
VS. HEAD DAMPING RATE

B_H	ΔF
$50 \frac{N \cdot s}{m}$	138 N
$130 \frac{N \cdot s}{m}$	130 N
$250 \frac{N \cdot s}{m}$	123 N
$500 \frac{N \cdot s}{m}$	120 N
$1000 \frac{N \cdot s}{m}$	124 N

TABLE 3.11

CONTACT FORCE PER DISPLACEMENT INPUT VS. FREQUENCY
FRAME DAMPING

Frame Damping	1 Hz	2 Hz	3 Hz	4 Hz
0	$1,540 \frac{N}{m}$	$48,700 \frac{N}{m}$	$6,025 \frac{N}{m}$	$4,560 \frac{N}{m}$
$30 \frac{N \cdot s}{m}$	$1,550 \frac{N}{m}$	$20,270 \frac{N}{m}$	$6,004 \frac{N}{m}$	$4,615 \frac{N}{m}$
$60 \frac{N \cdot s}{m}$	$1,580 \frac{N}{m}$	$12,200 \frac{N}{m}$	$5,911 \frac{N}{m}$	$4,660 \frac{N}{m}$
$100 \frac{N \cdot s}{m}$	$1,671 \frac{N}{m}$	$8,540 \frac{N}{m}$	$5,700 \frac{N}{m}$	$4,700 \frac{N}{m}$
$200 \frac{N \cdot s}{m}$	$1,946 \frac{N}{m}$	$5,216 \frac{N}{m}$	$5,005 \frac{N}{m}$	$4,700 \frac{N}{m}$
$300 \frac{N \cdot s}{m}$	$2,180 \frac{N}{m}$	$4,070 \frac{N}{m}$	$4,370 \frac{N}{m}$	$4,590 \frac{N}{m}$
$400 \frac{N \cdot s}{m}$	$2,353 \frac{N}{m}$	$3,549 \frac{N}{m}$	$3,907 \frac{N}{m}$	$4,430 \frac{N}{m}$
$500 \frac{N \cdot s}{m}$	$2,469 \frac{N}{m}$	$3,270 \frac{N}{m}$	$3,580 \frac{N}{m}$	$4,255 \frac{N}{m}$

TABLE 3.12

CONTACT FORCE VARIATION vs. FROM DAMPING RATE

B_f	ΔF
$30 \frac{N \cdot s}{m}$	130 N
$60 \frac{N \cdot s}{m}$	120 N
$100 \frac{N \cdot s}{m}$	123 N
$200 \frac{N \cdot s}{m}$	123 N
$500 \frac{N \cdot s}{m}$	136 N

formance degrades. Like the head, the baseline frame has too little damping.

Since both the head and frame are underdamped, a third damping study was done where both head and frame elements are varied. The frame damping was varied from 30 $\frac{N \cdot s}{m}$ to 200 $\frac{N \cdot s}{m}$ and the head from 75 $\frac{N \cdot s}{m}$ to 500 $\frac{N \cdot s}{m}$. Data from the frequency and time simulations are summarized in Tables 3.13 and 3.14. The best response was obtained with a frame damping of 60 $\frac{N \cdot s}{m}$ and a head damping of 500 $\frac{N \cdot s}{m}$.

One-Way Damping

One-way damping, or damping that acts in the downward direction only, has been suggested as a way to improve performance [2]. Damping of this type would move easily toward the catenary but would resist moving away from it. A time simulation was run to see how the addition of one-way frame damping would affect performance. Two-way frame damping was set 30 $\frac{N \cdot s}{m}$ while one-way frame damping was varied from 30 $\frac{N \cdot s}{m}$ to 100 $\frac{N \cdot s}{m}$. The time simulation results are summarized in Table 3.15. The best one-way damper was only Table to equal the best two-way damper.

Since one-way damping resists downward motion more than upward motion, it lessens the drop in contact force that occurs at the towers. However, if more two-way damping is used instead, it does not let the catenary displace as much in the middle of the span. If the catenary is displaced less, it forces the pantograph down a smaller distance as the tower is approached. Since the pantograph has less downward inertia, the drop in contact will be small. Figure 3.32 shows the displacement plot for a pantograph with 100 $\frac{N \cdot s}{m}$ frame damping and Figure 3.33 shows the same plot for

TABLE 3.13

COMBINED DAMPING STUDY,
FREQUENCY RESPONSE

B_f = 30 $\frac{N \cdot s}{m}$

B_H	1 Hz	2 Hz	3 Hz	4 Hz
75 N·s/m	1,554 N/m	22,570 N/m	5,715 N/m	4,022 N/m
130 N·s/m	1,560 N/m	21,300 N/m	5,800 N/m	9,280 N/m
250 N·s/m	1,550 N/m	17,300 N/m	6,840 N/m	5,640 N/m
500 N·s/m	1,510 N/m	16,910 N/m	8,440 N/m	6,470 N/m

B_f = 60 $\frac{N \cdot s}{m}$

B_H	1 Hz	2 Hz	3 Hz	4 Hz
75 N·s/m	1,595 N/m	13,380 N/m	5,662 N/m	4,053 N/m
130 N·s/m	1,587 N/m	12,570 N/m	5,911 N/m	4,660 N/m
250 N·s/m	1,568 N/m	11,650 N/m	6,761 N/m	5,684 N/m
500 N·s/m	1,531 N/m	12,440 N/m	8,323 N/m	6,498 N/m

B_f = 100 N·s/m

B_H	1 Hz	2 Hz	3 Hz	4 Hz
75 N·s/m	1,684 N/m	8,737 N/m	5,415 N/m	4,074 N/m
130 N·s/m	1,671 N/m	8,543 N/m	5,703 N/m	4,698 N/m
250 N·s/m	1,645 N/m	8,444 N/m	6,525 N/m	5,718 N/m
500 N.s/m	1,601 N/m	8,971 N/m	8,007 N/m	6,506 N/m

B_f = 200 N·s/m

B_H	1 Hz	2 Hz	3 Hz	4 Hz
75 N·s/m	1,965 N/m	5,236 N/m	4,729 N/m	4,033 N/m
130 N·s/m	1,945 N/m	5,216 N/m	5,005 N/m	4,694 N/m
250 N.s/m	1,906 N/m	5,321 N/m	5,750 N/m	5,704 N/m
500 N·s/m	1,854 N/m	5,850 N/m	7,026 N/m	6,433 N/m

TABLE 3.14

COMBINED DAMPING STUDY,
TIME RESPONSE

B_f = 30 $\frac{N \cdot s}{m}$

B_H	ΔF
130 N·s/m	130 N
250 N·s/m	123 N
500 N·s/m	120 N

B_f = 60

B_H	ΔF
130 N·s/m	120 N
250	119 N
500	118 N

B_f = 100 N·s/m

B_H	ΔF
130 N·s/m	123 N
250 N·s/m	124 N
500 N·s/m	125 N

B_f = 200 N·s/m

B_H	ΔF
75 N·s/m	123 N
130 N·s/m	123 N
250 N·s/m	127 N
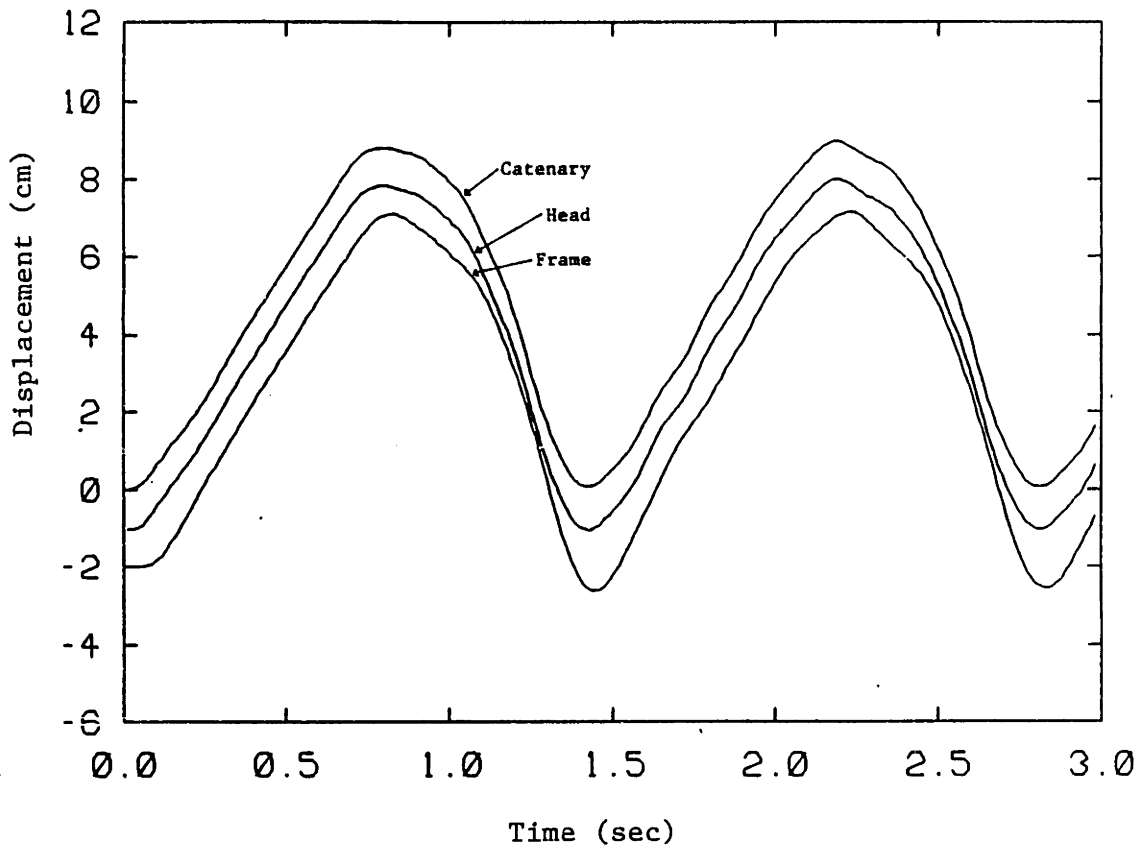
FIGURE 3.32: DISPLACEMENT OF CATENARY, HEAD, AND
FRAME vs. TIME, 100 N-s/m FRAME DAMPING
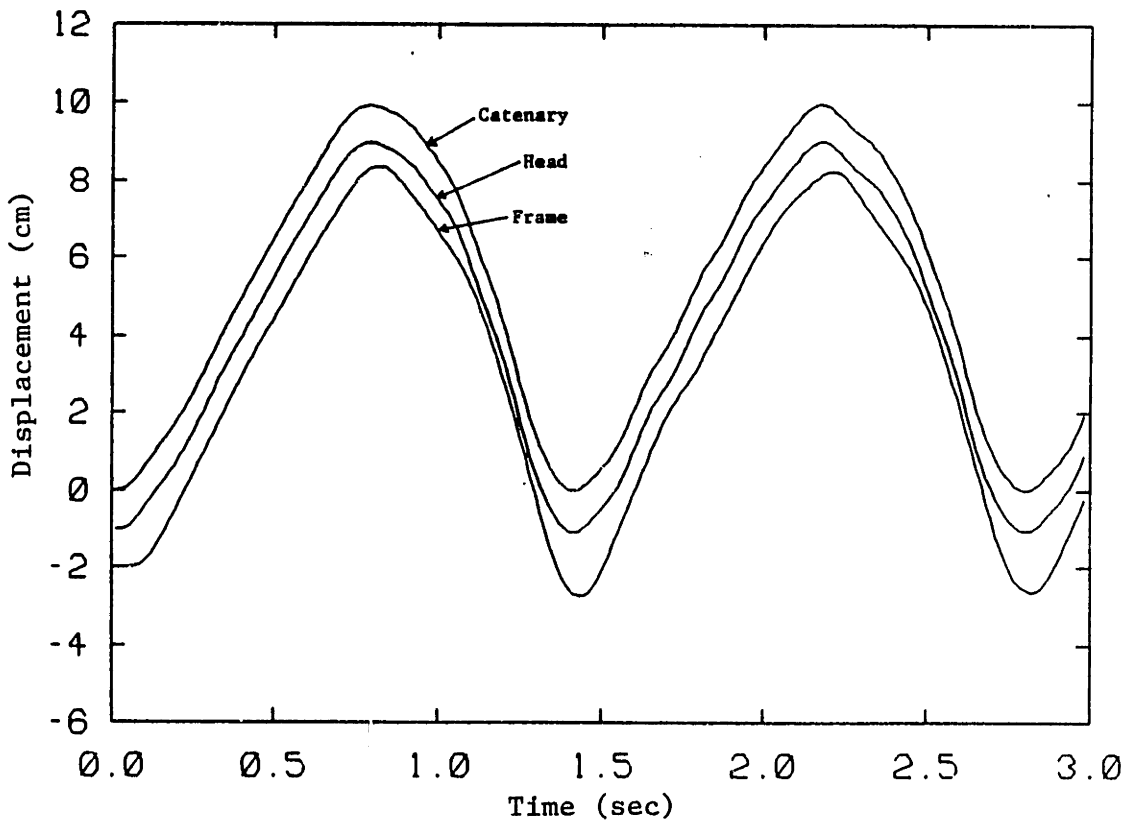
FIGURE 3.33: DISPLACEMENT OF CATENARY, HEAD, AND
FRAME vs. TIME, 100 N-s/m FRAME DAMPING

$30 \frac{N \cdot s}{m}$ frame damping plus $60 \frac{N \cdot s}{m}$ one-way frame damping. It can be seen that the catenary displacement is 1 cm smaller for the two-way case.

One-way damping offers no advantages over two-way damping for the cased considered.

3.4.4 Stiffness to Ground

Stiffness to ground was varied on the baseline pantograph from 0 to 2500 N/m. The time response date is summarized in Table 3.16. A small amount of frame stiffness, 500 N/m, reduces contact force variation by 64% (see Figure 3.34). With a frame spring, the pantograph cannot displace the catenary as much as it did in the zero stiffness case. Since displacements are smaller, the vertical inertial forces developed are less and dynamic excitation is attenuated.

As stiffness to ground is increased beyond 500 N/m, performance degrades. The catenary's spring rate is very high at the towers and decreases as midspan is approached, so the pantograph must displace the catenary more between towers to maintain nominal pressure with the wire. Since frame stiffness restrictes pantograph motion, the contact force becomes unacceptably small between spans. Choosing the best stiffness is a compromise between allowing enough catenary displacement to maintain adequate contact force and not introducing excessive dynamic excitation.

Dynamic excitation becomes worse with increasing train velocity. The compromise between reducing dynamic excitation and allowing enough catenary displacement to maintain adequate contact force results in larger

TABLE 3.15

ONE-WAY FRAME DAMPING (2-way damping = $30 \frac{N \cdot s}{m}$)

Contact Force Variation vs. One-Way Damping

One-Way Frame Damper	ΔF
30 N·s/m	123 N
60 N·s/m	120 N
100 N·s/m	123 N

TABLE 3.16

CONTACT FORCE VARIATION VS. FRAME SPRING RATE

K_f	ΔF
250 N/m	72.7 N
500 N/m	46.1 N
1,000 N/m	58.6 N
2,500 N/m	56.3 N
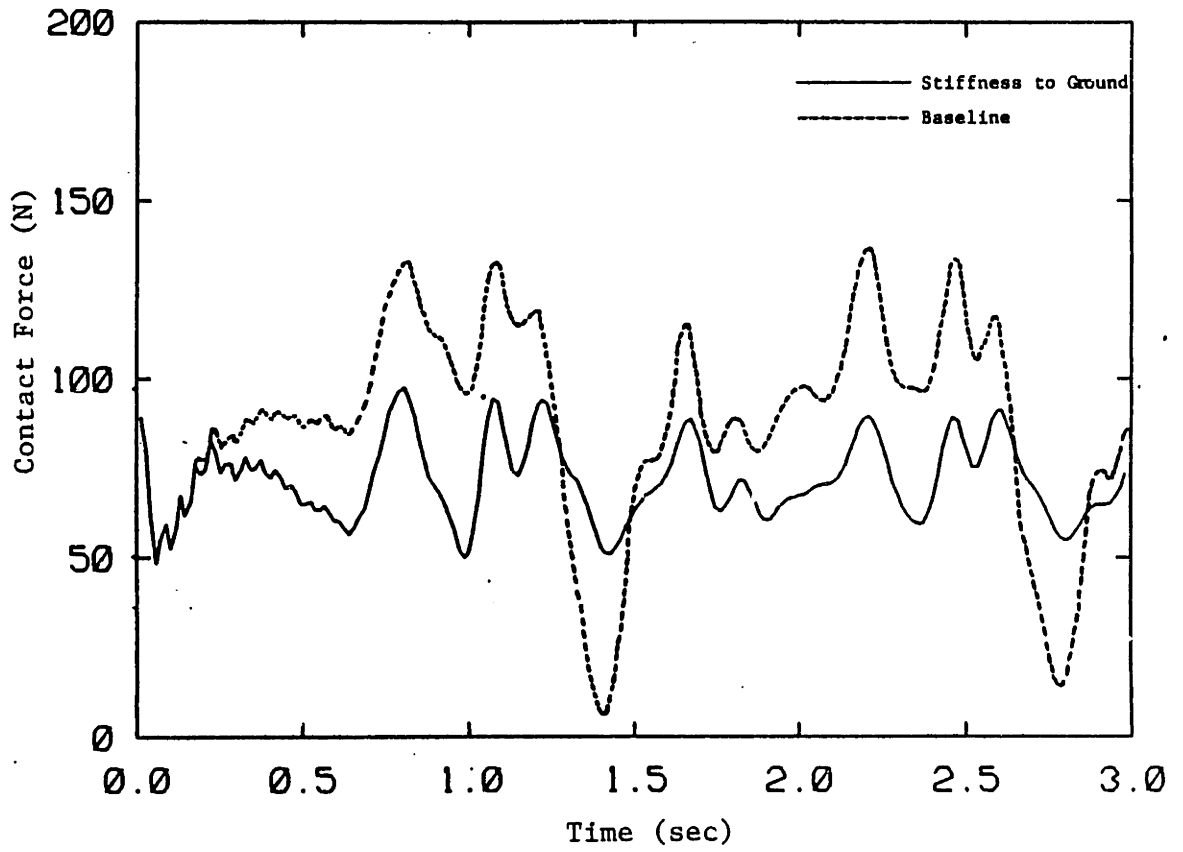
FIGURE 3.34: COMPARISON OF BASELINE AND STIFFNESS TO
GROUND PANTOGRAPHS, 170 km/hr

frame stiffnesses for optimum performance as velocity increases. The best performance at 225 km/hr is with a spring rate of 1000 N/m, and at 275 km/hr it is 1500 N/m.

Unfortunately, stiffness to ground cannot be implemented on most all existing systems. When a tunnel is approached, the catenary height may drop as much as 1.5m. If the pantograph had a 500 N/m frame stiffness and had to compress 1.5 m, a 760 N force would be applied to the frame. This is clearly unacceptable. Stiffness to ground may have some applications on lines specifically designed for high speed, as in the Japanese system, where great effort has been made to keep the wire height constant.

3.4.5 Suspension Comparison

Because of the tunnel problem, pantograph frame suspensions must be designed to operate over a wide range of heights, typically 0.5 to 2.0 m. A nominal contact force must be sustained with the wire, so the suspension must be able to provide a constant uplift force over this range. Zero stiffness to ground must be maintained because of the high forces that a finite stiffness value would apply to the frame over a large excursion.

There are two suspension types that currently dominate pantograph design. One uses springs in combination with a cam or link system to provide a constant uplift force. When modelled, the spring suspension looks like a constant uplift force and a damper (see Figure 3.35a). In the other design, a pneumatic cylinder is used to provide constant uplift force. The model of this suspension, shown in Figure 3.35b, is a constant uplift force with a spring and damper in series.
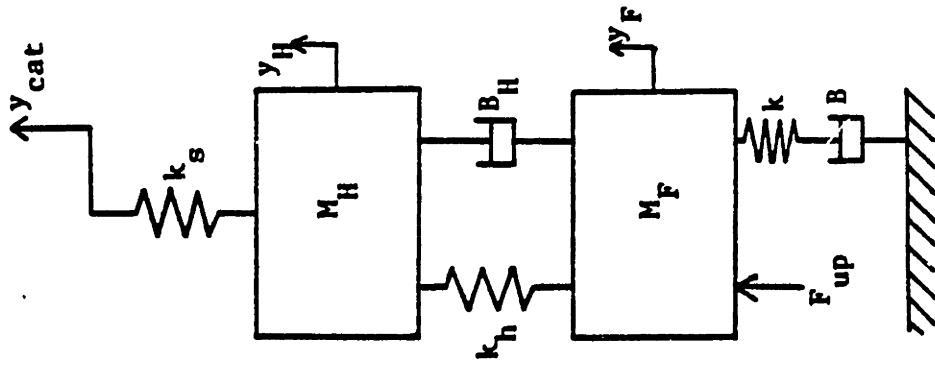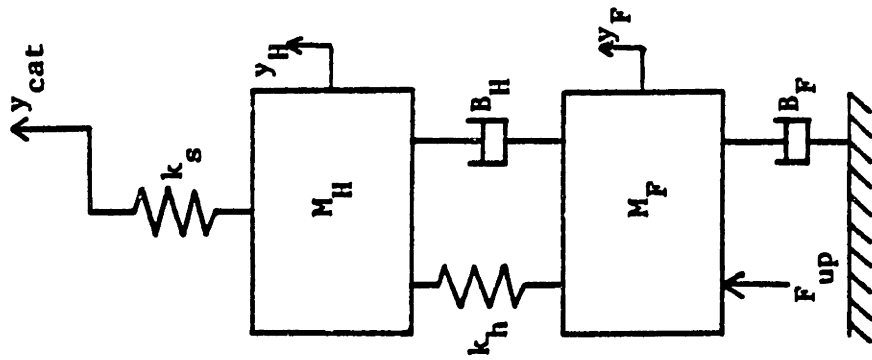
FIGURE 3.35: SPRING SUSPENSION PANTOGRAPH
MODEL AND AIR CYLINDER SUSPENSION
PANTOGRAPH MODEL

As the value of damping on the airspring suspension becomes very large, the system begins to resemble an uplift force in parallel with a frame spring. Since a finite stiffness to ground is unacceptable, an upper limit on damping must be set. Wire height gradients can have an amplitude as large as 1.5 m and a gradient as steep as 0.5% during a tunnel approach [11]. To pick a limit on damping, a train traveling at 150 km/hr will not be allowed to apply more than 50 N across the damper. A 150 km/hr under a 0.5% gradient yields a vertical velocity of $\hat{}$.20 m/s. Dividing the maximum damper force by the vertical velocity gives a maximum damper value of $250 \frac{N \cdot s}{m}$.

The frequency response program was run to evaluate different suspension spring and damping rates. The better values were run in the time simulation and it was found that a spring rate of 1000 N/m and a damping of $250 \frac{N \cdot s}{m}$ gave the smallest contact force variation. At 170 km/hr the airspring suspension's contact force variation was 42% lower than the best spring suspension (Figure 3.36). A comparison of the contact force variations for each suspension is given below. As explained in the last section, stiffness to ground reduces high velocity dynamic excitation. Since the damper develops high forces when vertical velocities are high, the spring has the greatest effect when needed most.

TABLE 3.17

CONTACT FORCE VARIATION FOR SPRING AND AIR CYLINDER SUSPENSION

Speed	ΔF, Spring Suspension	ΔF, Air Cylinder Suspension
135 km/hr	39.1 N	50.0 N
170 km/hr	120 N	84.4 N
225 km/hr	Loss of Contact	146 N
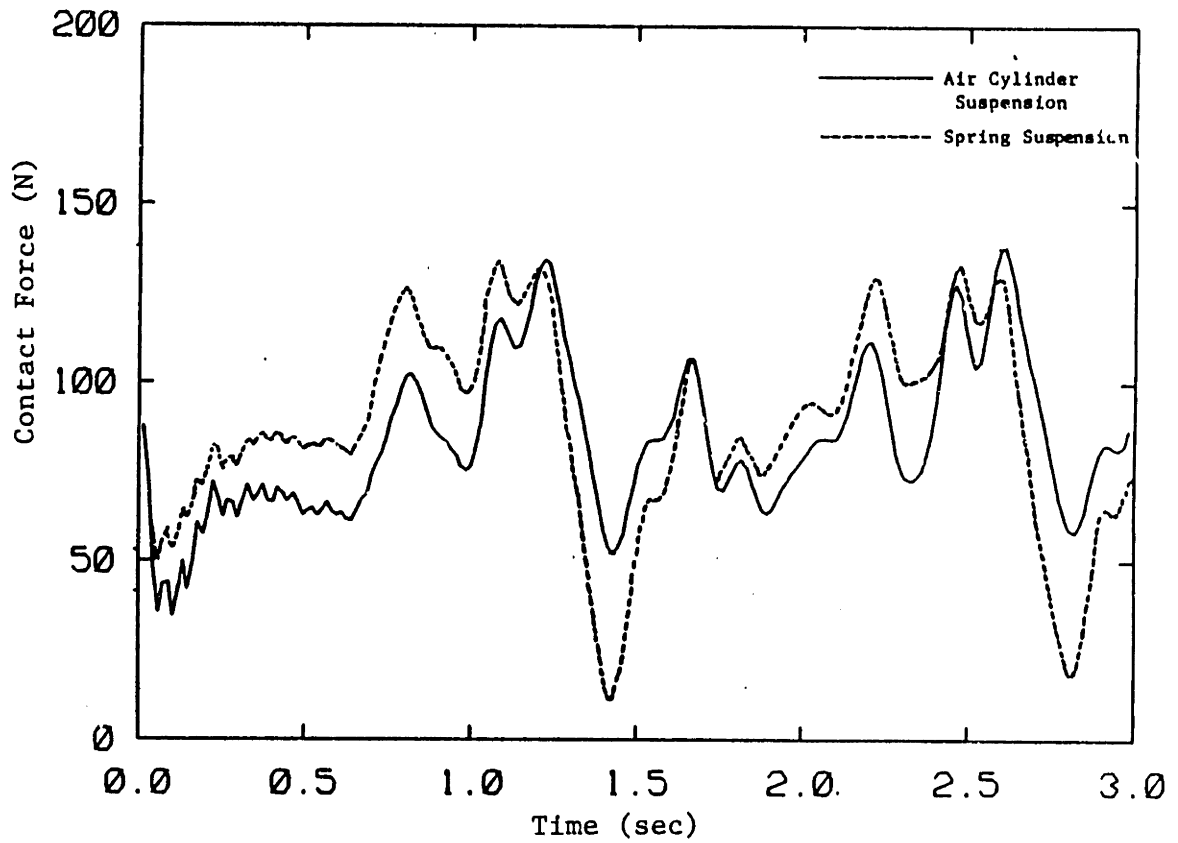
FIGURE 3.36: COMPARISON OF AIR CYLINDER SUSPENSION
AND SPRING SUSPENSION PANTOGRAPHS,
170 km/hr

3.5 Optimized Pantograph

With the results of the parameter studies, an optimized set of pantograph parameters has been formed. It was shown that reducing both head and frame mass was important to improve pantograph performance. A lightweight pantograph using graphite or an other lightweight material would probably perform very well. However, this would introduce many questions about the sturdiness of the structure. It was finally decided to use the masses of the baseline system since they represent the masses of a well-designed pantograph. This also shows what kind of improvements are possible on existing pantographs.

The airspring suspension showed a large performance improvement over the spring suspension. It is used here with the parameters that were chosen in the last section. A softer head suspension was also found to improve performance. A value of 3500 N/m is used here. With a reduced head spring it is also necessary to adjust the head damping. Several values were run in both the time and frequency simulations and the best one was found to be $100 \frac{N \cdot s}{m}$. The parameters for the ideal pantograph are found in Table 3.18.

TABLE 3.19

CONTACT FORCE VARIATION VS. SPEED FOR BASELINE AND IDEAL PANTOGRAPH

Speed	ΔF, Baseline	ΔF, Ideal
135 km/hr	54.7 N	48.4 N
170 km/hr	130 N	72.6 N
225 km/hr	Loss of Contact	119 N

TABLE 3.18

IDEAL PANTOGRAPH PARAMETERS

Head Mass:	91 kg	20 lb
Frame Mass:	17.2 kg	38 lb
Stiffness of the Pantograph Shoe:	82.3 kN/m	470 lb/in
Stiffness Between the Head and Frame:	3,500 N/m	20 lb/in
Stiffness of series suspension spring:	1,000 N/m	5.71 lb/in
Damp Between Head and Frame:	$100 \frac{N \cdot s}{m}$	0.572 lb-sec/in
Damping of series suspension Damper:	$250 \frac{N \cdot s}{m}$	1.43 lb-sec/in
Uplift Force:	90 N	20.2 lb

Table 3.19 shows the Contact Force Variation vs. speed for the base-
line and ideal pantographs. The ideal pantograph performed slightly
better at low speeds and significantly better at high speeds. Figure 3.37
compares the contact force for the baseline and ideal systems at 170 kph.
The optimized pantograph performed much better than the baseline system.

3.6 Active Control

In this section a frame-actuated controller is designed using optimal
control techniques. A frame-actuated design was chosen for several
reasons. Frame dynamics are largely responsible for most losses of con-
tact. Many pantographs, including the Brecknell-Willis, already have a
pneumatic cylinder on the frame to provide uplift force and could be
modified for active control. A head-actuated design would require the
actuator to move with the pantograph, increasing the overall mass and
thus degrading performance.

The pantograph model used for the control design is the same two-mass
model developed in Section 2. The equations for the model using full
state feedback control are also developed there. The model is shown in
Figure 3.38a. The wire height, y_{cat}, cannot be realistically measured.
For design purposes the catenary is modelled as a constant spring whose
value is the average catenary stiffness, k_{ave}. Figure 3.38b shows this
scheme.

A diagram of the proposed controller is shown in Figure 3.39. The
control input is a linear combination of the states plus the desired up-
lift force:
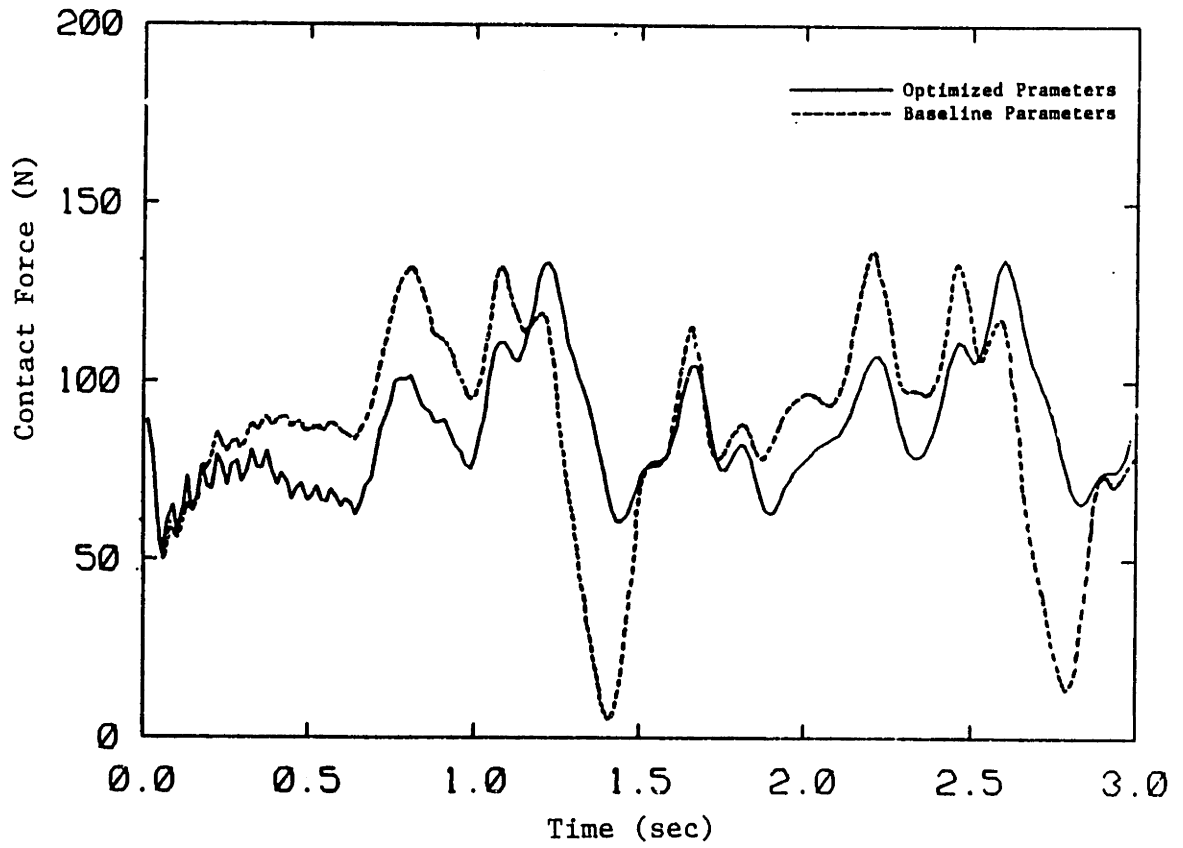
FIGURE 3.37: CONTACT FORCE COMPARISON OF OPTIMIZED AND
BASELINE PANTOGRAPH, 170 km/hr
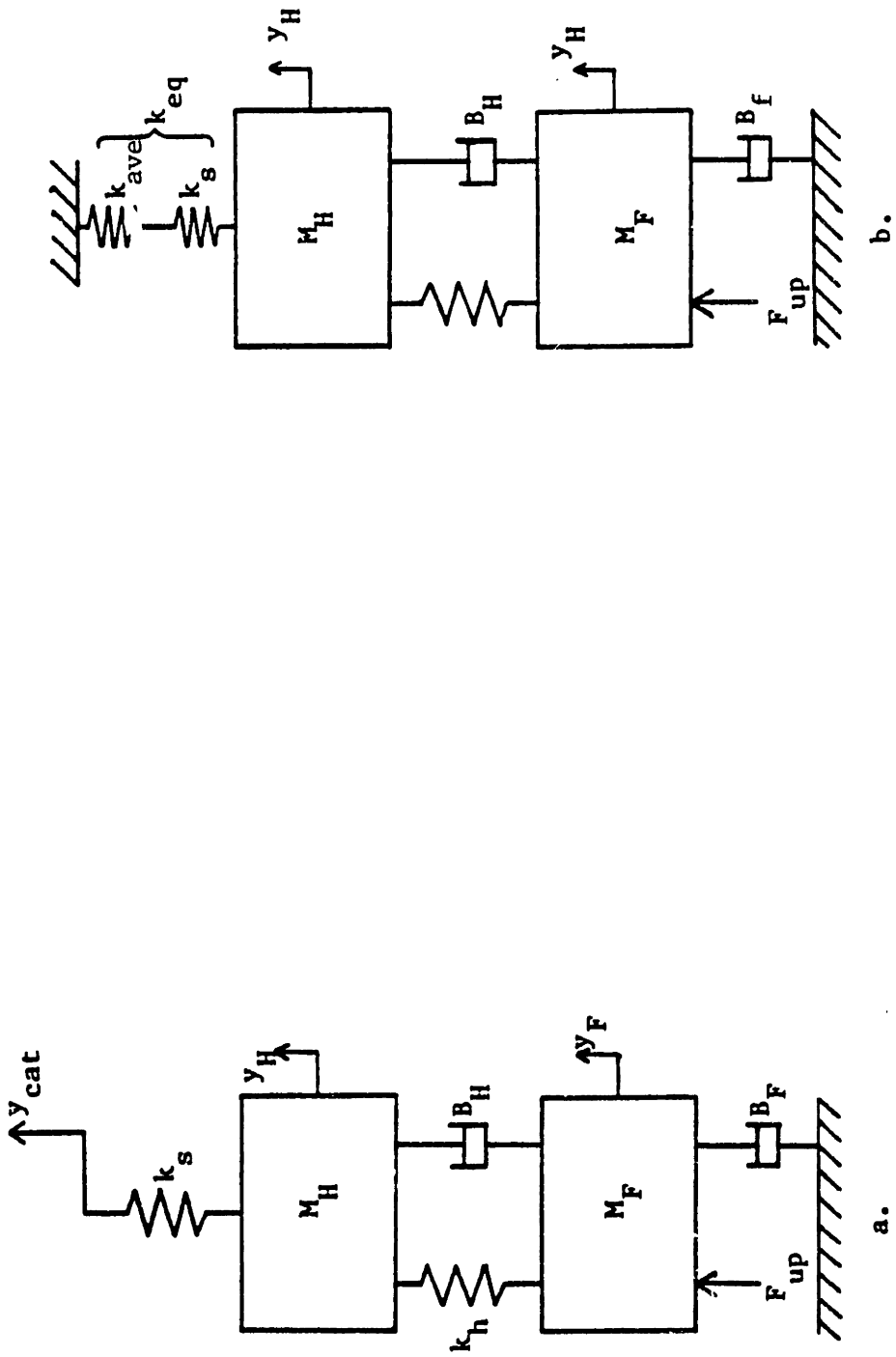
FIGURE 3.38: PANTOGRAPH MODELS
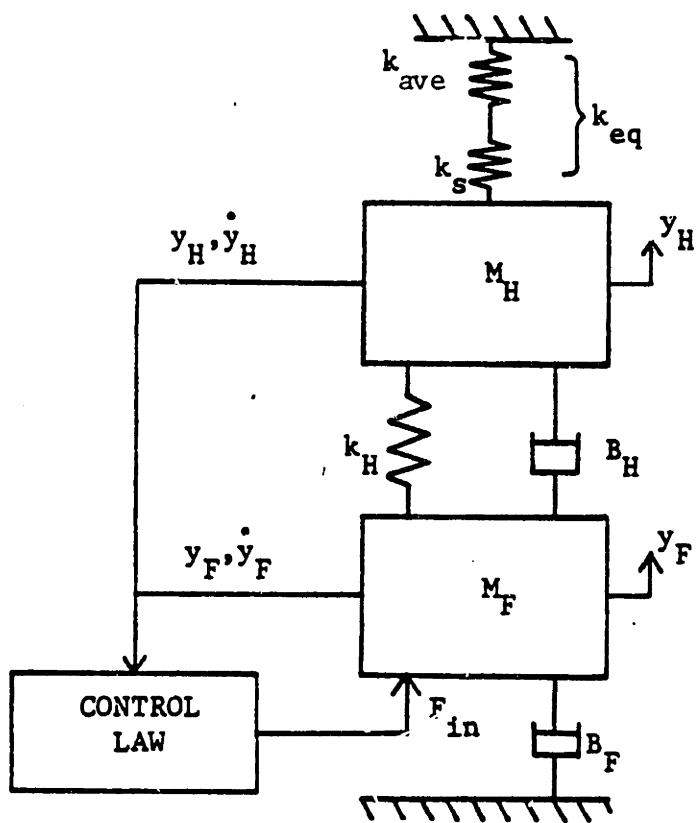
FIGURE 3.39: ACTIVE PANTOGRAPH MODEL

$$F_{in} = C_1 y_H + C_2 \dot{y}_H + C_3 y_F + C_4 \dot{y}_F + F_{up}$$

where:

C_1, C_2, C_3, and C_4 are the controller gains

F_{up} is the uplift force

y_H, $\dot{y}_H$, y_F, $\dot{y}_F$ are the pantograph states as defined in Figure 3.38.

The controller gains are selected by minimizing the quadratic cost function:

$$J = \int_0^t (\underline{y}^T \underline{Q} \, \underline{y} + F_{in}^T R \, F_{in}) dt)$$

where:

$\underline{y}$ state variable vector

F_{in} control force

$\underline{Q}$ state weighting matrix

via the Matrix Riccati Equation [28]. When the pantograph approaches a speed where loss of contact occurs, it experiences high head and frame velocities. So the $\underline{Q}$ weighting matrix is chosen to penalize high velocities. Because of the tunnel problem, the pantograph must be able to make large excursions. So there are no penalties associated with displacements. The chosen Q matrix is:

$$Q = \begin{bmatrix} 0 & 0 & 0 & 0 \\ 0 & \dfrac{1}{(0.13 \text{ m/s})^2} & 0 & 0 \\ 0 & 0 & 0 & 0 \\ 0 & 0 & 0 & \dfrac{1}{(0.14 \text{ m/s})^2} \end{bmatrix}$$

The R weighting factor is chosen to keep the control force from becoming unreasonably large. A value of 10^{-5} was used for design purposes. The pantograph parameters used are the baseline values.

The Matrix Riccati Equation is solved using the COPT software package at M.I.T.'s Joint Computer Facility. The resulting gains are given below:

$$C_1 = -27,500 \text{ N/m}$$
$$C_2 = 897 \frac{\text{N} \cdot \text{s}}{\text{m}}$$
$$C_3 = 27,500 \text{ N/m}$$
$$C_4 = 2,392 \frac{\text{N} \cdot \text{s}}{\text{m}}$$

The contact force and displacement plots for an actively-controlled pantograph using these gains are given in Figures 3.40 and 3.41. The controller increases the overall contact force fluctuation but does reduce the drop in contact force at the towers.

In order to improve active-pantograph performance· some modifications must be made. Since a simpler controller is more desirable, the number of measurements made will be reduced. Feeding back frame velocity effectively adds a damper from the frame to ground. Since the gain on $\dot{y}_F$ is simply a
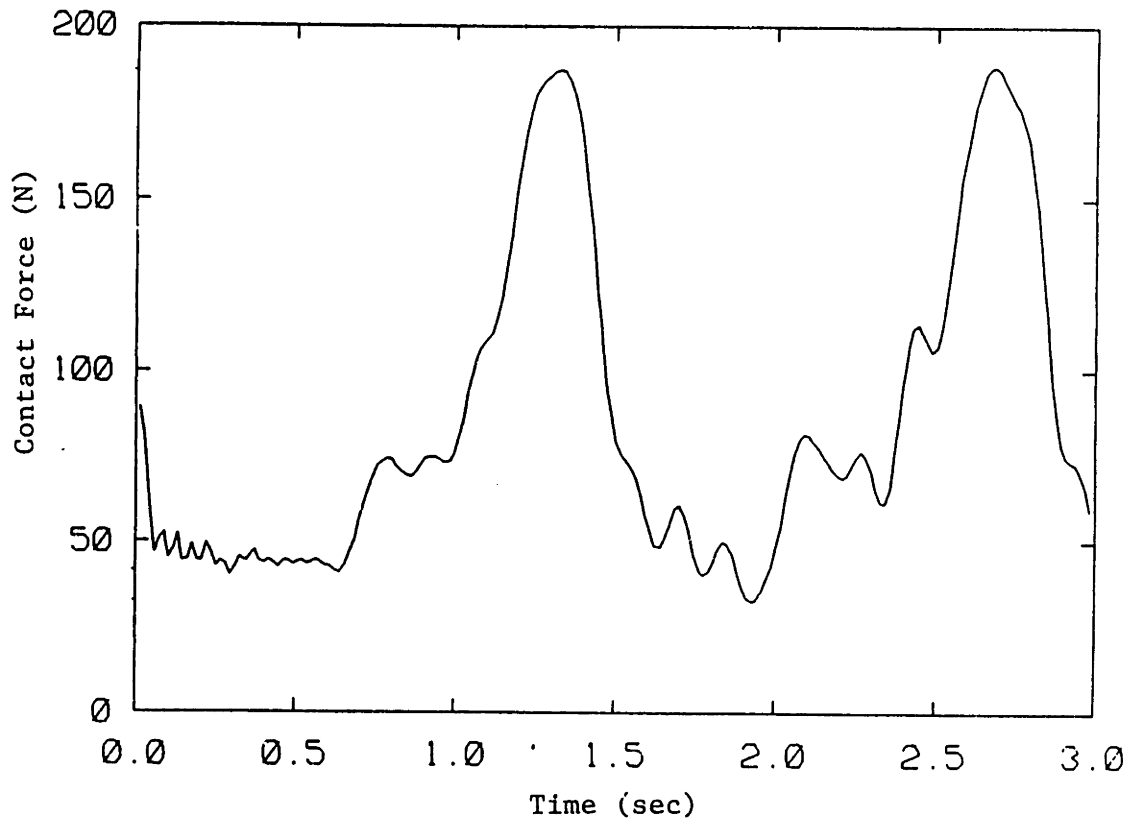
FIGURE 3.40:   CONTACT FORCE FOR FULL STATE
               FEEDBACK PANTOGRAPH, 170 km/hr
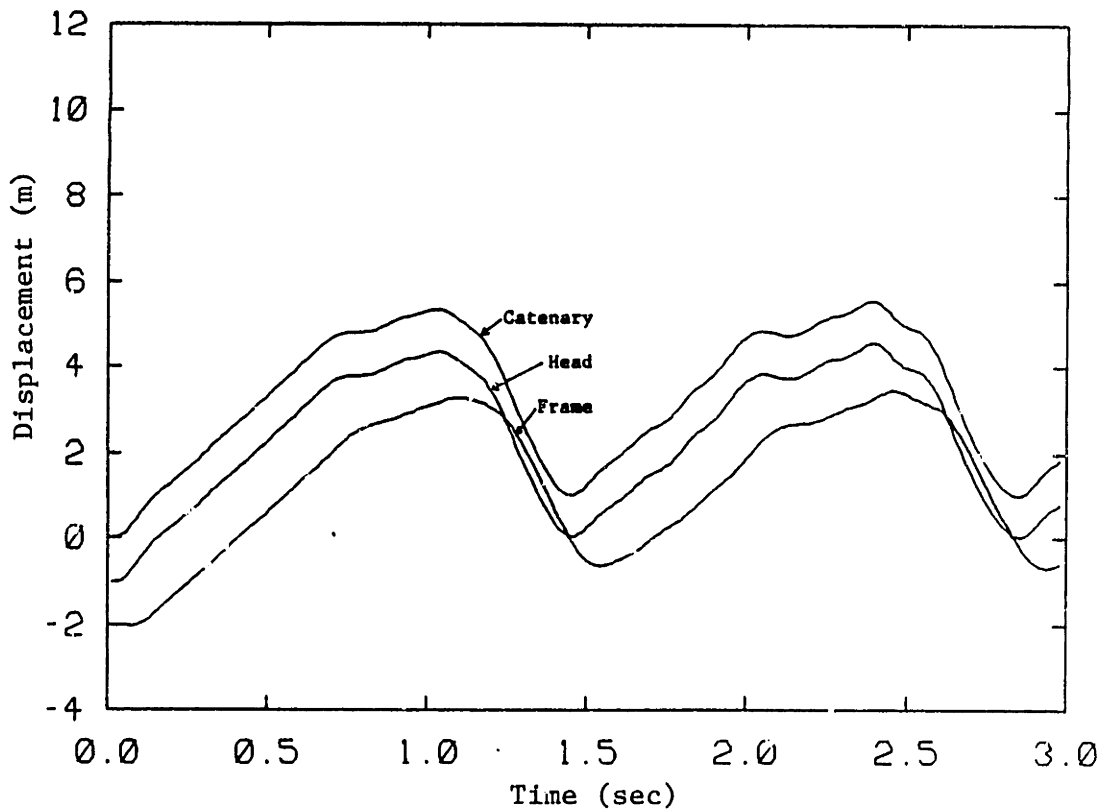
FIGURE 3.41:   DISPLACEMENT OF CATENARY, HEAD, AND
               FRAME vs. TIME, FULL STATE FEEDBACK
               PANTOGRAPH, 170 km/hr

damper, its effect can be included passively by increasing the value of frame damping. Head velocity is the most difficult measurement to make. Feeding it back only adds more damping to the frame. Since this measurement is the hardest to obtain accurately and contributes little to improved performance, it will be neglected. This leaves only two states that are measured, head and frame displacements. The schematic diagram of the controlled pantograph (Figure 3.39) is still valid. However, the control law is now simplified to:

$$F_{in} = C_1 y_H + C_3 y_F + F_{up}$$

Frame damping and control gains are varied and their resulting frequency responses studied. The more promising values are tested in the time simulation. To comply with the tunnel requirement, it was determined in section 3.4.5 that frame damping must not exceed $250 \frac{N \cdot s}{m}$. The restriction is observed here. The Riccati equation also recommends the position gains be equal in magnitude and opposite in sign to ensure that there is no static stiffness to ground. This condition is also adhered to. Since the gains are restricted to being of equal magnitude, only two parameters are varied, gain magnitude and frame damping. The smallest variation in contact force is achieved with gains of:

$$C_1 = -70,000 \text{ N/m}$$

$$C_2 = 0.0 \qquad \text{(no head velocity feedback)}$$

$$C_3 = 70,000 \text{ N/m}$$

$$C_4 = 0.0 \qquad \text{(frame velocity feedback replaced with damper)}$$

and a frame damping value of 250 $\frac{N \cdot s}{m}$. All other parameters are baseline

values; the parameters are summarized in Table 3.20.

Even though the gain on frame displacement, C_3, is effectively a

stiffness to ground, it cannot be replaced by a spring because of the

tunnel problem. To accomodate a one meter frame motion the actuator would

have to overcome a 70,000 N/m spring force; control forces of this mag-

nitude are unacceptably high. The controller gains are restricted to being

equal and opposite so the control law can be written as:

$$F_{in} = k(y_F - y_H) + F_{up}$$

where:

$$k = C_3 = -C_1$$

Both the head and frame are forced to move when a tunnel is ap-

proached. Since their difference is much smaller in magnitude than the

motion of either one, the control force will be kept at acceptable levels

if both displacements are fed back through equal and opposite gains.

Figure 3.42 compares the contact force for the active pantograph and

the baseline pantograph at 170 kph. Active control reduces contact force

fluctuations by 58%. Figure 3.43 shows the control force versus time.

The control force fluctuation is 132 N and its magnitude never exceeds

140 N. These forces are small and are well within the range of available

actuators. Table 3.21 gives the contact force fluctuations for the active

and baseline pantographs at several speeds. Minimum and maximum control

forces are also given for the active case.

TABLE 3.20

ACTIVE PANTOGRAPH PARAMETERS

Head Mass:	9.1 kg	20 lb
Frame Mass:	17.2 kg	38 lb
Stiffness of Pantograph Shoe:	82.3 kN/m	470 lb/in
Stiffness Between Head and Frame:	7,000 N/m	40 lb/in
Damping Between Head and Frame:	$130 \frac{N \cdot s}{m}$	0.743 lb sec/in
Damping Between Frame and Ground:	$250 \frac{N \cdot s}{m}$	1.43 lb sec/in
Uplift Force:	90 N	20.2 lb
Control Gains:		
c_1	$-70,000 \frac{N}{m}$	-400 lb/in
c_2	0.0	0.0
c_3	$70,000 \frac{N}{m}$	400 lb/in
c_4	0.0	0.0
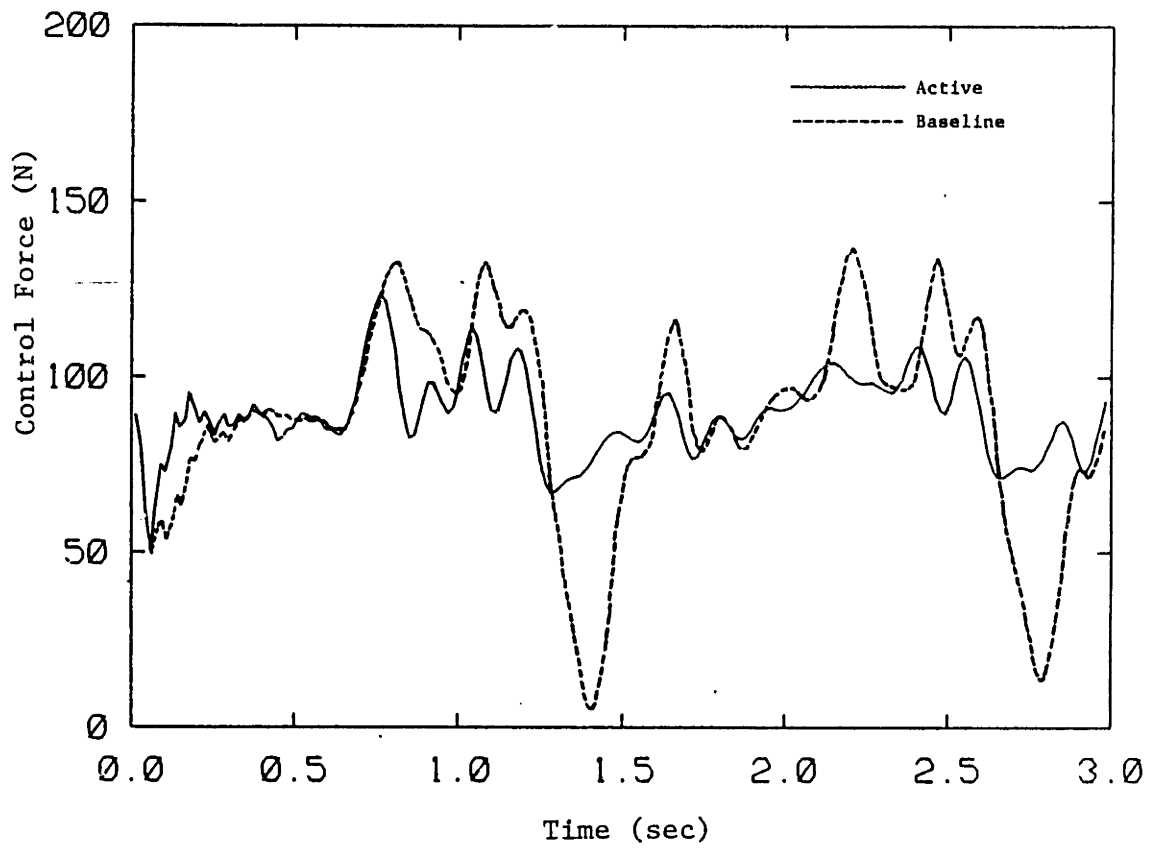
FIGURE 3.42: CONTACT FORCE COMPARISON FOR ACTIVE
AND BASELINE PANTOGRAPH, 170 km/hr
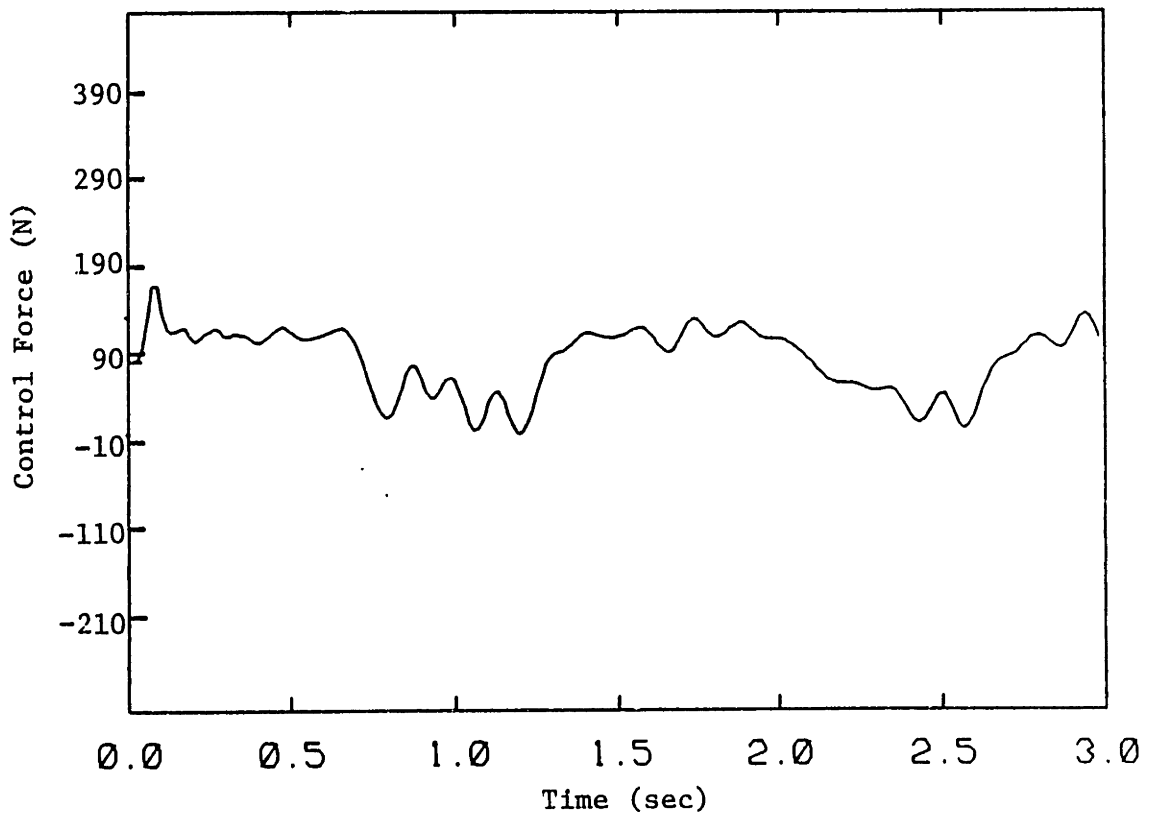
FIGURE 3.43: CONTROL FORCE FOR ACTIVE PANTOGRAPH,
170 km/hr

-99-

TABLE 3.21

CONTACT FORCE VARIATION FOR ACTIVE AND BASELINE PANTOGRAPHS

Speed	ΔF, Passive System	ΔF, Active System	Maximum Control Force	Minimum Control Force
135 km/hr	54.7 N	25.9 N	127.5 N	40.0 N
170 km/hr	130 N	54.7 N	140 N	8.75 N
225 km/hr	Loss of Contact	128 N	203 N	-110 N

Active control performs better at all speeds.

Active simulations were also made under the baseline catenary with 8 cm of sag. Runs were made at velocities of 220 km/hr and 250 km/hr. The contact force variations are 64.8 N and 110 N respectively.

In section 3.4.2 it was shown that a reduced head spring rate improved performance. Table 3.22 gives the parameters for an active pantograph with the best heat suspension parameters. Figure 3.44 compares the contact force variation for the active pantograph with the best head suspension with the optimum passive pantograph from section 3.5 at 170 km/hr. The active system has 25% smaller contact force variation. Table 3.23 compares the best active and passive systems at different speeds.

TABLE 3.23

CONTACT FORCE VARIATION FOR ACTIVE AND OPTIMUM PANTOGRAPH

Speed	ΔF, Passive System	ΔF, Active System	Maximum Control Force	Minimum Control Force
135 km/hr	48.4 N	25.0 N	131 N	40.0 N
170 km/hr	72.6 N	54.7 N	146 N	2.50 N
225 km/hr	119 N	120 N	221 N	-119 N

TABLE 3.22

ACTIVE PANTOGRAPH WITH IMPROVED HEAD SUSPENSION

Head Mass:	91 Kg	20 lb
Frame Mass:	17.2 Kg	38 lb
Stiffness of Pantograph Shoe:	82.3 KN/m	470 lb/in
Stiffness Between Head and Frame:	3,500 N/m	20 lb/in
Damping Between Head and Frame:	$100 \frac{N \cdot s}{m}$	0.572 lb sec/in
Damping Between Frame and Ground:	$250 \frac{N \cdot s}{m}$	1.42 lb sec/in
Uplift Force:	90 N	20.2 lb

Control Gains

c_1	-70,000 N/m
c_2	0.0
c_3	70,000 N/m
c_4	0.0
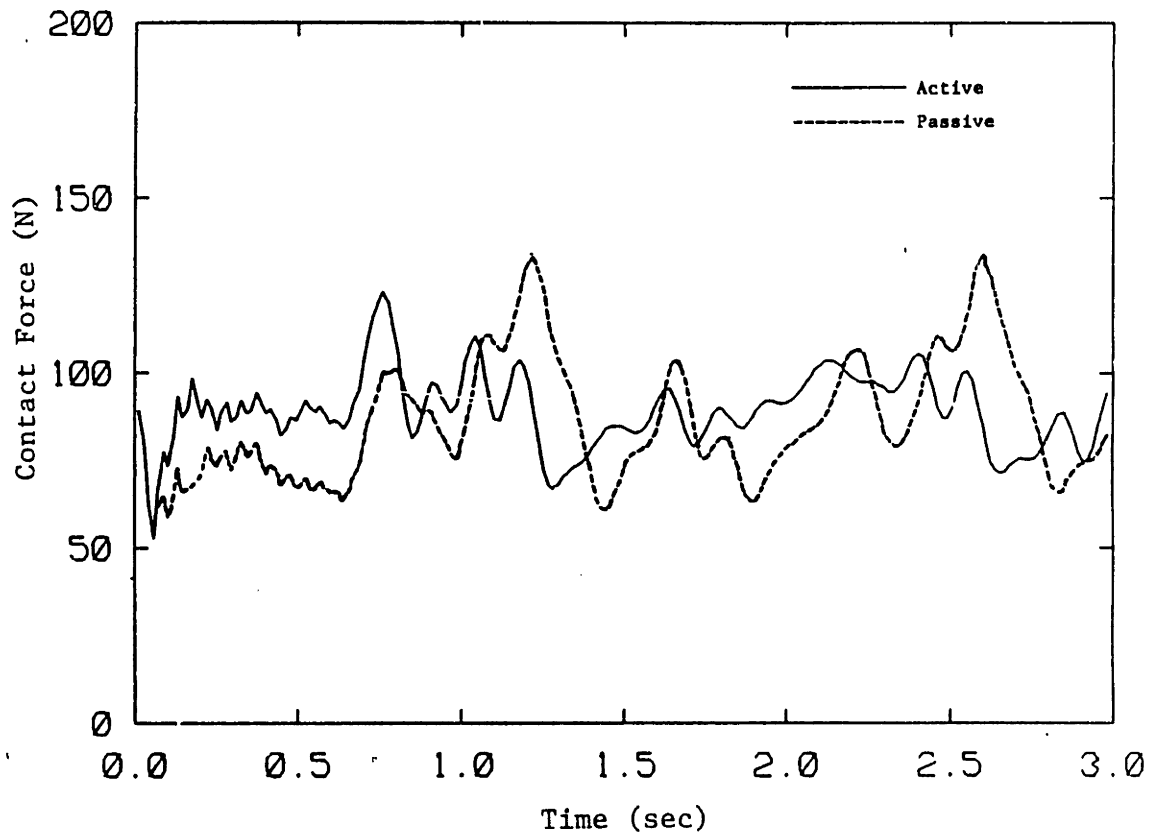
FIGURE 3.44:   CONTACT FORCE COMPARISON OF BEST PASSIVE
AND BEST ACTIVE SYSTEM, 170 km/hr

The active pantograph performs much better at low and intermediate speeds. At higher speeds, however, performance for the optimized-passive pantograph and the active pantograph are about the sane.

3.7 Two Pantograph Simulation

The system model is capable of running two arbitrarily spaced pantograph under the same catenary to test the case where two pantographs are mounted on the same train. In this section two baseline pantographs are run under the baseline catenary at 150 km/hr. They are spaced five passenger car lengths apart (130 m).

Figures 3.45 through 3.51 show the time history of the contact wire shape at 0.1 second intervals. The first shape given is at t = 2.6 sec, 0.5 sec before the second pantograph comes on line; it shows that the catenary is vibrating with a peak to peak amplitude of 3.5 cm. Figure 3.47 shows both the first and second pantographs moving toward the center of their respective spans. The catenary's displacement by the first pantograph is nearly linear. However, the second pantograph displaces the catenary in a more uneven manner. The less uniform response is due to the catenary's vibrations caused by the first pantograph. Figure 3.48 shows both pantographs as each approaches the end of their spans; the catenary's descent is much less uniform for the second pantograph.

Figures 3.52 and 3.53 show the displacement plots for the first and second pantographs respectively. The displacement plot for the first pantograph rises and descends fairly smoothly. However, for the second
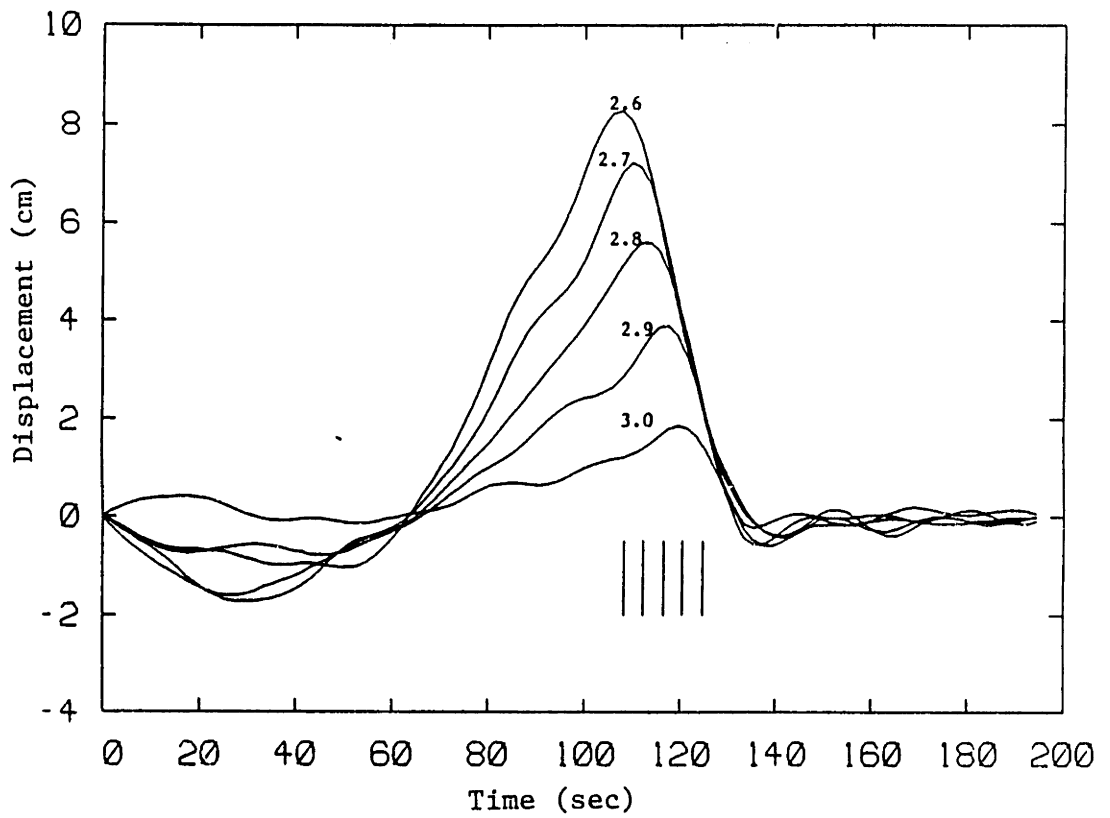
FIGURE 3.45: CATENARY SHAPE FOR TWO PANTOGRAPH CASE
2.6 TO 3.0 SECONDS
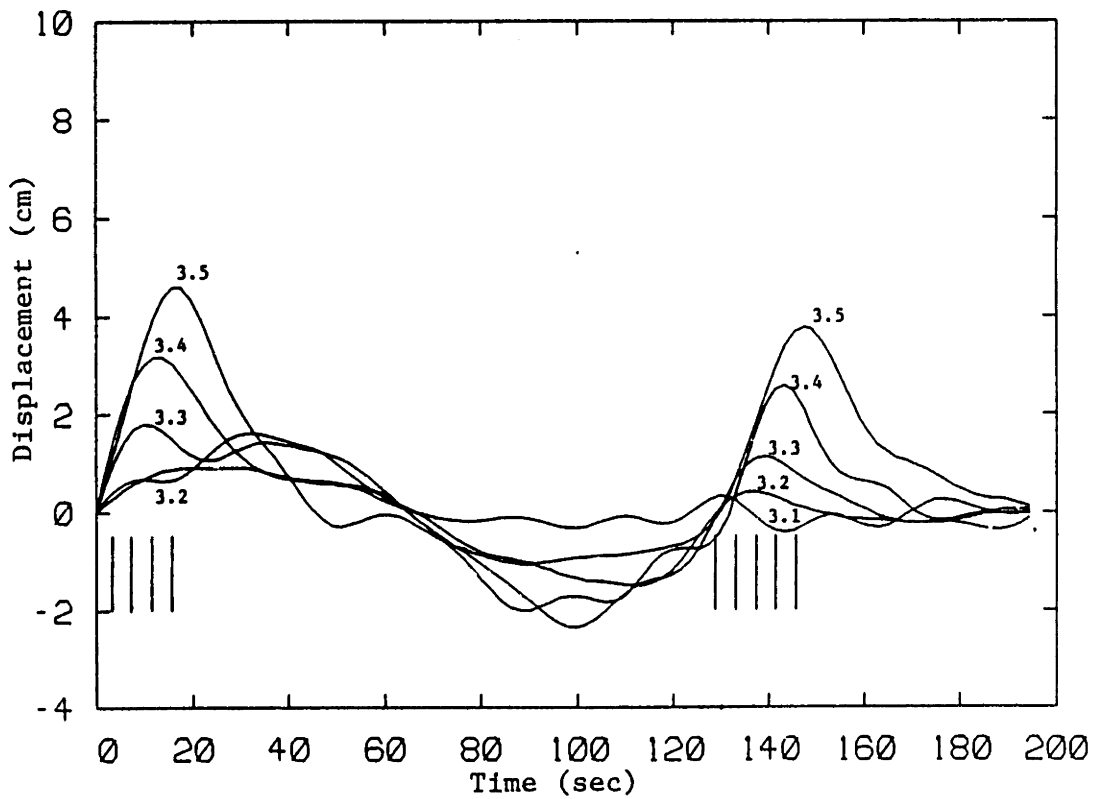
FIGURE 3.46: CATENARY SHAPE FOR TWO PANTOGRAPH CASE
3.1 TO 3.5 SECONDS

-104-
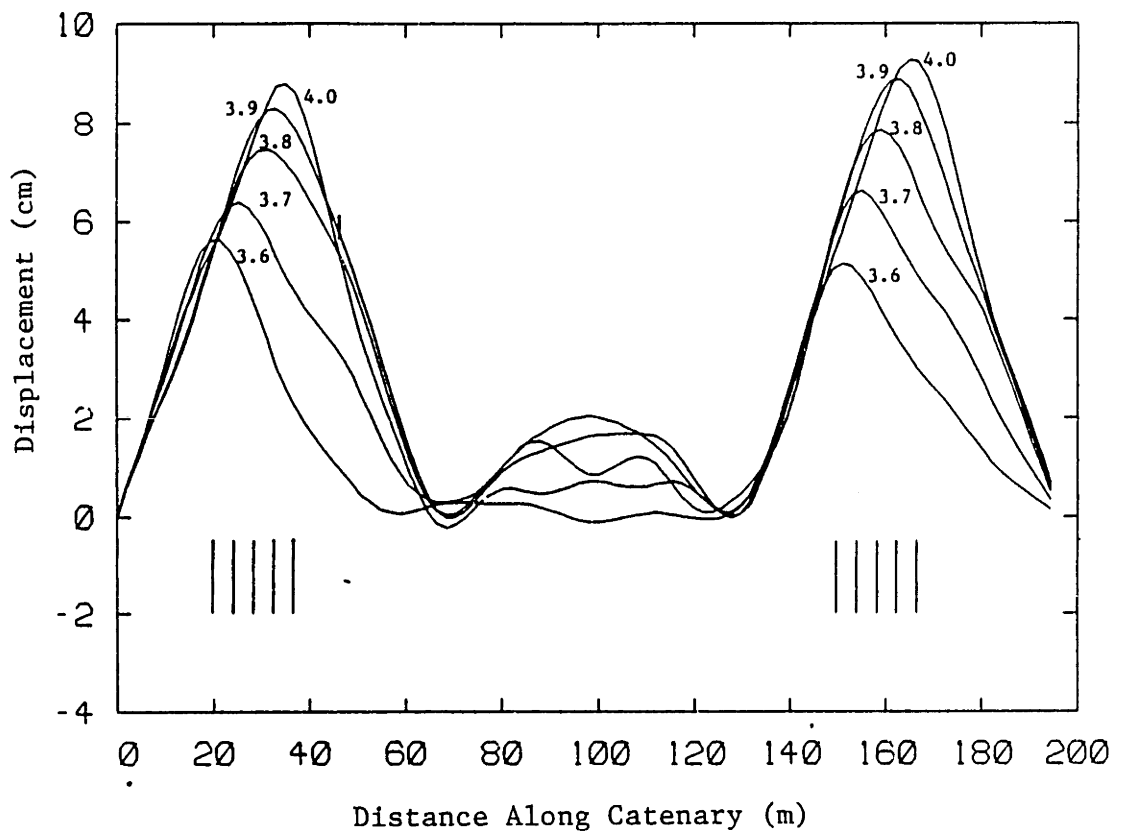
FIGURE 3.47: CATENARY SHAPE FOR TWO PANTOGRAPH
CASE 4.1 TO 4.5 SECONDS
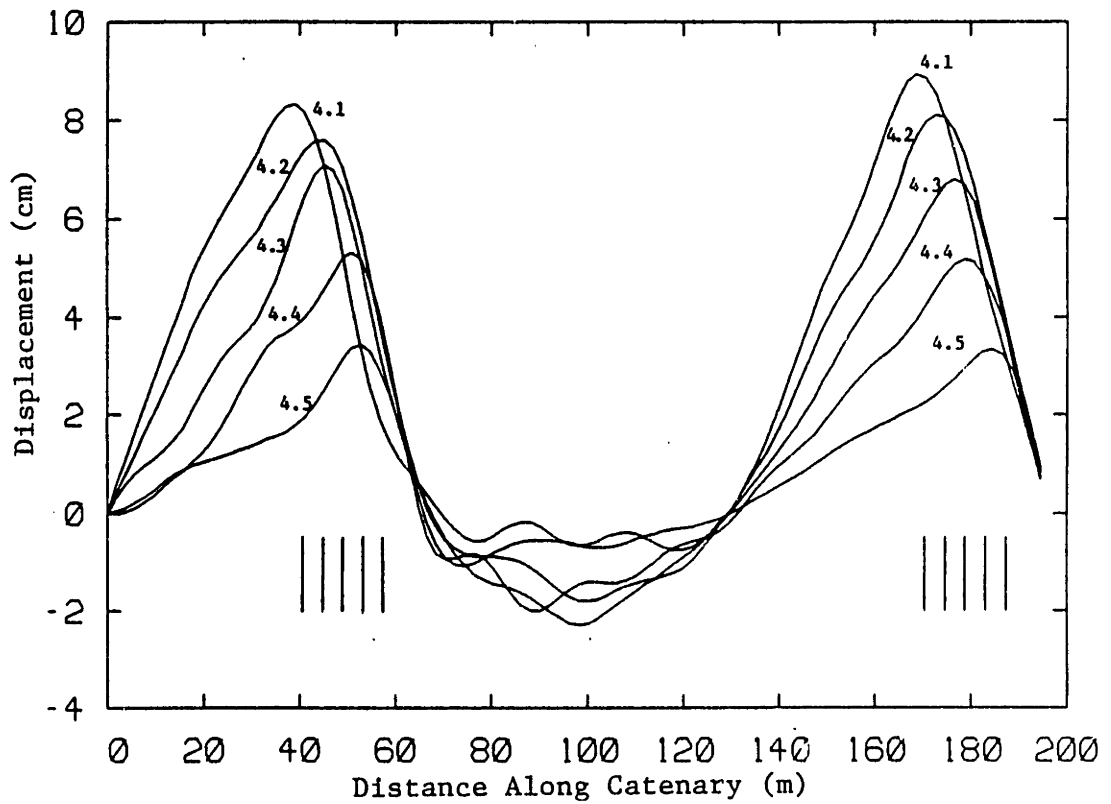
FIGURE 3.48: CATENARY SHAPE FOR TWO PANTOGRAPH
CASE 4.1 TO 4.5 SECONDS
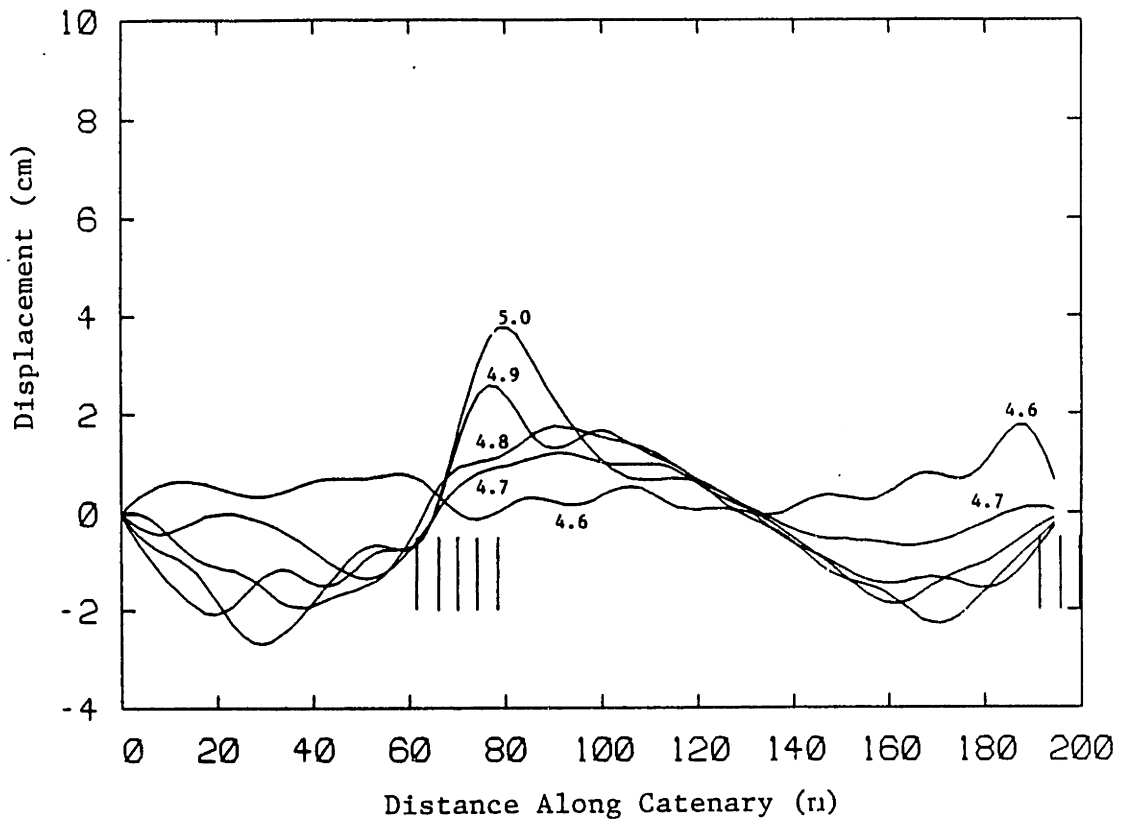
FIGURE 3.49: CATENARY SHAPE FOR TWO PANTOGRAPH
CASE 4.6 TO 5.0 SECONDS
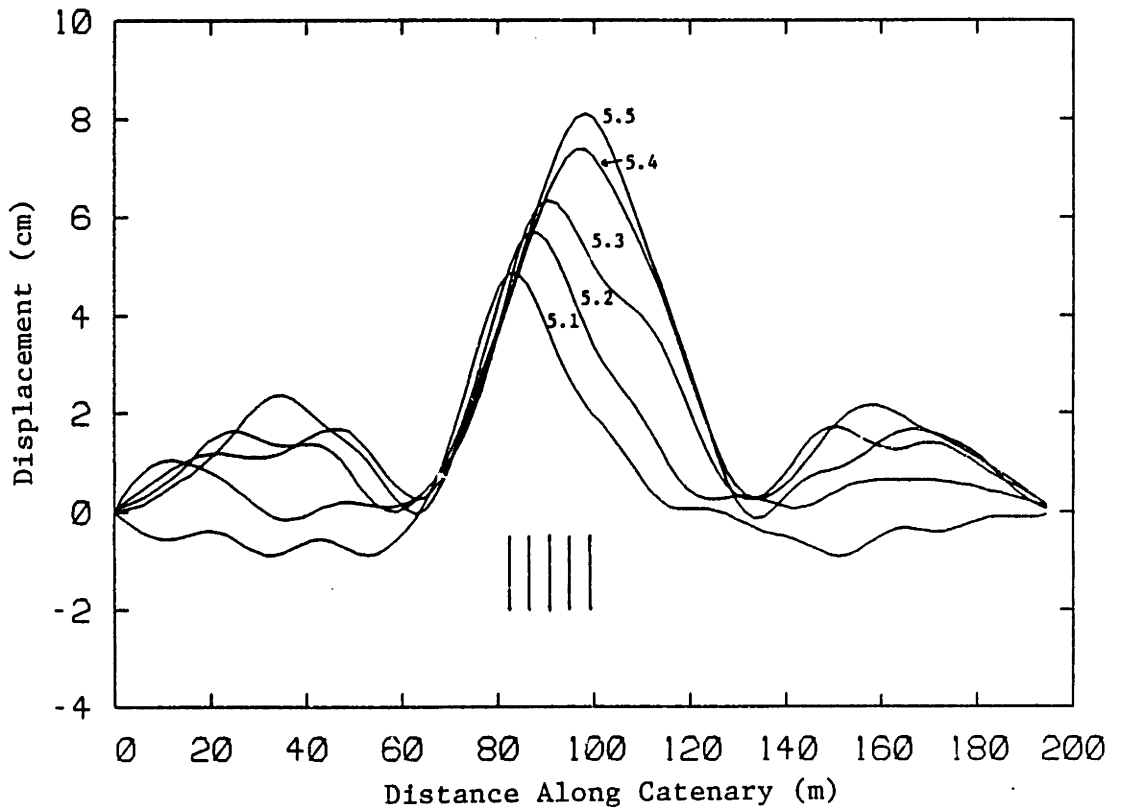
FIGURE 3.50: CATENARY SHAPE FOR TWO PANTOGRAPH
CASE 5.1 TO 5.5 SECONDS
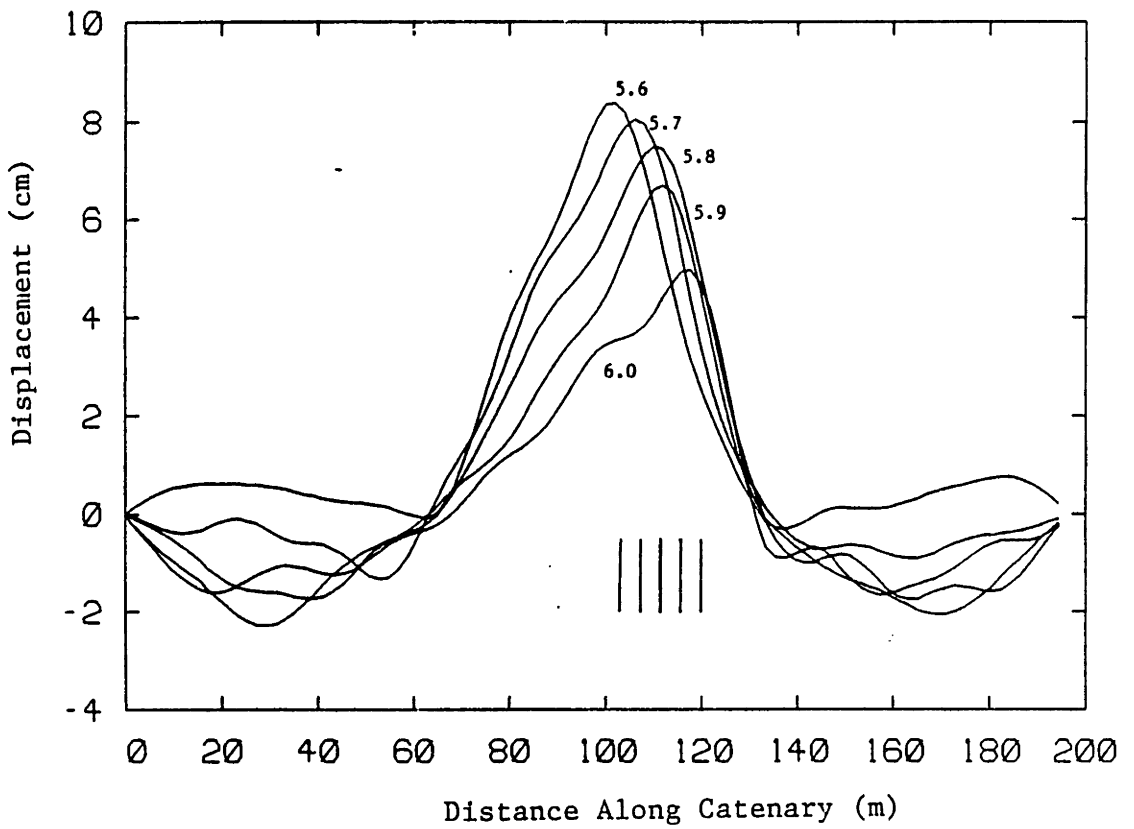
FIGURE 3.51: CATENARY SHAPE FOR TWO PANTOGRAPH CASE
5.6 TO 6.0 SECONDS
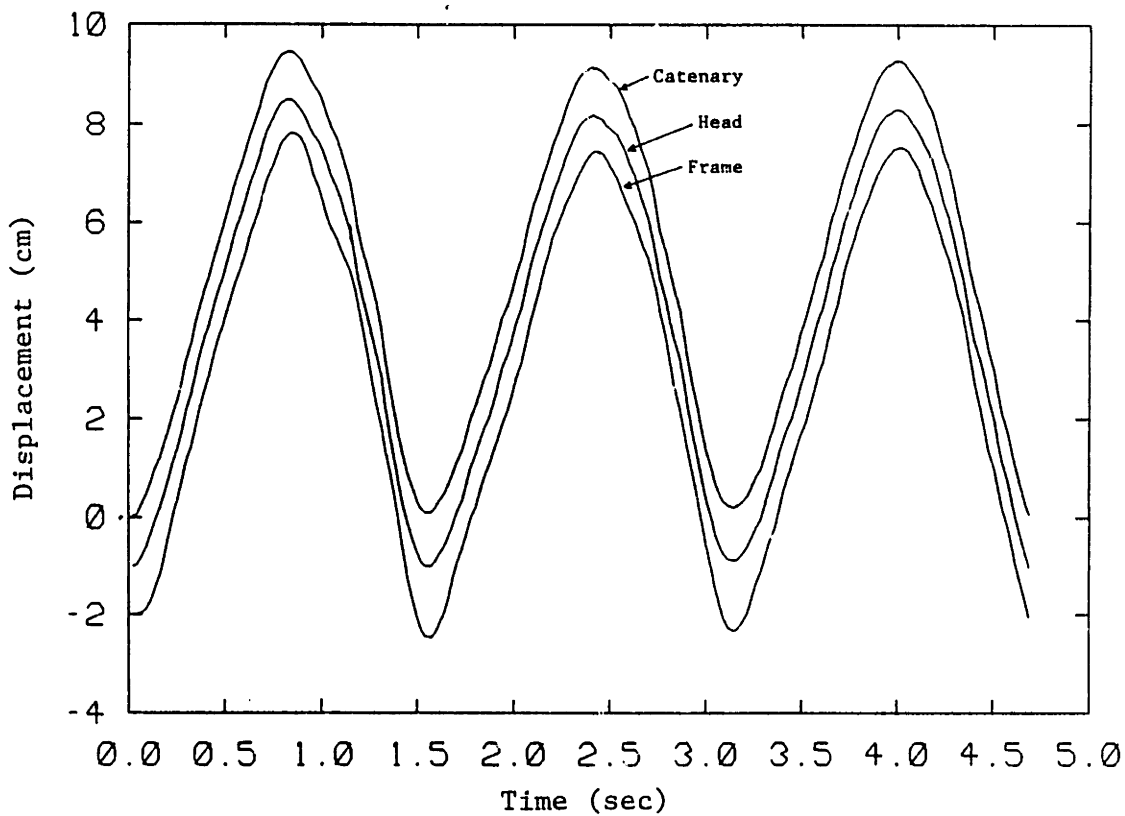
FIGURE 3.52:   DISPLACEMENT OF CATENARY, HEAD,
AND FRAME vs. TIME.   FIRST PANTOGRAPH
FOR TWO PANTOGRAPH CASE
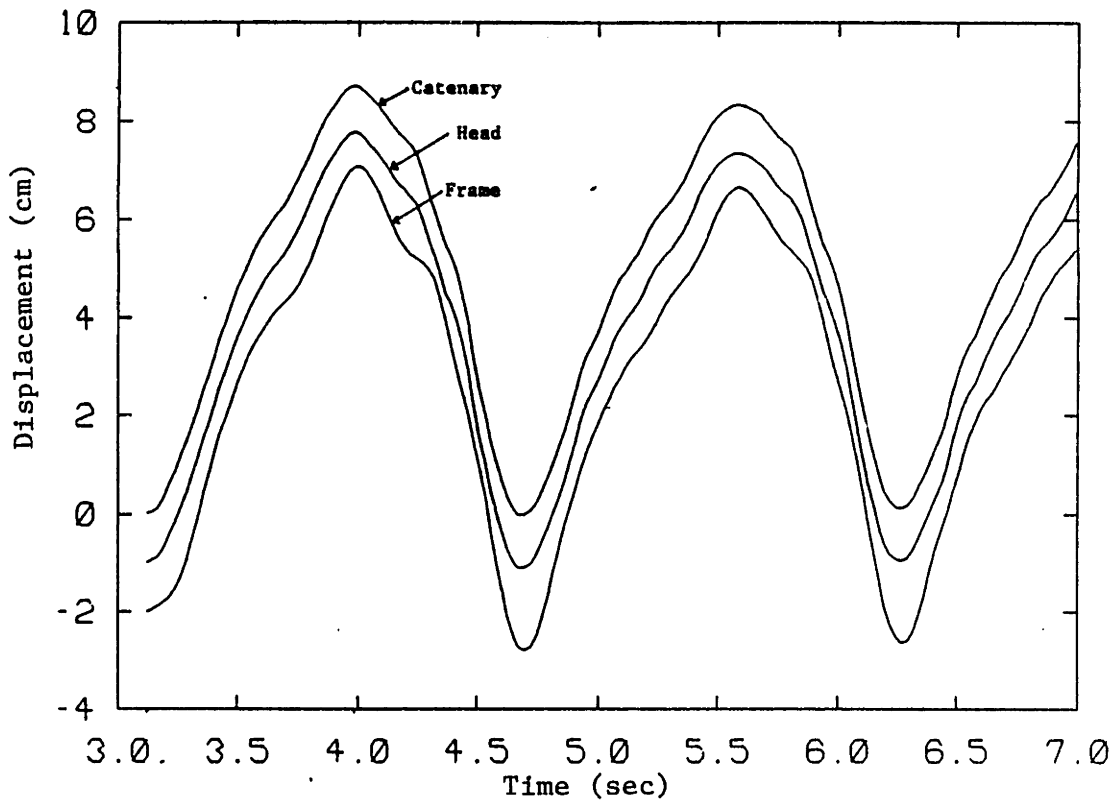
FIGURE 3.53:   DISPLACEMENT OF CATENARY, HEAD,
AND FRAME vs. TIME.   SECOND PANTOGRAPH
FOR TWO PANTOGRAPH CASE

-108-

pantograph, displacements do not change as uniformly. Catenary vibrations have a noticeable effect on the head trajectory. The maximum displacement for the second pantograph is nearly one centimeter less than for the first. The smaller displacement is due to the catenary vibrating in the downward direction when the pantograph reaches its peak displacement.

Contact force plots for both pantographs are given in Figures 3.54 and 3.55. Peaks and troughs in contact force occur in the same locations along the catenary. However, the magnitude of these fluctuations are larger for the second pantograph. Contact force fluctuation is 27% higher for the second pantograph. The increase in size of fluctuations is due to the difficulty the pantograph has in tracking the catenary's vibrations.
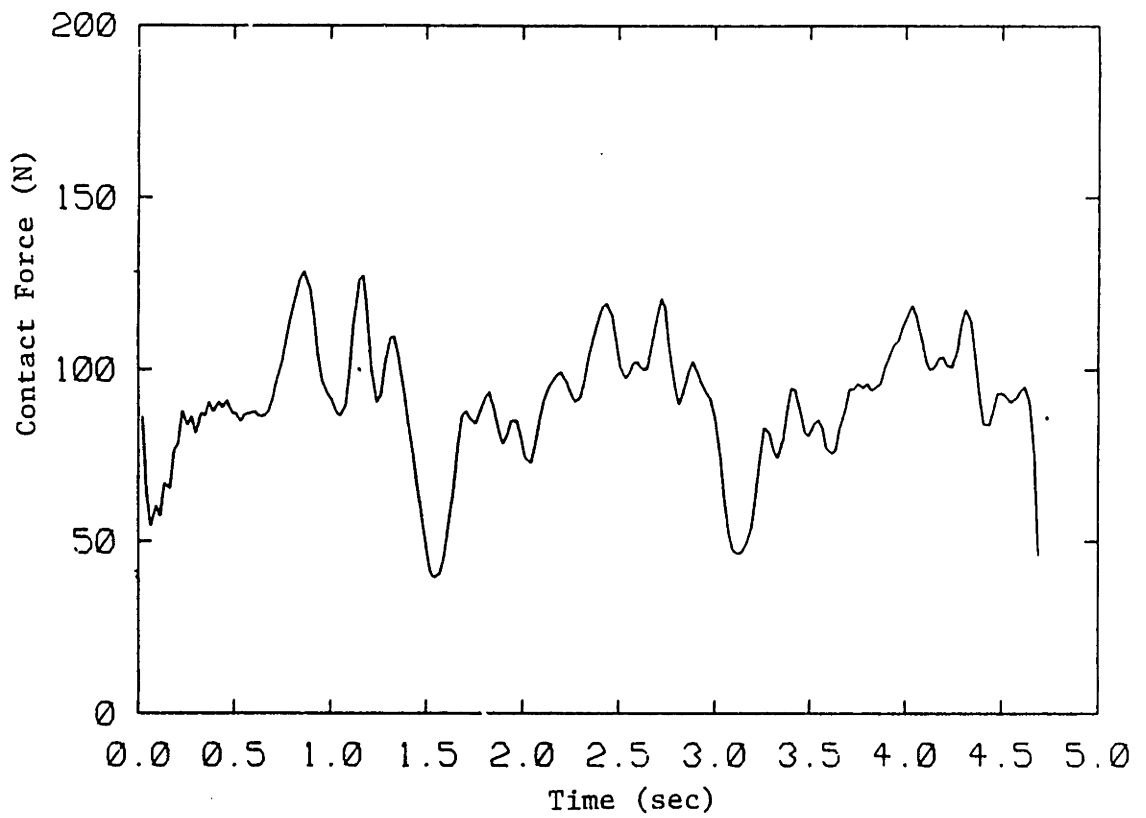
FIGURE 3.54:   CONTACT FORCE vs. TIME
               FIRST PANTOGRAPH FOR TWO PANTOGRAPH CASE
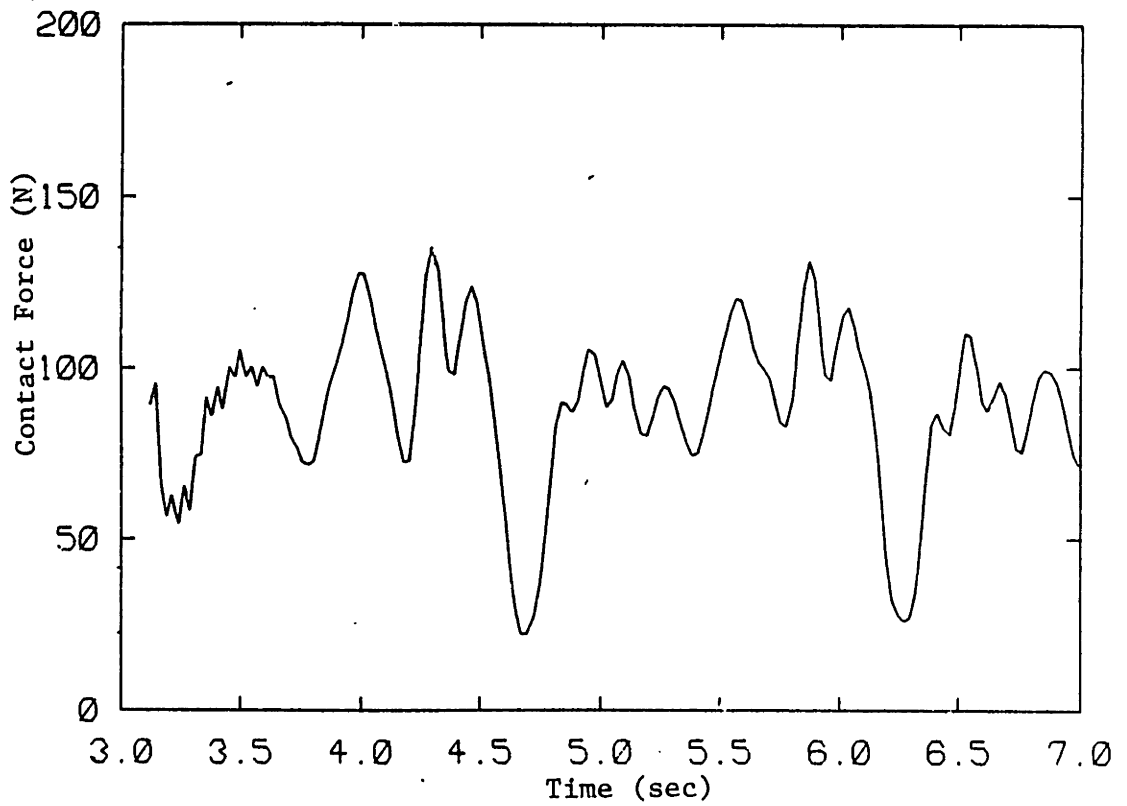
FIGURE 3.55:   CONTACT FORCE vs. TIME
               SECOND PANTOGRAPH OF TWO PANTOGRAPH CASE

-110-

CHAPTER 4

CONCLUSION

In this research, two analytical models were developed to describe the dynamics of pantograph-catenary systems. The first was a time-domain simulation of one or two pantographs traveling under a catenary. The second was a frequency-response simulation for the pantograph. These models were used to evaluate the dynamic effects of alternate catenary materials, to investigate the influence of pantograph parameters on performance, and to evaluate new pantograph configuration.

Rising copper costs have increased interest in all-aluminum catenaries. Besides reducing material costs, results showed aluminum catenaries offer substantial performance improvement. Contact force variation at 170 km/hr for the aluminum catenary was 51% lower than the copper contact wire catenary. Loss of contact occurred at 260 km/hr for aluminum as opposed to 175 km/hr for the baseline case. Catenary vibrations that occur after the pantograph has passed were much smaller for the aluminum case. An aluminum catenary's ability to dissipate energy at a faster rate may make it more suitable for applications where two pantographs are run under the same catenary. The wear rate for aluminum, however, is higher than coppers.

A small amount of catenary sag was found to improve performance. The catenary is most compliant at the center of a span. As the pantograph moves toward midspan it attempts to overcome the sag by moving the cable up, it encounters inertial resistance which increases the

apparent stiffness of the catenary. Proper sag reduces the pantograph

vertical gross motion and the vertical momentum developed. Smaller

vertical momentum yields smaller contact force fluctuations. A desirable

value of sag was found to be 80% of the maximum catenary displacement

for the zero sag case.

In this study the influence of pantograph parameters on performance

was investigated. It is generally agreed that reducing pantograph head

mass improves performance. Keeping the frame mass small also was shown

to be equally important. A soft head suspension was also found to improve

performance. Halfing the head spring rate to 3500 N/m reduced the

contact force variation by 13%. Increased damping also yielded performance

improvements. When head damping was increased from 130 N·s/m to 500 N·s/m

contact force fluctuation dropped 8.3%. Doubling frame damping to 60 N·s/m

resulted in a 8.3% performance improvement.

There are two suspension types that currently dominant pantograph

design. One uses springs in combination with a cam or link system to

provide a constant uplift force. The other uses a pneumatic cylinder

to provide uplift force. The suspension parameters that yielded the

best performance for each design were found and then compared with each

other. At 170 km/hr the pneumatic suspension's contact force variation

was 30% lower than the spring suspension's.

Using results from the parameter and suspension studies, an optimal

set of pantograph parameters was formed. At 170 km/hr the optimum panto-

graph contact force variation was 44% lower than the baseline case. Most

of the improvement was due to differences in the frame suspensions.

Using modern control techniques, a frame-actuated, active controller was designed. The control force is a function of the head and frame displacement. The active pantograph contact force variation was 58% lower than the baseline case and 25% less than the optimum passive pantograph at 170 km/hr. However, as speed increases performance for the optimum passive pantograph and the active pantograph became similar.

Several references give the maximum speed a train should travel as 30% to 40% of the catenary wave speed. With an improved pantograph this design speed can be raised. Simulations have been made as high as 53% of the catenary wave speed with an active pantograph under a sagging catenary. At this speed the pantograph maintained an acceptable contact force at all times. It was found that pantographs could be successfully run at 50% of the wave speed.

Simulations were made with two pantographs running under the same catenary. Catenary vibrations caused by the first pantograph make it more difficult for the second pantograph to maintain contact. The second pantograph experiences higher frequency inputs than the first pantographs. Since the second pantograph received different frequency inputs, characteristics of a good first pantograph may not necessarily describe best second pantograph. Parameter and configuration studies should be done on the second pantograph to determine the optimum design.

APPENDIX A

CATENARY MODEL DEVELOPMENT[1]

This appendix develops the equations of motion and the natural modes
for a simple style, two wire catenary.

A.1 Modal Analysis Review

A system of n degrees of freedom has n natural modes. Associated with
each mode is a natural frequency, ω, and a natural mode shape, ϕ. The mode
shapes of a dynamic linear system are orthogonal and therefore system dis-
placements can be expressed as a sum of the natural modes multiplied by
appropriate, time-varying modal amplitudes, or modal response functions, a
technique known as modal decomposition. [Ref. 29, 30]

$$y(x,t) = \Sigma \; \phi_i(x) \; z_i(t) \qquad (A.1)$$

where

$y(x,t)$ = the time varying displacement of the system

$\phi_i(x)$ = the ith natural mode shape

$z_i(t)$ = the modal amplitude of the ith mode

i = the mode number

The mode shape, ϕ, depends only upon position; and the modal amplitude,
z, depends only upon time. When a system is excited in a natural mode,
the system and all the system elements, maintain the same relative
displacements to each other, and the mode shape describes this relation.

_____

[1]The pantograph-catenary model derivation presented here first appeared
in Armbruster [17]. The derivation has been modified to include the
following new effects: catenary sag, a full state feedback controller
for the pantograph, the ability to run two pantographs under the same
catenary, and a choice of two frame suspensions: a spring and damper in
parallel or a spring and damper in series. Some changes have also been
made to the text to correct errors and make the presentation clearer.

Once the mode shapes are known, the dynamics of the system are determined by the amplitudes, $z(t)$.

The benefit of separating the motion into modal components is the modes may be considered independently and the equations reduce to simple, linear, second order, differential equations of the form:

$$M_i \ddot{z}_i(t) + C_i \dot{z}_i(t) + K_i z_i = Q_i \qquad (A.2)$$

where

z_i = the ith modal amplitude

M_i = the modal mass of the ith mode

C_i = the modal damping of the ith mode

K_i = the modal stiffness of the ith mode

Q_i = the forcing function of the ith mode

The modal mass, M_i, is defined by

$$M_i = \int_0^\ell \rho \, \phi_i^2 \, dx \qquad (A.3)$$

where ρ is the lineal density.

The modal damping is defined by equation (A.4) and must be distributed proportional to the mass to ensure orthogonality of the modes.

$$C_i = \int_0^\ell c(x) \, \phi_i^2 \, dx \qquad (A.4)$$

where $c(x)$ is the damping (distributed proportional to mass)

The modal stiffness, K_i, is given by

$$K_i = \int_0^\ell k(x) \, \phi_i^2 \, dx \qquad (A.5)$$

where $k(x)$ represents the spring constants and effective stiffnesses along the length.

The forcing function, Q_i is:

$$Q_i(t) = \int_0^\ell f(x,t) \, \phi_i \, dx \qquad \text{(A.6)}$$

where $f(x,t)$ is the applied force (time and position varying). The natural frequency of the system when vibrating in the ith mode is given by equation and follows from the natural frequency of a simple system as:

$$\omega_i = \sqrt{K_i/M_i} \qquad \text{(A.7)}$$

An efficient way to express equation (A.2) is in terms of the natural frequency, the damping ratio and the modal mass as:

$$M_i \ddot{z}_i(t) + 2M_i \xi_i \omega_i \, \dot{z}_i(t) + M_i \omega_i^2 \, z_i(t) = Q_i \qquad \text{(A.8)}$$

Once the mode shapes and frequencies are known, the time response of each mode is determined by equation (A.8) and the total system response is determined by applying equation (A.1) and summing up the individual responses.

A.2 Catenary Model Description

The response of the catenary is determined by writing the displacement of each wire as a Fourier sine-series expansion. The equations of motion are derived using the amplitudes of the sine terms and Lagrange's method, and are used to obtain the natural frequencies and natural mode shapes of the catenary. Using these modes the equations for the catenary are written in modal form along with the equation for a pantograph model. These equations are solved

-116-

using a fourth-order Runge-Kutta numerical integration routine.

The model of the catenary is shown in Figure A.1, and incorporates the following features:

- Simple Catenary with a contact wire and a messenger wire.

- Variable spacing allowed between the towers and between the droppers.

- Contact and support wires are each modeled with a bending stiffness, constant tension, and a uniform density.

- Damping distributed proportional to the mass of the wires to ensure orthogonality of the modes.

- The two wires are connected by droppers. These are modeled as massless springs, K_1 through K_p.

- The mass of the droppers is not directly included but is modeled by distributing it evenly along, and equally between the two wires.

- The top wire is connected to flexible towers modeled as springs S_1 through S_Q.

- The ends of both wires must have zero displacement but are allowed to have any angle

- A constant gravitational force can be applied to the catenary to induce a desired amount of sag.

- The ability for more than one pantograph to travel under the catenary.

A.3 Catenary Equation Development

Using Fourier analysis the shape of a finite length, L, can be represented in terms of a sum of both sine and cosine terms, each term with an appropriate amplitude. For the catenary, let $y(x,t)$ describe the displacement of the catenary wire, both as a function of position, x, and of time, t. The boundary conditions require zero displacements of the two ends ($x=0$ and $x=L$); therefore, no cosine terms
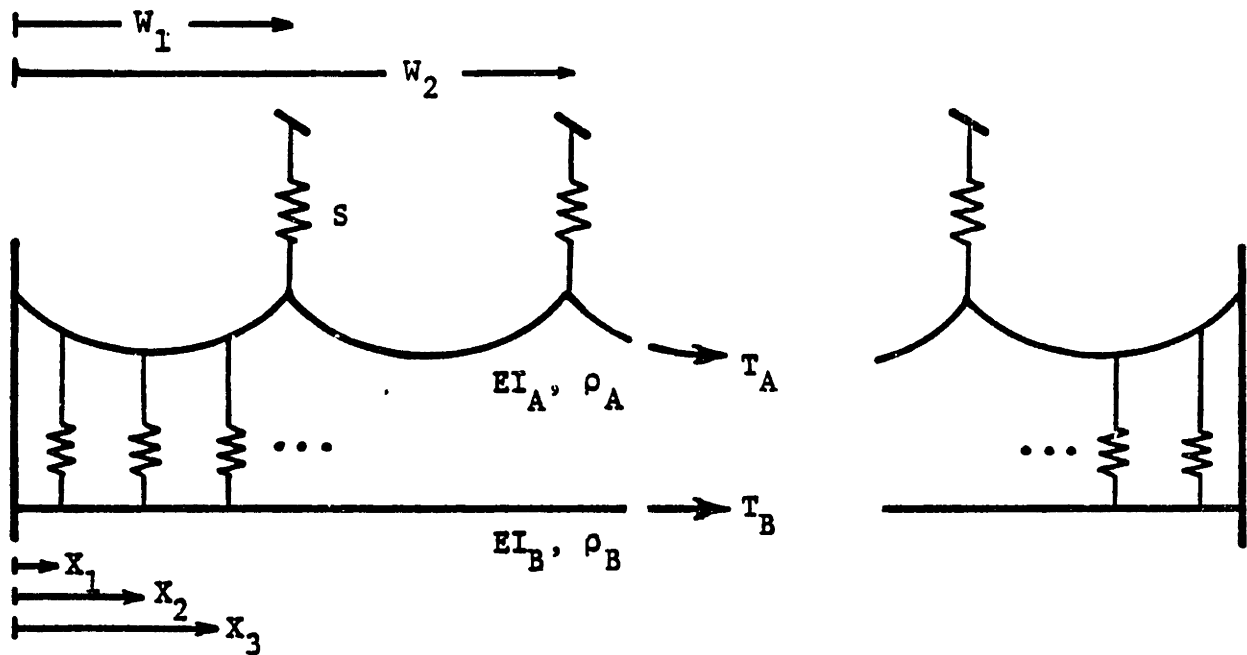
Tower Stiffness: S

Dropper Stiffness: K

Distance to the jth Tower: W_j

Distance to the ith Dropper: X_i

Stiffness of the Two Wires: EI_A, EI_B

Density of the Two Wires: ρ_A, ρ_B

Tension in the Two Wires: T_A, T_B

FIGURE A.1: CATENARY MODEL

may exist. The two wires, the contact and the support wire, are written

separately and as functions of sine terms only as:

$$y_A(x,t) = \sum_m A_m(t) \sin(\frac{m\pi x}{L}) \qquad \text{Upper Wire} \qquad (A.9a)$$

$$y_B(x,t) = \sum_m B_m(t) \sin(\frac{m\pi x}{L}) \qquad \text{Lower Wire} \qquad (A.9b)$$

where

y_A = the displacement of the upper wire

y_B = the displacement of the lower wire

A_m = the amplitude of the mth sine term for the upper wire

B_m = the amplitude of the mth sine term for the lower wire

x = the distance along the catenary

L = the total length of the catenary

m = an integer. Designates the harmonic number.

The shape of these wires is time varying, therefore, the amplitudes A_m

and B_m are time varying and can be written $A_m(t)$ and $B_m(t)$. Since they

describe the shape of the whole catenary at all times the amplitudes can

be used to write the equations of motion for the catenary, and obtain the

natural modes of the catenary.

The catenary equations are developed using a Lagrange formulation.

Each sine wave is an admissable motion, and the amplitudes provide a

sufficient and convenient set of generalized coordinates.

To use Lagrange's method the expression for the kinetic coenergy[+]

and the potential energy are written in terms of the generalized

coordinates. The kinetic coenergy, T^*, for a lumped system is:

[+]For a linear system the kinetic coenergy equals the kinetic energy.

$$T^* = 1/2 \; Mv^2 \qquad (A.10)$$

Or, for a continuous system

$$T^* = 1/2 \int_{x=0}^{\ell} \rho \, \dot{y}^2 \, dx \qquad (A.11)$$

and for the two wires of the catenary:

$$T^* = 1/2 \int_{0}^{\ell} \rho_A \dot{y}_A^2 + \rho_B \dot{y}_B^2 \, dx \qquad (A.12)$$

Differentiating equation (A.9) with respect to time yields:

$$\dot{y}_A = \sum_m \dot{A}_m \sin\left(\frac{m\pi x}{L}\right) \qquad (A.13a)$$

$$\dot{y}_B = \sum_m \dot{B}_m \sin\left(\frac{m\pi x}{L}\right) \qquad (A.13b)$$

Inserting these equations into Equation (A.12):

$$T^* = 1/2 \int_{0}^{\ell} \rho_A \left[\sum_m \dot{A}_m \sin\left(\frac{m\pi x}{L}\right)\right]^2 + \rho_B \left[\sum_m \dot{B}_m \sin\left(\frac{m\pi x}{L}\right)\right]^2 dx \qquad (A.14)$$

Evaluating the integral gives the final result for the kinetic co-energy:

$$T^* = \frac{\rho_A L}{4} \sum \dot{A}_m^2 + \frac{\rho_B L}{4} \sum \dot{B}_m \qquad (A.15)$$

The potential energy of the system equals the sum of all the potential energies. They are: the tension in the wires, the bending of the wires, the displacement of the dropper springs, and the displacement

-120-

of the tower springs:

$$V = V_{TEN} + V_{BEND} + V_{DROP} + V_{TOW} \qquad (A.16)$$

where

V = the total potential energy

V_{TEN} = the potential energy due to the tension in wires

V_{BEND} = the potential energy due to the bending stiffness

V_{DROP} = the potential energy due to the dropper springs

V_{TOW} = the potential energy due to the tower springs

In general the potential energy is the integral of force, f, and dis-placement, r.

$$V = \int_{0}^{r} f \cdot dr \qquad (A.17)$$

For the potential energy due to tension, V_{TEN} is the integral along the length of the cable of the incremental potential energy, δV_{TEN}:

$$V_{TEN} = \int_{0}^{\ell} \delta V_{TEN} \qquad (A.18)$$

where

$$V_{TEN} = T(dS - dx) \qquad (A.19)$$

dx = free length of wire

dS = length of displaced wire

T = tension in wire

-121-

A diagram of an element of a displaced wire is given below:
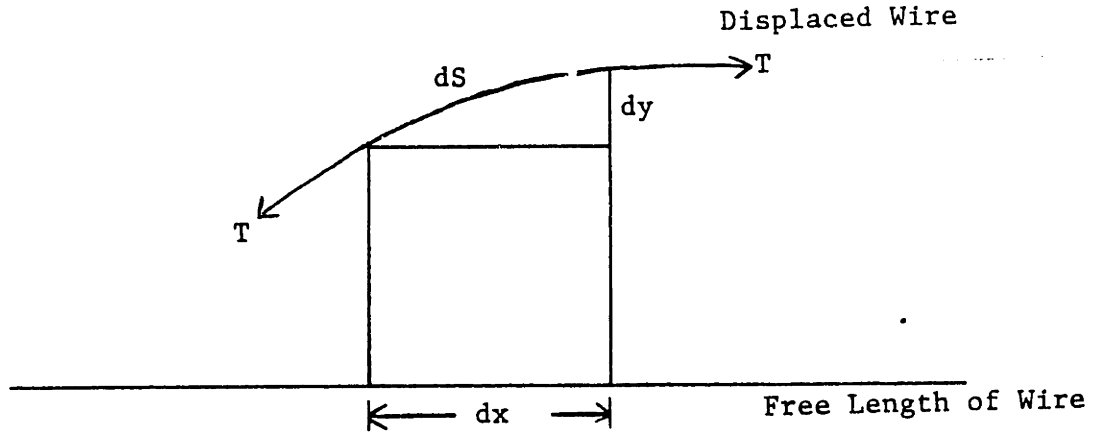
FIGURE A.2:   TENSIONED WIRE ELEMENT

Using the Pathagarian theorem, dS can be approximated as:

$$dS^2 = dx^2 + dy^2 \qquad (A.20)$$

Letting

$$dy = \frac{dy}{dx} dx \qquad (A.21)$$

and substituting into (A.20) yields

$$dS^2 = dx^2 + (\frac{dy}{dx})^2 dx^2 \qquad (A.22)$$

or

$$dS = \sqrt{1 + (\frac{dy}{dx})^2} dx \qquad (A.23)$$

Using the binomial expansion and neglected higher orger terms by assuming $\frac{dy}{dx}$ small:

$$dS = [1 + 1/2 (\frac{dy}{dx})^2] dx \qquad (A.24)$$

by substituting (A.24) into (A.19) the expression for δV_{TEN} becomes:

$$V_{TEN} + T \; 1/2 \; (\frac{dy}{dx})^2 \; dx \qquad (A.25)$$

Substituting the above expression into (A.18) gives the equations for V_{TEN}:

$$V_{TEN} = 1/2 \; T \int_o^\ell (\frac{dy}{dx})^2 \; dx \qquad (A.26)$$

The potential energy may now be evaluated using equation (A.9) for the displacement. Evaluating $\frac{dy}{dx}$ and substituting for the top wire gives:

$$V_{TEN,A} = 1/2 \; T_A \int_o^\ell \left[\sum_m \frac{m\pi}{L} \; A_m \; \cos(\frac{m\pi x}{L}) \right]^2 \; dx \qquad (A.27)$$

Evaluating this integral

$$V_{TEN,A} = \frac{T_A \pi^2}{4L} \; \sum_m m^2 A_m^2 \qquad (A.28)$$

Adding in the effect of the lower wire B, the final expression for the potential energy due to tension effects is obtained:

$$V_{TEN} = \frac{T_A \pi^2}{4L} \sum_m m^2 A_m^2 + \frac{T_B \pi^2}{4L} \sum_m m^2 B_m^2 \qquad (A.29)$$

An expression for the potential energy due to the bending stiffness of the cable may be derived as:

$$V_{BEND} = \int_0^\ell \frac{M_b^2}{2EI} dx \qquad (A.30)$$

where

    M_b is the bending moment

    E Young's Modular

    I Area moment of inertia

From the mechanics of solids

$$M_b \approx \frac{\partial^2 y}{\partial x^2} EI \qquad (A.31)$$

Plugging into equation (A.30) yields:

$$V_{BEND} = \int_0^\ell \frac{EI}{2} \left(\frac{\partial^2 y}{\partial x^2} \right)^2 dx \qquad (A.32)$$

The second derivative of displacement is obtained from equation (A.9) as:

$$\frac{d^2 y}{dx^2} = \sum_m - A_m \frac{m^2 \pi^2}{L^2} \sin\left(\frac{m \pi x}{L}\right) \qquad (A.33)$$

Substituting equation (A.30) yields (for upper wire)

-124-

$$V_{BEND,A} = \int_0^{\ell} \sum_m - A_m \frac{m^2\pi^2}{L^2} \sin\left(\frac{m\pi x}{L}\right) \, dx \qquad (A.34)$$

Evaluating the integral gives

$$V_{BEND,A} = \frac{EI_A\pi^4}{4L^3} \sum_m m^4 A_m^2 \qquad (A.35)$$

Adding in the effect of the other wire, the final expression for the potential energy due to bending effects is obtained:

$$V_{BEND} = \frac{EI_A\pi^4}{4L^3} \sum_m m^4 A_m^2 + \frac{EI_B\pi^4}{4L^3} \sum_m m^4 B_m^2 \qquad (A.36)$$

The potential energy in the droppers and the towers must be evaluated. These elements are both modeled as linear springs. The potential energy for a linear spring is

$$V_{SPR} = 1/2 \ K \ \Delta^2 \qquad (A.37)$$

For the dropper springs Δ represents the difference between the upper and lower wires.

$$\Delta = y_A - y_B \qquad (A.38)$$

The potential energy for the droppers must be evaluated at each dropper location $x = X_1, X_2, \ldots X_p$

$$V_{DROP} = 1/2 \ \sum_{j=1}^{P} K_j \ (y_A - y_B)^2 \Big|_{x=X_j} \qquad (A.39)$$

Using equation (A.9) for the displacement, the potential energy for the dropper springs is

$$V_{DROP} = 1/2 \sum_{j=1}^{P} K_j \left[\sum_m (A_m - B_m) \sin\left(\frac{m\pi X_j}{L}\right) \right]^2 \tag{A.40}$$

The potential energy for the support springs is now evaluated, and must be done at each tower location $x = W_1, W_2, \ldots W_Q$

$$V_{TOW} = 1/2 \sum_{j=1}^{Q} S_j \left. y_A^2 \right|_{x=W_j} \tag{A.41}$$

where S_j = the stiffness of the jth tower

Substituting equation (A.9) for the displacement the potential energy of the support tower springs may be derived

$$V_{TOW} = 1/2 \sum_{j=1}^{Q} S_j \left[\sum_m A_m \sin\left(\frac{m\pi W_j}{L}\right) \right]^2 \tag{A.42}$$

Substituting equation (A.29), (A.36), (A.40), and (A.42) into equation (A.16) yields an expression for the total potential energy:

$$V_{TOTAL} = \frac{T_A \pi^2}{4L} \sum_m m^2 A_m^2 + \frac{T_B \pi^2}{4L} \sum_m m^2 B_m^2$$

$$+ \frac{EI_A \pi^4}{4L^3} \sum_m m^4 A_m^2 + \frac{EI_B \pi^4}{4L^3} \sum_m m^4 B_m^2$$

$$+ 1/2 \sum_{j=1}^{P} K_j \left[\sum_m (A_m - B_m) \sin\left(\frac{m\pi X_j}{L}\right) \right]^2$$

$$+ 1/2 \sum_{j=1}^{Q} S_j \left[\sum_m A_m \sin\left(\frac{m\pi W_j}{L}\right) \right]^2 \tag{A.43}$$

With the expression for the kinetic coenergy and the potential

energy determined, written above in equation (A.15) and (A.43),

Lagrange's method can be used to develop the equations of motion

for the catenary. In order to determine the natural modes, it is

only necessary to investigate the unforced homogeneous case (no input,

no damping). For any admissable motion of the catenary Lagrange's

equation must be satisifed:

$$\frac{d}{dt}\left(\frac{\partial L}{\partial \dot{\xi}}\right) - \frac{\partial L}{\partial \xi} = 0 \qquad\qquad (A.44)$$

where

$$L = T^* - V$$

ξ = generalized coordinate

The generalized coordinate are A_m and B_m, the amplitude of the sine

terms. Each sine wave (or combination of waves) is an admissable

motion, therefore for each m Lagrange's equations must be satisfied.

$$\frac{d}{dt}\left(\frac{\partial L}{\partial \dot{A}_m}\right) - \frac{\partial L}{\partial A_m} = 0 \qquad\qquad (A.45a)$$

$$\frac{d}{dt}\left(\frac{\partial L}{\partial \dot{B}_m}\right) - \frac{\partial L}{\partial B_m} = 0 \qquad\qquad (A.46b)$$

Using equation (A.15). The first part of equation (A.45) can be

evaluated

$$\frac{\partial L}{\partial \dot{A}_m} = 1/2 \, \rho_A L \, \dot{A}_m \qquad \text{(A.46a)}$$

$$\frac{\partial L}{\partial \dot{B}_m} = 1/2 \, \rho_B L \, \dot{B}_m \qquad \text{(A.46b)}$$

Taking the time derivative gives

$$\frac{d}{dt}\left(\frac{\partial L}{\partial \dot{A}_m}\right) = 1/2 \, \rho_A L \, \ddot{A}_m \qquad \text{(A.47a)}$$

$$\frac{d}{dt}\left(\frac{\partial L}{\partial \dot{B}_m}\right) = 1/2 \, \rho_B L \, \ddot{B}_m \qquad \text{(A.47b)}$$

The second half of equation (A.45) is evaluated using equation (A.44):

$$-\frac{\partial L}{\partial A_m} = \frac{T_A \pi^2}{2L} m^2 A_m + \frac{EI_A \pi^4}{2L^3} m^4 A_m$$

$$+ \sum_{j=1}^{P} K_j \sin(\frac{m\pi X_j}{L}) \sum_{r} (A_r - B_r) \sin(\frac{r\pi X_j}{L}) \qquad \text{(A.48)}$$

$$+ \sum_{j=1}^{Q} S_j \sin(\frac{m\pi W_j}{L}) \sum_{r} A_r \sin(\frac{r\pi W_j}{L})$$

where r sums over the same range as m, i.e., $A_r = A_m$ for $r = m$

Similarly:

$$- \frac{\partial L}{\partial B_m} = \frac{T_B \pi^2}{2L} m^2 B_m + \frac{EI_B \pi^4}{2L^3} m^4 B_m$$

$$- \sum_{j=1}^{P} K_j \sin\left(\frac{m\pi X_j}{L}\right) \sum_r (A_r - B_r) \sin\left(\frac{r\pi X_j}{L}\right) \tag{A.49}$$

Lagrange's equation, equation (A.45),

$$\frac{d}{dt} \left(\frac{\partial L}{\partial \dot{A}_m}\right) - \frac{\partial L}{\partial A_m} = 0 \tag{A.45a}$$

can be written for each m as:

$$\left(\frac{\rho_A L}{2}\right) \ddot{A}_m + \left(\frac{T_A \pi^2 m^2}{2L} + \frac{EI_A \pi^4 m^4}{2L^3}\right) A_m$$

$$+ \sum_{j=1}^{P} K_j \sin\left(\frac{m\pi X_j}{L}\right) \sum_r (A_r - B_r) \sin\left(\frac{r\pi X_j}{L}\right)$$

$$+ \sum_{j=1}^{Q} S_j \sin\left(\frac{m\pi W_j}{L}\right) \sum_r A_r \sin\left(\frac{r\pi W_j}{L}\right) = 0 \tag{A.50}$$

With a similar expression for B_m

This equation is a function of the amplitudes and their second derivative and is of the form:

$$\alpha \ddot{A}_m + \beta A_m + \gamma = 0 \tag{A.51}$$

where γ is a function of A_m and B_m.

Because the catenary model is a linear system it is free to vibrate in its natural mode(s). And, true for all linear systems, it has as many modes as degrees of freedom. In a natural mode the motion of the system will be harmonic (sinusoidal). Therefore, the amplitudes term A_m and B_m must also be harmonic, and:

$$\ddot{A}_m = -\omega^2 A_m \qquad\qquad (A.42)$$

$$\ddot{B}_m = -\omega^2 B_m$$

where

ω = the natural frequency of the mode

m = the number of the sine term

Substitution equation (A.52) into equation (A.50) yields:

$$\omega^2 A_m = \left(\frac{T_A \pi^2 m^2}{\rho_A L^2} + \frac{EI_A \pi^4 m^4}{\rho_A L^4} \right) A_m$$

$$+ \frac{2}{\rho_A L} \sum_{j=1}^{P} \left[K_j \sin\left(\frac{m\pi X_j}{L}\right) \sum_r (A_r - B_r)\sin\left(\frac{r\pi X_j}{L}\right) \right] \qquad (A.53)$$

$$+ \frac{2}{\rho_A L} \sum_{j=1}^{Q} \left[S_j \sin\left(\frac{m\pi W_j}{L}\right) \sum_r A_r \sin\left(\frac{r\pi W_j}{L}\right) \right]$$

$$\omega^2 B_m = \frac{T_B \pi^2 m^2}{\rho_B L^2} + \frac{EI_B \pi^4 m^4}{\rho_B L^4} B_m$$

$$\frac{2}{\rho_B L} \sum_{j=1}^{P} \left[K_j \sin(\frac{r\pi X_j}{L}) \sum_r (A_r - B_r) \sin(\frac{4\pi X_j}{L}) \right] \qquad (A.54)$$

A double sum such as

$$\sum_{i=1}^{I} [R_i \times \sum_{j=1}^{J} S_j] \qquad (A.55)$$

can be rewritten as

$$\sum_{j=1}^{J} [S_j \times \sum_{i=1}^{I} R_i] \qquad (A.56)$$

Therefore we can rewrite equation (A.53) as:

$$\omega^2 A_m = (\frac{T_A \pi^2 m^2}{\rho_A L^2} + \frac{EI_A \pi^4 m^4}{\rho_A L^4}) A_m$$

$$+ \sum_r \left[A_r \cdot \frac{2}{\rho_A L} \sum_{j=1}^{P} K_j \sin(\frac{m\pi X_j}{L}) \sin(\frac{r\pi X_j}{L}) \right]$$

$$- \sum_r \left[B_r \cdot \frac{2}{\rho_A L} \sum_{j=1}^{P} K_j \sin(\frac{m\pi X_j}{L}) \sin(\frac{r\pi X_j}{L}) \right]$$

$$+ \sum_r \left[A_r \cdot \frac{2}{\rho_A L} \sum_{j=1}^{Q} S_j \sin(\frac{m\pi W_j}{L}) \sin(\frac{r\pi W_j}{L}) \right] \qquad (A.57)$$

which can be reduced further to:

$$\omega^2 A_m = \alpha(m) A_m + \sum_r A_r \sigma_{AA}(m,r) + \sum_r B_r \sigma_{AB}(m,r) \tag{A.58}$$

where:

$$\alpha(m) = \frac{T_A \pi^2 m^2}{\rho_A L^2} + \frac{EI_A m^4}{\rho_A L^4}$$

$$\sigma_{AA}(m,r) = \frac{2}{\rho_A L} \sum_{j=1}^{P} K_j \sin\left(\frac{m\pi X_j}{L}\right) \sin\left(\frac{r\pi X_j}{L}\right)$$

$$+ \sum_{j=1}^{Q} S_j \sin\left(\frac{m\pi W_j}{L}\right) \sin\left(\frac{r\pi W_j}{L}\right)$$

$$\sigma_{BB}(m,r) = \frac{2}{\rho_A L} \sum_{j=1}^{P} \sin\left(\frac{m\pi X_j}{L}\right) \sin\left(\frac{r\pi X_j}{L}\right)$$

Similarly equation (A.54) can be written as:

$$\omega^2 B_m = \beta(m) B_m + \sum_r A_r \sigma_{BA}(m,r) + \sum_r B_r \sigma_{BB}(m,r) \tag{A.59}$$

where:

$$\beta(m) = \frac{T_B \pi^2 m^2}{\rho_B L^2} + \frac{EI_B \pi^4 m^4}{\rho_B L^4} \tag{A.60}$$

$$\sigma_{BA}(m,r) = -\frac{2}{\rho_B L} \sum_{j=1}^{P} K_j \sin\left(\frac{m\pi X_j}{L}\right) \sin\left(\frac{r\pi X_j}{L}\right)$$

$$\sigma_{BB}(m,r) = \frac{2}{\rho_B L} \sum_{j=1}^{P} K_j \sin\left(\frac{m\pi X_j}{L}\right) \sin\left(\frac{r\pi X_j}{L}\right)$$

Equations (A.58) and (A.59) can be written in matrix form

$$
\omega^2 [I]
\begin{bmatrix}
A_1 \\
\vdots \\
A_m \\
B_1 \\
\vdots \\
B_M
\end{bmatrix}
=
\begin{bmatrix}
\alpha(1) & & & & & \\
& \ddots & & & & \\
& & \alpha(m) & & & \\
& & & \beta(1) & & \\
& & & & \ddots & \\
& & & & & \beta(m)
\end{bmatrix}
\begin{bmatrix}
A_1 \\
\vdots \\
A_m \\
B_1 \\
\vdots \\
B_m
\end{bmatrix}
+
\left[
\begin{array}{c|c}
\sigma_{AA} & \sigma_{AB} \\
\hline
\sigma_{BA} & \sigma_{BB}
\end{array}
\right]
\begin{bmatrix}
A_1 \\
\vdots \\
A_m \\
B_1 \\
\vdots \\
B_m
\end{bmatrix}
$$

$$\underbrace{\qquad}_{\Gamma} \qquad \underbrace{\qquad\qquad}_{\Xi} \qquad \underbrace{\quad}_{\Gamma} \qquad\qquad \underbrace{\qquad\qquad}_{\Theta} \qquad \underbrace{\quad}_{\Gamma}$$

(A.60)

Or as

$$\omega^2 [I] \; \Gamma \;=\; [\Xi + \Theta]\Gamma \tag{A.61}$$

Letting

$$H \;=\; [\Xi + \Theta] \tag{A.62}$$

The final form of the catenary equations is obtained:

$$\omega^2 \, I \, \Gamma \;=\; H\Gamma \tag{A.63}$$

The eigenvalues of the matrix H give the natural frequencies squared. The eigenvalues are the same as finding the roots of the character-istic equation:

$$DET(\lambda I - H) \;=\; 0 \tag{A.64}$$

The eigenvector for each eigenvalue gives the set of amplitudes for each mode.

Denoting λ_i as the ith eigenvalue of the matrix, and Γ_{ij} as the jth element of the ith eigenvector we obtain

$$\omega_i = \sqrt{\lambda_i} \tag{A.65}$$

The amplitudes are:

$$A_{im} = \Gamma_{im} \tag{A.66}$$

$$B_{im} = \Gamma_{i(m+M)} \tag{A.67}$$

The natural mode shapes are:

$$\phi_i = \sum_{m=1}^{M} A_{im} \sin\left(\frac{m\pi x_A}{L}\right) + \sum_{m=1}^{M} B_{im} \sin\left(\frac{m\pi x_B}{L}\right) \tag{A.67}$$

where

M = the maximum number of sine terms considered in the sum

There are 2M natural modes resulting from this technique. Inspection of the modes shows approximately half in the lower frequency range and the other half in a much higher frequency range. The half in the high frequency range are not indicative of the true natural modes, but are a consequence of the solution technique using a finite number of sine terms. These higher modes should not be considered in the system response.

The above method determines the natural mode shapes. With the natural modes known, the response of the system is most effectively calculated using modal analysis. The response of each mode can be

found using equation (A.8)

$$M_i \ddot{z}_i(t) + 2M_i \xi_i \omega_i \dot{z}_i(t) + M_i \omega_i^2 z_i(t) = Q_i \qquad (A.8)$$

where

$z_i(t)$ = the ith modal response function or modal amplitude

Q_i = the ith modal forcing function

ω_i = the ith natural frequency

M_i = the ith modal mass (a scalar)

ξ_i = the ith damping ratio

There will be N modal response equations, where N in the number of modes considered.

The displacement of the catenary as a function of time is given by the sum of the individual modal responses:

$$y(x,t) = \sum_{i=1}^{N} \phi_i(x) z_i(t) \qquad (A.1)$$

Sag is incorporated into the model through the model forcing function:

$$Q_i = \int_0^\ell f(x,t) \phi_i(x) dx \qquad (A.6)$$

where

$f(x,t)$ = the applied force distribution

ϕ_i = the ith mode shape

Since sag is induced by gravity, a force which is time invariant and distributed proportionally to wire mass, the applied force distribution is a constant. So the modal forcing function becomes:

$$Q_{i,sag} = \int_0^{\ell} G \, \phi_i(x) \, dx \qquad (A.68)$$

where

G = the gravitational force distribution, a constant.

To determine G the modal catenary equations of motion are solved for the static case. G's value is determined such that the sag at midspan corresponds to a desired value.

The coupling between the pantograph and the catenary also comes from the modal forcing function, Q_i. The forcing function due to pantograph interaction depends only upon the mode shape and the contact force. Since the pantograph equations are developed independently of the catenary equations, any pantograph model can be used to obtain the contact force. There is also no limit as to how many pantograph can be run under a given catenary.

To get the total modal forcing function for a given mode, the modal forcing function due to sag and each pantograph are summed:

$$Q_i = Q_{i,sag} + Q_{i,pant1} + Q_{i,pant2} \qquad (A.69)$$

APPENDIX B

PANTOGRAPH-CATENARY INTERACTION

This appendix develops the equations of motion for the pantograph, shows the coupling of the pantograph equations with the natural modes of the catenary, and discusses the simulation technique for the response of the total system.

B.1 Pantograph Model

The pantograph model is a two mass model with nonlinear suspension elements. It makes no attempt to model geometric nonlinearities or vibration of the pantograph's links. The model does, however, include the following features.

- The motion of the pantograph is modeled with two masses. The first represents the pantograph head and the second the pantograph frame.

- The stiffness of the contact strips and pantograph shoe are modeled by a linear spring, K_s.

- The stiffness between the head and frame is modeled by a linear spring, K_H.

- Mechanical stops are included to limit the relative motion between head and frame.

- The uplift force is modeled by a constant force, F_o.

- Two types of damping elements between the head and the frame are modeled: linear and one-way damping.

- There are two suspension choices: the first is a linear spring, linear damper, and a one-way damper in parallel. (Figure B.1). The second is a linear spring and damper in series (Figure B.2).
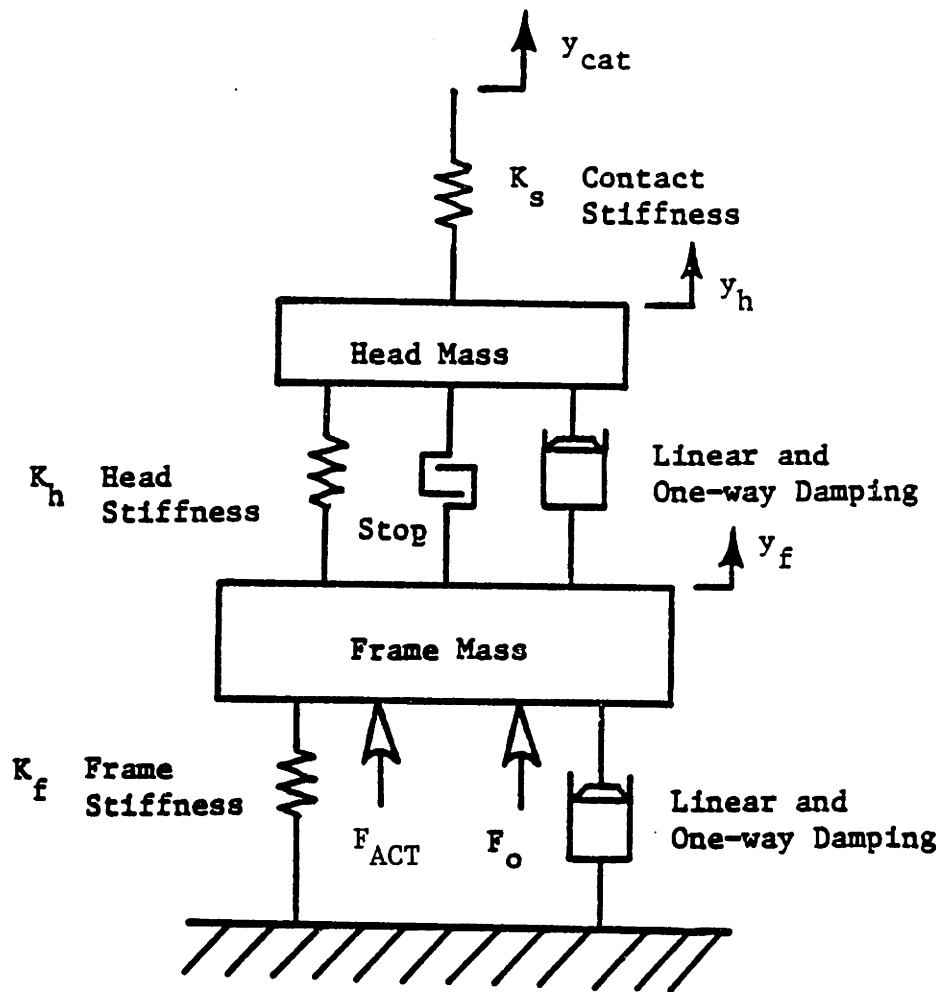
FIGURE B.1: PANTOGRAPH MODEL, FIRST SUSPENSION OPTION
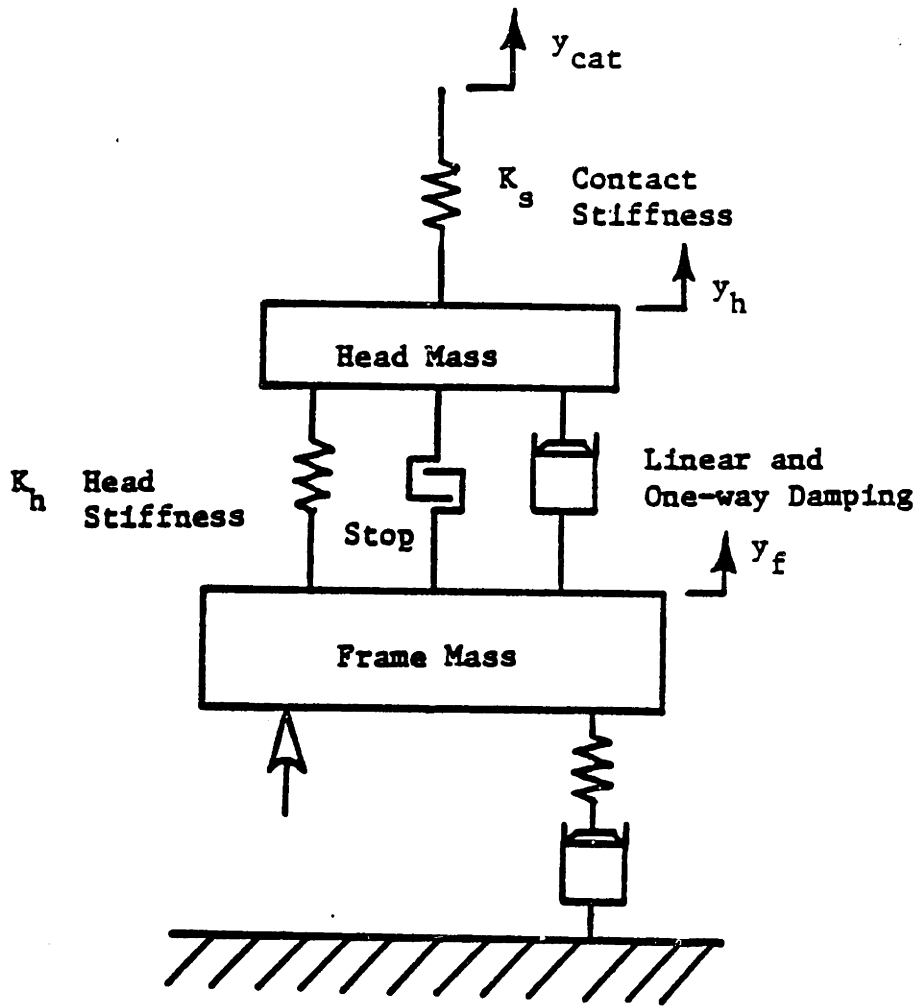
FIGURE B.2: PANTOGRAPH MODEL, SECOND SUSPENSION OPTION

● The model contains a full-state feedback, frame-actuated, active controller.

The pantograph equation of motion will first be developed for the linear case; nonlinearities will be added later. The equations of motion for the linear pantograph are easily derived by summing forces on its two masses. The equations of motion for the parallel spring, damper suspension case (Figure B.1) are:

$$M_h \ddot{y}_h + B_h(\dot{y}_h - \dot{y}_f) + K_h(y_h - y_f) = F_c \qquad (B.1)$$

$$M_f \ddot{y}_f + B_h(\dot{y}_f - \dot{y}_h) + B_f \dot{y}_f + K_h(y_f - y_h) + K_f y_f = 0$$

$$(B.2)$$

where

F_c	=	the dynamic contact force
y_h	=	the displacement of the head mass
y_f	=	the displacement of the frame mass
M_h	=	the head mass
M_f	=	the frame mass
B_h	=	the damping between the head and frame
B_f	=	the damping between the frame and base
K_h	=	the stiffness between the head and frame
K_f	=	the stiffness between the frame and base

The contact force, F_c, is determined from the interaction of the pantograph and catenary. The interaction is modeled by a spring with stiffness typical of the flexure of the contact strips. Therefore, the contact force is:

$$F_c = K_s(y_{cat} - y_h) \qquad\qquad (B.3)$$

where

y_{cat} = the displacement of the lower

y_h = the displacement of the pantograph head

K_s = the stiffness of the contact strip

F_o = the static applied uplift force

When the pantograph loses contact with the catenary the contact force is set to zero and the two systems are considered separately until the pantograph regains contact.

The pantograph model can also be implemented with a full-state feedback controller. The control force is applied to the frame (see Figure B.1) and is a linear function of all the pantograph state variables:

$$F_{act} = -(C_1 y_h + C_2 \dot{y}_h + C_3 y_F + C_4 \dot{y}_F)$$

where

F_{act} = the active control input

C_1 = the gain on head position

C_2 = the gain on head velocity

C_3 = the gain on frame position

C_4 = the gain on frame velocity

The pantograph equations of motion with the active control force are:

$$M_h\ddot{y}_h + B_h(\dot{y}_h - \dot{y}_f) + K_h(y_h - y_f) = F_c$$

$$M_f\ddot{y}_f + B_h(\dot{y}_f - \dot{y}_h) + B_f\dot{y}_f + K_h(y_f - y_h) + K_f y_f = F_{act}$$

Some pantographs have suspensions that are more accurately modeled by a spring and damper in series (Figure B.2). The equations of motion are found by summing forces on the masses and the point between the frame suspension spring and damper. In addition to the position and velocity of the two masses, the position between the suspension spring and damper is also a state-variable. The equations of motion are:

$$M_h\ddot{y}_h + B_h(\dot{y}_h + \dot{y}_f) + K_h(y_h - y_f) = F_c$$

$$M_f\ddot{y}_f + B_h(\dot{y}_f - \dot{y}_h) + K_h(y_f - y_h) + K_{sf}(y_f - y_s) = 0$$

$$B_{sf}\dot{y}_s + K_{sf}(y_s - y_f) = 0$$

where

y_s = the position between the frame suspension's spring and damper

B_{sf} = the series suspension's damping rate

K_{sf} = the series suspension's spring rate

The above provides the linear equations for the simulation's pantograph models. The nonlinear effects included in the models are now developed. To simulate these nonlinear elements the set of linear equations are augmented with the nonlinearities.

To limit the motion between the head and the frame, a mechanical stop is included in the model. At each time step the distance between the head and frame is checked to ensure the stops have not been hit. If they have been the head and frame are constrained to move together until motion is reversed and the stops are freed.

One-way or unidirectional damping is also included in the full nonlinear model. This is not an element of any current pantograph, but it is included to assess its benefit for future pantographs. A one-way damper is a damper which resists motion in only one direction. In the simulation, extra damping was added to the model whenever the velocity between the head and frame was negative (the head moving away from the wire). If the velocity was positive, no extra damping was applied. The same relationship held for the one-way damper attached between the frame and base.

B.2 Coupling Between the Models

The coupling between the pantograph and catenary comes exclusively through the contact force. When the pantograph is in contact with the catenary the motion of the pantograph head (more precisely, the top of the spring K_s) and the lower catenary wire are identical, and the contact force has a non-zero value which is determined from their mutual interaction. When the pantograph loses contact, the contact force becomes zero and the position of the pantograph and catenary are independent until the pantograph regains contact. Only during momentary losses of contact are the pantograph and catenary two separate systems. At all

other times, they are directly coupled: they share the same position and they share the same force.

The contact force enters the pantograph equations in equation (B.1) as the variable F_c. It enters the catenary model equations as part of the modal forcing function. The relationship for the modal forcing function is given in Appendix A as equation (A.6)

$$Q_i(t) = \int_0^\ell f(x,t) \, \phi_i \, dx \qquad \text{(Eqn A.6)}$$

where

$Q_i(t)$ = the forcing function of the ith mode

ϕ_i = the mode shape of the ith mode

$f(x,t)$ = the applied force distribution (units of force/length)

There is a forcing function equation for each mode. Therefore, at every time step the forcing function is calculated for each mode, and then using this forcing function each individual modal response is calculated from the second order differential equation in equation (A.8).

Since the contact force is applied to the lower wire only the B terms of each mode need be considered. Equation (A.6) therefore becomes:

$$Q_i = \int_0^\ell f(x,t) \sum_m B_{im} \sin\left(\frac{m\pi x}{L}\right) dx \qquad \text{(B.4)}$$

If the force is applied at a single point and moves with a velocity, V the position of the applied force is Vt.

$$Q_i = F_c(t) \sum_m B_{im} \sin\left(\frac{m \pi Vt}{L}\right) \qquad (B.5)$$

where

$F_c(t)$ = the applied contact force (units of force)

This is easily generalized for multiple pantographs. For two pantographs the forcing function is:

$$Q_i = F_1 \sum_m B_{im} \sin\left(\frac{m \pi Vt}{L}\right) + F_2 \sum_m B_{im} \sin\left(\frac{m \pi (Vt - X_p)}{L}\right) \qquad (B.6)$$

where F_1 = the contact force of the first pantograph

F_2 = the contact force of the second pantograph

X_p = the distance between the first and second pantograph

B.3 Simulation Technique

To simulate the dynamic response of the pantograph and catenary the equations of motion for both were solved simultaneously using a fourth order Runge Kutta integration technique. The catenary equations (N equations, where N equals the number of modes), the two pantograph equations (equations B.1 and B.2) and the nonlinear elements were written into Fortran code. The response of each modal amplitude, z, and the response of the pantograph is calculated at each time step. The position of the catenary wire at each instant is given by equation A.1 and summing up the individual modes. The time is then incremented and the process repeated until the final time of the simulation is reached. Figure B.2 summarizes the technique used in the dynamic simulation.

```
┌─────────────────────────────────┐
│    READ IN THE EIGENVALUES AND   │
│ EIGENVECTORS: I.E. THE FREQUENCIES│
│      AND SINE AMPLITUDES FOR     │
│         THE NATURAL MODES        │
└─────────────────────────────────┘
                │
┌─────────────────────────────────┐
│     CALCULATE THE MODAL MASSES   │
└─────────────────────────────────┘
                │
┌─────────────────────────────────┐
│         CALCULATE MODAL          │
│        FORCING FUNCTION          │
│        Qᵢ, DUE TO SAG            │
└─────────────────────────────────┘
                │
┌─────────────────────────────────┐
│     CALCULATE THE N MODAL        │
│     FORCING FUNCTIONS, Qᵢ,       │
│     AND THE CONTACT FORCE        │
│     FOR THIS TIME STEP           │
└─────────────────────────────────┘
                │
┌─────────────────────────────────┐
│     FORM THE N CATENARY          │
│     EQUATIONS AND THE 2          │
│     PANTOGRAPH EQUATIONS         │
└─────────────────────────────────┘
                │
┌─────────────────────────────────┐
│    CALCULATE THE RESPONSE OF     │
│     THE N MODAL AMPLITUDES       │
│     AND THE DISPLACEMENT OF      │
│    THE PANTOGRAPH VARIABLES      │
│        FOR THIS TIME STEP        │
└─────────────────────────────────┘
                │
┌─────────────────────────────────┐
│       INCREMENT THE TIME         │
└─────────────────────────────────┘
                │
┌─────────────────────────────────┐  No
│          FINISHED ?              │──────┐
└─────────────────────────────────┘      │
                │ Yes
┌─────────────────────────────────┐
│       OUTPUT THE TIME            │
│       HISTORY OF THE             │
│       VARIABLES OF               │
│         INTEREST                 │
└─────────────────────────────────┘
```
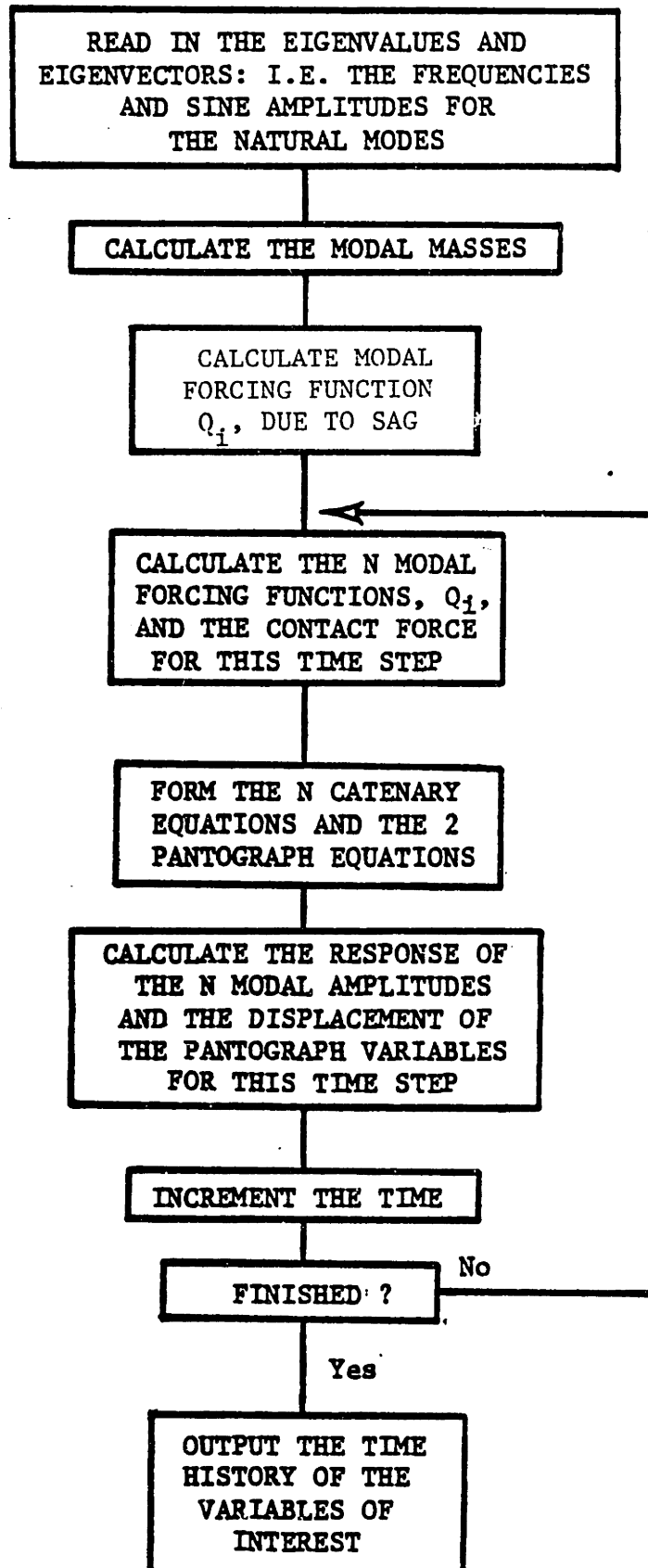
FIGURE B.3:   FLOW CHART FOR THE DYNAMIC SIMULATIONS

REFERENCES

1. Boissonnade, Pierre, and Dupont, "SNCF Tests Collection Systems for Highspeeds," International Railway Journal, October, 1975.

2. Boissonnade and Pierre, "Catenary Design for High Speeds," Rail International, March, 1975, pp 205-217.

3. Boissonnade, Pierre, and Dupont, "Current Collection with Two-Stage Pantographs on the New Paris-Lyon Line," Railway Gazette International, October 1977.

4. Gostling, R.J. and Hobbs, A.E.W., "The Interaction of Pantographs and Overhead Equipment: Practical Applications of a New Theoretical Method," paper presented at Institute of Mechanical Engineers, Derby Branch, February 1981.

5. Coxen, D.J., Gostling, R.J. and Whitehead, K.M., "Evolution of a Simple High-Performance Pantograph," Railway Gazette, January 1980.

6. Communications of the O.R.E., "Behavior of Pantographs and Overhead Equipment at Speeds Above 160 km/hr, "Rail International, January 1972.

7. Belyaev, I.A., Vologine, V.A., and Freifeld, A.V., "Improvement of Pantograph and Catenaries and Method of Calculating Their Mutual Interactions at High Speeds," Rail International, June 1977, pp 309-328.

8. Peters, John, "Dead Line Testing of the Faiveley Single and Dual Stage Pantographs on the RTT Catenary Systems," U.S. Department of Transportation Technical Report FRA/TCC-81/01.

9. Coxen, D.J., Gostling, R.J., and Whiteland, K.M., "Evolution of a Simple High-Performance Pantograph", Railway Gazette, January 1980.

10. Vesely, G.C., "Modeling and Experimentation of Pantograph Dynamics," S.M. Thesis, Massachusetts Institute of Technology, 1983.

11. Sikorsky Aircraft, "Design and Development of a Servo-Operated-Pantograph for High Speed Trains," U.S. DOT, Final Report, Contract No. 7-35415, July 1970.

12. Wann, L.M., "Improvement of a Pantograph for High Speed Train," S.M. Thesis, Massachusetts Institute of Technology, 1980.

13. Vinayalinyam, T., "Computer Evaluation of Controlled Pantographs for Current Collection From Simple Catenary Overhead Equipment at High Speed," J-DSMC.

14. Thomet, Michael, "Catenary and High Speed Power Collection," Joint ASME, IEEE Railroad Technical Conference, Conference Paper C76 458-5 IA, 1976.

15. Communications of O.R.E., "Behavior of Pantographs and Overhead Equipment at Speeds Above 160 km/h," Rail International, January 1972.

16. Sell, R.G., Prince, G.E. and Twine, D., "An Experimental Study of the Overhead Contact System for Electric Traction at 25 kV," Proceedings of the Institute of Mechanical Engineers, Britain, 1964-65.

17. Armbruster, K., "Modeling and Dynamics of Pantograph-Catenary Systems for HIgh Speed Trains," S.M. Thesis, Department of Mechanical Engineering, Massachusetts Institute of Technology, 1983.

18. Thomas, A.G., "Aluminum Conductors in Transport Systems," Electrical Times, June 16, 1966, pp 889-891.

19. Carlson, L.E. and Griggs, G.E., "Aluminum Catenary Quarterly Report," Prepared for the D.O.T., Contract Number DOT-FR-9154, February 1981.

20. Morris, R.B., "Application of an Analogue Computer to a Problem of Pantograph and Overhead Line Dynamics," Proceedings of the Institute of Mechanical Engineers, Britain, 1964-65.

21. Gilbert, G. and Davies, H.E.H., "Pantograph Motion on a Nearly Uniform Railway Overhead Line," Proceedings of the IEEE, Volume 113, pp 485, 1966.

22. Abbott, M.R., "A Numerical Method for Calculating the Dynamic Behavior of a Simple Catenary Overhead Contact System for Electric Railway Traction," Royal Aircraft Establishment, Technical Report 67156, 1967.

23. Levy, S., Bain, J.A. and Leclerc, E.J., "Railway Overhead Contact Systems, Catenary-Pantograph Dynamics for Power Collection at High Speeds," Journal of Engineering for Industry, ASME Paper 68-RR2, November 1968.

24. Scott, P.R. and Rothman, M., "Computer Evaluation of Overhead Equipment for Electric Railroad Traction," IEEE Transactions on Industry Applications, Volume 1A-10, No. 5, September/October 1974.

25. Willets, T.A. and Edwards, D.R., "Dynamic-Model Studies of Overhead Equipment for Electric Railway Traction - Part 1, Simple Catenary Equipment," Proceedings of the Institute of Electrical Engineers, Volume 113, April 1966, p 690.

26. Hobbs, A.E.W., "Accurate Prediction of Overhead Line Behavior," Railway Gazette International, September 1977, pp 3339-343.

27. Carlson, L.E. and Griggs, G.E., "Aluminum Catenary System Quarterly Report," Prepared for the D.O.T., Contract Number DOT-FR-9154, September 1980.

28. Kwakernaak, H. and Sivan, R., "Linear Optimal Control Systems," Wiley-Interscience, New York, 1972.

29. Biggs, J.M., "Introduction to Structural Dynamics," McGraw-Hill Book Company, New York, 1964.

30. Clough, R.W. and Penzien, J., "Dynamics of Structures," McGraw-Hill Book Company, New York, 1975.